

T-3100

The Effect of Fluid Pore Pressure on
the Formation and Stability of Sand Arches

by

Paul M. Winslow

ProQuest Number: 10782729

All rights reserved

INFORMATION TO ALL USERS

The quality of this reproduction is dependent upon the quality of the copy submitted.

In the unlikely event that the author did not send a complete manuscript and there are missing pages, these will be noted. Also, if material had to be removed, a note will indicate the deletion.



ProQuest 10782729

Published by ProQuest LLC (2018). Copyright of the Dissertation is held by the Author.

All rights reserved.

This work is protected against unauthorized copying under Title 17, United States Code
Microform Edition © ProQuest LLC.

ProQuest LLC.
789 East Eisenhower Parkway
P.O. Box 1346
Ann Arbor, MI 48106 – 1346

T-3100

A thesis submitted to the Faculty and the Board of Trustees of the Colorado School of Mines in partial fulfillment of the requirements for the degree of Master of Science, Petroleum Engineering.

Golden, Colorado

Date June 18, 1985

Signed: Paul M. Winslow
Paul M. Winslow

Approved: Dr. Ramona M. Graves
Dr. Ramona M. Graves
Thesis Advisor

Golden, Colorado

Date June 18, 1985

Craig W. Van Kirk
Dr. Craig W. Van Kirk
Head, Department of
Petroleum Engineering

Abstract

This investigation studies the effect of fluid pore pressure on the formation and stability of sand arches. The experimentation was conducted in an 87 inch long steel test cell with a 16 inch internal diameter (I.D.). The cell is equipped with hydraulic jacks mounted on the top and bottom of the cell, capable of applying 5000 psig vertical grain-to-grain stress. The effective sand pack length, with the jacks in place, is 52.75 inches. Additionally, the cell has two, 8 inch plexiglass ports for viewing the sand arches. These ports have a 4 inch simulated casing machined into them. This casing section runs longitudinally up the inside of the cell. A 1/2 inch I.D. pipe extends from the casing surface of the port, through the port, to simulate a perforation. Thus as hydrocarbons are produced out the port, arches can be observed forming around the perforation in the casing. Finally, the cell is equipped with three gauges mounted triaxially in the middle of the sand pack, behind the producing port. These gauges monitor sand pack stress.

The experimentation was conducted using 20/40 Gopher State frac sand. The fluid saturation within the sand pack consisted of a pendular water saturation with mineral spirits being the non-wetting, flowing phase.

Experimentation was conducted at constant fluid pore pressures of 900, 450, and 200 psig. Tests were run at each of these pore pressure levels on sand packs with 3000, 2250, 1500, and 750 psig applied vertical stress. This data showed arch stability to be an inverse function of fluid pore pressure and an increasing function of vertical stress. As the fluid pressure is increased, arch stability decreases, as measured by the flowrate at which an arch fails. Likewise an increase in vertical stress, strengthens an arch allowing it to remain stable to higher flowrates. Of these two functions, fluid pore pressure has the greater effect on arch stability, than does vertical stress.

TABLE OF CONTENTS

	<u>Page</u>
Abstract	iii
List of Figures	vii
List of Tables	x
Acknowledgements	xi
Introduction	1
Practical Applications	3
Literature Survey	5
- Introduction	5
- Methods of Sand Control	6
- Open-Hole Gravel Pack	7
- Inside-Casing Gravel Pack	11
- Sand Consolidation	15
- Gravel Resin Slurries	24
- Re-Stressing the Formation	26
- Sand Arching	26
- Rock Mechanics	48
Equipment Design	52
- Sand Cell	52
- Plexiglass Ports	54
- Hydraulic Jacks	56
- Strain Gauges	57
- Flow Equipment	63

	<u>Page</u>
- Pressure Transducers	69
- Water Injection System	69
Experimental Procedure	70
Discussion of Results	74
- Data Collection	74
- Arch Formation and Stability	91
- Fluid Pore Pressure Effects	94
- Stress Effects	109
- Grain Crushing Analysis	127
Conclusions	141
Recommendations	143
- Equipment Improvement	143
- Future Experimentation	145
Nomenclature	149
Cited References	151
Appendix	154
- Experimental Procedure Outlined	154

List of Figures

<u>Figure</u>		<u>Page</u>
1	Hole Underreamer (1)	8
2	Open-Hole Gravel Pack (1)	9
3	Open-Hole Gravel Pack with Open-Hole Packers (1)	12
4	Inside Casing Gravel Pack (1)	13
5	Chemical Consolidation Cross-Section (1) . .	16
6	Payzone Packer Illustration (6)	27
7	Terzaghi's Trap-Door Apparatus (9)	29
8	Hall and Harrisberger's Arching Apparatus (11)	32
9	Tippie and Kohlhaas' Arching Apparatus (13) .	37
10	Colorado School of Mines Sand Cell (16) . . .	41
11	Bratli and Risnes' Arching Apparatus (20) . .	45
12	Colorado School of Mines Sand Cell, Cross-Sectional View (22)	53
13	Plexiglass Ports Cross-Section	55
14	Hydraulic Jack System Diagram (22)	58
15	Triaxial Mounting of Strain Gauges (22) . . .	59
16	Gauge Positioning, Cross-Sectional View (22)	60
17	Gauge Calibrating Test Cell (22)	62
18	Strain Gauge Calibration, #58899 (F) (22) . .	64
19	Strain Gauge Calibration, #58896 (G) (22) . .	65
20	Strain Gauge Calibration, #58898 (H) (22) . .	66

<u>Figure</u>		<u>Page</u>
21	Flow Equipment Schematic(22)	67
22	Arch Cross-Sectional View	92
23	Flowrate at Arch Failure vs. Pore Pressure, 3000, 2250, 1500, and 750 psig Vertical Stress	97
24	Flowrate at Arch Failure vs. Pore Pressure, 3000 psig Vertical Stress	98
25	Flowrate at Arch Failure vs. Pore Pressure, 2250 psig Vertical Stress	99
26	Flowrate at Arch Failure vs. Pore Pressure, 1500 psig Vertical Stress	100
27	Flowrate at Arch Failure vs. Pore Pressure, 750 psig Vertical Stress	101
28	Flowrate at Arch Failure vs. Vertical Stress, Comparison to Benton's(22) Data	103
29	Flowrate at Arch Failure vs. Horizontal Stress, Comparison to Benton's(22) Data	104
30	Flowrate at Arch Failure vs. Vertical Stress, 900, 450, and 200 psig Pore Pressure	112
31	Flowrate at Arch Failure vs. Vertical Stress, 900 psig Pore Pressure	113
32	Flowrate at Arch Failure vs. Vertical Stress, 450 psig Pore Pressure	114
33	Flowrate at Arch Failure vs. Vertical Stress, 200 psig Pore Pressure	115
34	Flowrate at Arch Failure vs. Horizontal Stress, Both gauges H and G	117
35	Flowrate at Arch Failure vs. Horizontal Stress, Gauge H	118
36	Flowrate at Arch Failure vs. Horizontal Stress, Gauge G	119

<u>Figure</u>	<u>Page</u>
37	Horizontal Stress Comparison 121
38	Flowrate at Arch Failure vs. Stress Ratio . 124
39	Vertical Stress vs. Horizontal Stress (H) . 125
40	Vertical Stress vs. Horizontal Stress (G) . 126
41	Flowrate at Arch Failure vs. Net Effective Stress 128
42	Grain Size Distribution, Initial and Final Sand Samples 132
43	Grain Size Distribution, Blow-up Section . . 133
44	Grain Size Distribution, Crush Test Data . . 136
45	Grain Size Distribution, Blow-up Section . . 137
46	Effect of Pore Pressure on Sand Grain Crushing ⁽¹¹⁾ 138

List of Tables

<u>Table</u>		<u>Page</u>
1	Hall and Harrisberger (11) Data	33
2	Fluid Properties of Mineral Spirits	75
3	Raw Laboratory Data	77
4	Flowrate at Arch Failure vs. Fluid Pressure Data	96
5	Reduced Data	110
6	Sand Samples Sieve Analysis	130
7	Crush Test Sieve Analysis	135

Acknowledgements

The author wishes to express his sincere gratitude to the Petroleum Engineering Department of the Colorado School of Mines for the use of its facilities for this graduate study. The author also wishes to thank Arco Oil and Gas Company, Chevron Oil Field Research Company, Marathon Oil Company, and Tenneco Oil Exploration and Production for their funding of this project. Additionally, the author would like to thank John Benton for his assistance with experimental knowledge and especially Jeff Bolke for his invaluable assistance in data collection. Finally a special word of thanks to the author's advisor, Dr. R. M. Graves, and committee members Dr. J. W. Crafton, and R. S. Thompson.

Introduction

Sand production is a severe problem in unconsolidated and friable sand reservoirs. The flow of sand into the wellbore causes rapid erosion of both the casing and down hole equipment as well as surface equipment. This situation becomes very costly when equipment is constantly being replaced. Not only is the equipment expensive to replace, but workover costs and lost production from down time also contribute to the cost. Several options are available to the oil industry to eliminate or at least cut down on this problem.

Traditionally sand production has been curtailed through the use of gravel packs, sand screens and liners, and through chemical consolidation. The gravel packs and screens are designed to cause sand bridging of the formation sand, which eliminates the influx of sand. Chemical consolidation involves increasing the bonding strength between sand grains to artificially consolidate the sand. Besides the cost encountered in using these techniques, they tend to reduce the productivity of the formation, by reducing the near wellbore permeability.

Because of this reduction of productivity using mechanical and chemical techniques, recent studies have shifted to a natural method of sand control. This method

involves the formation of a stable sand arch around the perforations in a casing. It has been shown experimentally that sand will arch across a hole, under certain conditions. The formation and stability of these arches is a function of the sand type, stress conditions, fluid type and pressure, fluid saturations, permeability, and flowrates across the arch.

The arching behavior of sand has been investigated by numerous individuals and companies. The most current and ongoing experimentation is being conducted in the Petroleum Engineering Department at the Colorado School of Mines. Much of this research has focused on the effects of stress and fluid properties on the formation and stability of sand arches. Some work has also been done using different size frac sands and natural sands. Until this time, no concern has been given to the effects of fluid pore pressure in the sand pack. Previous work has been done at atmospheric pressure. This thesis will investigate the effects of pore pressure on arch formation and stability.

Practical Applications

- 1) Injection of water into the formation prior to bringing a well on production, will assure residual water saturation which is necessary for arch stability. In high productivity reservoirs, water should be injected and then the well brought on slowly until sand problems occur. At this point more water should be injected and the well brought on slowly again to a producing rate below that corresponding to sand production. The sand arches formed around the perforations will remain stable at this rate.
- 2) Wells completed in unconsolidated sands should be brought on to production gradually. This gradual rate increase being on the order of 0.5 BPD/perforation per hour. It was observed that sudden increases in flow-rate across sand arches often cause premature arch failure. Thus a gradual build-up in flowrate will allow for a higher sand-free production rate. This also applies when bringing a well back on production after a shut-in period. It was observed that arches remained intact when the flowrate was instantaneously shut in. These arches then remained stable when flow was initiated back across the arch, as long as the flowrate was initiated at a rate less than the rate

prior to shut-in. Once initiated at this lower rate, the flowrate could then be stepped up to the previous level without arch failure.

- 3) It was seen that arch stability increases with increasing overburden stress and decreasing fluid pore pressure. Thus the technique of sand control through the use of natural sand arches is best accomplished in deep, under or normally-pressured reservoirs. It is not a method advantageous for use in over-pressured shallow reservoirs. In these shallow reservoirs there is not sufficient energy in the form of grain-to-grain stress to sustain stable arches.
- 4) If stable sand arches form around perforations initially in a reservoir, they will remain stable as the reservoir is depleted as long as the production rate and water cut do not increase. It has been shown that arch stability is an inverse function of fluid pressure, so a depletion in reservoir pressure will tend to strengthen an arch.

Literature Survey

Introduction

The flow of sand into the wellbore is a result of overbalanced forces on the sand grains in the direction of the perforation. These forces include fluid drag from the flowing hydrocarbons, formation stresses, pore pressure, gravity, and any cohesive forces. Once these forces have become overbalanced and sand is being produced, various sand control techniques have to be used to re-establish formation integrity. These techniques typically include various types of gravel packs with screens or liners, in-situ chemical consolidation, and gravel resin slurries.

Another type of sand control can be utilized if initiated before massive sand production occurs. This involves creating the right conditions down hole to form and maintain a stable sand arch around each perforation. These arches can be maintained under certain flowrate or drawdown conditions. This flowrate depends on in-situ formation parameters such as formation stresses, fluid pore pressure, cohesive forces, and reservoir fluid properties.

The following is a discussion in further detail of the present understanding of sand arches as a means of sand control as well as a comprehensive overview of other sand control techniques. Additionally, a theoretical development is presented discussing the effect of fluid pore pressure on formation stress and on arch stability.

Methods of Sand Control

Sand production is a major concern in many reservoirs around the world. This sand production is a result of producing oil and gas from unconsolidated or friable sand reservoirs. Sand carried by the producing hydrocarbons causes serious problems for both downhole as well as surface equipment. Common problems associated with sand production include:

- 1) Shut-in production due to plugging. Sand will plug perforations, casing, tubing, surface flow lines, and will fill separators.
- 2) Equipment failure due to erosion from sand carried in the produced fluid. This erosion will cause holes in pipes as well as leaks in valves, flanges, chokes, and other flow line equipment.
- 3) Casing buckling or collapse due to the removal of sand from behind the casing.

These problems are not only costly to repair, but often can be quite dangerous as well. Leaks in surface equipment can present a serious fire or explosion hazard.

Several types of sand control are used to eliminate sand problems. These include gravel packing, chemical consolidation, resin coated sand slurries, re-stressing the formation, and sand arching. Each of these methods has its advantages and disadvantages, and thus are used under different reservoir conditions.

Open-Hole Gravel Pack

The most common type of sand control used is the open-hole gravel pack. Using this technique, the well is drilled to the top of the producing formation and casing is set. The producing formation is then drilled through and underreamed. Figure 1 shows this drilling process. A wire-wrapped screen or slotted liner is then hung from the casing and sized gravel is pumped in the annulus between the screen and the formation (Figure 2). Sufficient literature exists on gravel and screen sizing as well as actual packing procedures^{(1) (2)}, so these will not be discussed. The packed gravel and screen provide a bridging matrix for the reservoir sand thus significantly reducing if not eliminating sand production.

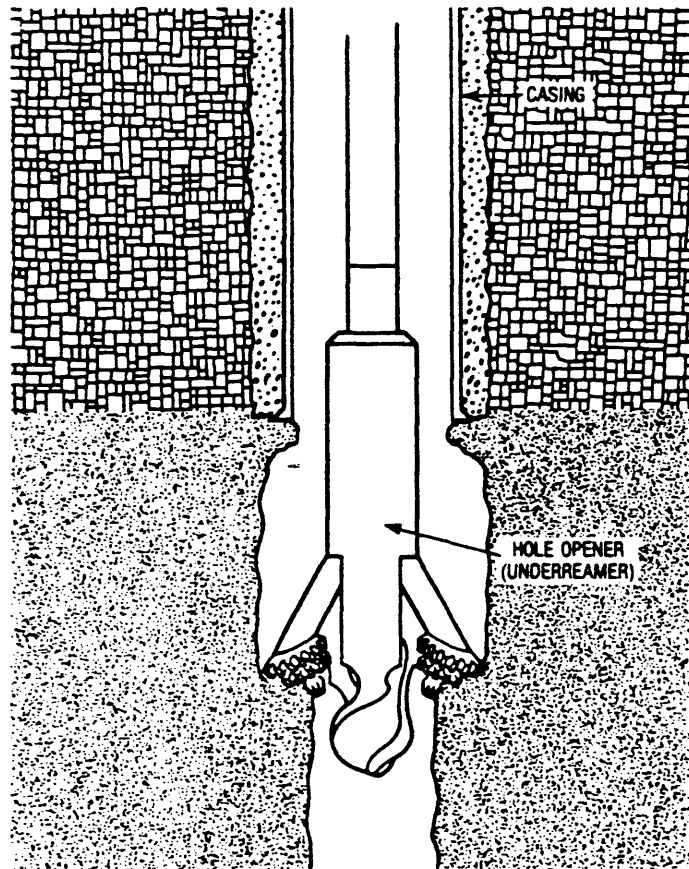


Figure 1

Hole Underreamer (After Suman, et al. ⁽¹⁾),

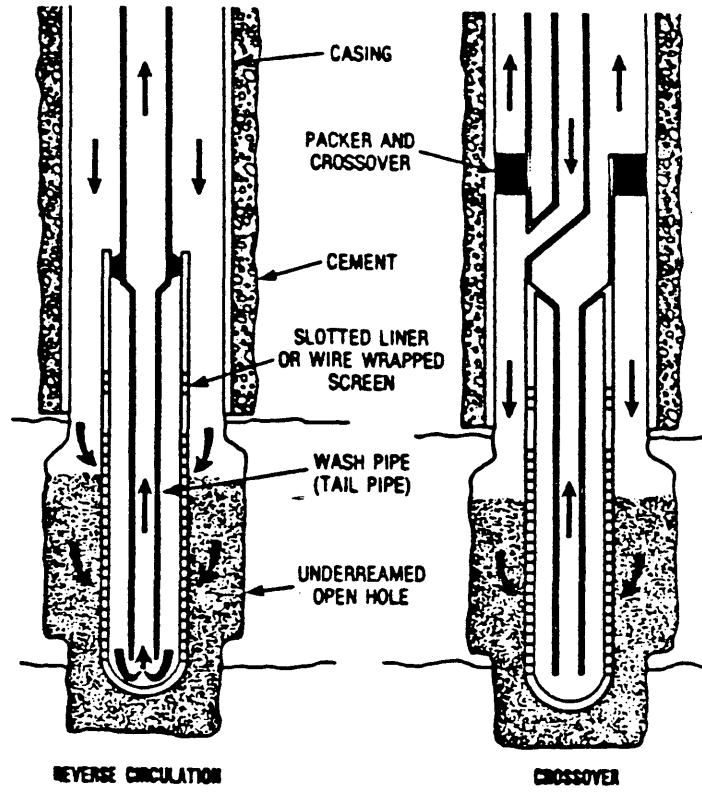


Figure 2
Open-Hole Gravel Pack
(After Suman, et al. ⁽¹⁾)

This method is especially good for thick reservoirs where zone selectivity to eliminate water encroachment is not necessary. Because the well is completed open-hole, the productivity is much higher than in a cased and perforated well. Also the radial flow of the well is enhanced due to the enlarging or underreaming of the hole. This allows for higher production rates.

To complete a well in this manner, the top and bottom of the formation have to be known in advance to stop drilling at the proper depths. To get around this problem, wells are often drilled through the producing formation, logged, and cased. The formation top and bottom are picked from the logs and a "window" is then cut in the casing. The formation is then underreamed and packed in the same open-hole fashion.

Another disadvantage in open-hole gravel packs is that the entire packed interval is in communication. Thus zone selectivity for production and squeezing is lost. Therefore, open-hole gravel packs are not commonly used where water or gas coning problems are associated due to the communication problems. Interbedded shale zones also cause problems. To solve these interbedded problems, open-hole inflatable packers can be set at selected intervals on blank joints in between sections of screen,

(Figure 3). This allows for some degree of zone separation. If the stringers are relatively thin, this technique is not practical.

Inside-Casing Gravel Pack

The second type of sand control used in the oil industry is a gravel pack within the casing. Here the well is drilled, cased, and perforated as usual, and then a screen is placed inside the casing opposite the perforations. The annulus between the screen and the casing wall is then packed with sand or gravel. Figure 4 shows a typical inside-casing gravel pack setup. Best results for sand-free production occur if sand is packed behind the casing and in the perforations as well as inside the casing.

The inside-casing gravel pack is best to use on thin zones or on multiple zone wells. It is also advantageous to use this type of gravel pack in wells that have interbedded water, gas, or shale zones. Since the hole is cased, only the hydrocarbon producing intervals are perforated. This isolates the producing zone from these other zones.

In multizone wells, the zones are separated by packers and are packed or completed separately. The casing used in such a well has to be fairly large. This is

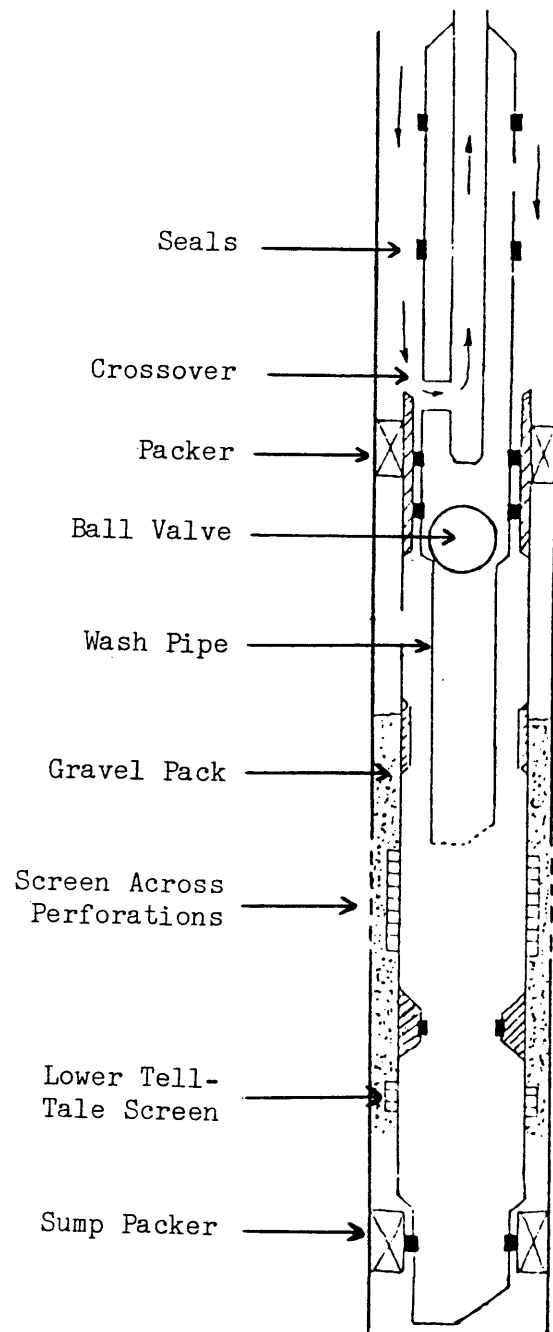


Figure 4

Inside-Casing Gravel Pack (After Suman, et al.⁽¹⁾)

due to the increased size of the upper screens, which have to be large in order to accommodate the extra tubing strings. Thus inside-casing gravel packs for multizoned wells are very costly. Not only is the extra down-hole equipment and larger casing expensive, but also the process is very time consuming which increases rig costs.

Another problem with inside-casing gravel packs is that the gravel pack causes production impairment at higher rates. This loss in productivity is due to the turbulent flow through the gravel pack and screen. Flow coming into the wellbore is concentrated into an area the size of the perforation opening. Studies show that the gravel pack does not diffuse this flow, so the flow across the pack is linear⁽²⁾. The radial flow entering the perforation is then forced into a constricted linear flow at very high velocity. It has been shown that this velocity is in the non-darcian or turbulent region for moderately high productivity wells. This turbulent flow causes a severe pressure drop across the gravel pack, that is noticed as a skin effect. This skin effect or productivity loss increases with increased production rate. Thus inside-casing gravel packs should not be used in high productivity formations.

Sand Consolidation

In-situ sand consolidation was developed as an alternative to inside-casing gravel packs. Chemicals are injected into the formation in order to cement the sand grains together around the perforations. The main advantage with this process over the inside-casing gravel pack, is that it will not impair the well productivity to the extent that the gravel pack does. Although the cementation process will slightly reduce the near wellbore permeability, the fact that there is no linear flow region across a gravel pack means that there will not be a large productivity loss due to the turbulent flow. Another advantage to having the casing interior free from sand and screens, is that on a multi-completion well, smaller casings can be used. Thus chemical consolidation is often used in multizoned wells, especially in the upper zones.

A typical in-situ cementation process involves injection of preflush, resin solution, catalyst, and overflush phases (Figure 5). The main purpose of the preflush is to clean the formation near the wellbore and to displace reservoir fluids that might contaminate the resin. This is one problem with plastic consolidation of sand grains. The plastic resins typically used are very sensitive to water, brine, isopropyl alcohol, hydraulic

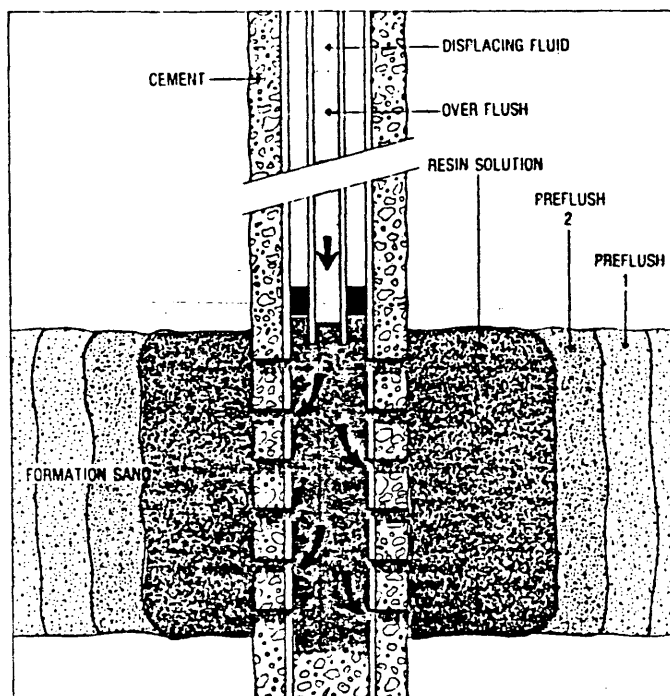


Figure 5
Chemical Consolidation Cross-Section
(After Suman, et al.⁽¹⁾)

fluids, acid, toluene, pipe dope, and diesel oil. Thus several preflush systems are typically used to safeguard resin contamination.

The resin solution is generally an epoxy, furfuryl alcohol (Furans), or phenol formaldehyde (Phenolic) solution. These coating plastics are carried in either an aqueous or hydrocarbon solvent. In addition the resin solution contains a coupling agent, and may contain a curing agent. Certain solutions incorporate the catalyst within the resin and others place the catalyst in the overflush.

There is both an advantage and disadvantage with placing the catalyst in the resin solution. One problem associated with chemical consolidation processes is that it is often difficult to expose all sand grains with each stage of the cementing process. Thus by placing the catalyst within the resin solution, complete contact is achieved between the resin and the catalyst. This assures complete setting of the plastic resin. The drawback to this is that if injection is blocked through the perforations, the resin will set inside the casing.

On the other hand if the catalyst is carried in the overflush stage, the resin can not set-up in the casing, but also the catalyst may not come in contact with all of the resin. This would result in an incomplete consolidation and sand production might occur.

The primary function of the overflush is to spread the resin and catalyst uniformly throughout the perforation area. The overflush forces residual resin to be deposited at grain-to-grain contacts. This accounts for the minimal reduction in permeability once the resin sets. The thickness of the resin film deposited controls this permeability as well as the compressive strength of the consolidated sand.

The key to successfully consolidating the sand grains in the wellbore region, is to uniformly spread or place the resin and catalyst. This is very difficult to accomplish, which accounts for the low success rate of 30-50% (2). Extreme care has to be taken in order to prevent contamination of the resins being used. These contaminants account for many of the consolidation failures. Additionally certain contaminants, especially brines, speed up the degradation process of the set plastics.

Thus formations consolidated with plastic resins may develop sand production problems later in the life of the well.

In addition to being sensitive to certain contaminants, these plastics are very sensitive to temperature. Temperature has two effects on these plastics. First as the temperature is increased, the setting time decreases. This makes proper placement difficult. Secondly, temperature has an accelerating effect on the degradation of the set plastic. Because of these, most chemical consolidation systems are not recommended above 300° F. This eliminates this type of sand control for any thermal recovery systems.

In-situ sand consolidation is best used for relatively short intervals, less than 10 feet. It is also helpful if the formation has a good quality sand with sufficient vertical permeability⁽¹⁾. This type of sand control is ideally suited for high pressure reservoirs and for upper zones in a multizoned well. Although the chemicals involved are relatively expensive, placement is less costly since a rig is not needed on the well.

As mentioned earlier, the main drawbacks are the plastics sensitivity to contaminants and temperature, and the difficulty in placement of the plastic resins. This

placement problem is compounded in formations where sand has already been produced. It has been shown that chemical distribution is poor in unstressed sands, and in sands where a cavity exists(2). In the case of the cavity already existing, the solution to the problem lies in using a high gravel content resin slurry. This will be discussed later in further detail.

In presenting a solution to the temperature and contaminant restraints of in-situ consolidation, several new techniques have been patented. These include metal plating(3) and silica cementing(4)(5) of the sand grains.

Strickland, et al.(3) presented a technique whereby sands are consolidated by plating the grain surfaces with either nickel or cobalt. In this process metal is deposited as a thin film on all exposed surfaces. Since the metallic layer is very thin, there is reported to be little permeability reduction. The compressive strength of this metallic consolidated sand is reported to be 40,000 psig at the wellbore. Unlike the plastic consolidations where the sand develops a fairly uniform compressive strength, the metal plating method develops a tapering strength, with maximum strength at the wellbore. This is advantageous because the wellbore is where the maximum strength is required.

Another advantage to this method is that the nickel and cobalt solutions are aqueous. This reduces the chance of contamination from formation waters. Also the plating process can be run in a fairly short time. Because the nickel and cobalt consolidate during the injection process, no shut-in time is required. This technique like the plastic consolidations can be run without a rig, which helps offset the cost involved in the chemicals.

For the nickel plating process, diesel oil is injected to remove all formation hydrocarbons from the near wellbore area. Isopropyl alcohol is then injected to activate the sand surfaces for the metal plating. This activating is done by depositing colloidal palladium on the exposed surfaces. A spacer is used to separate the activator from the plating solution, and saltwater is used to displace the plating solution.

Similar to the metal plating technique, two silica cementing methods have been developed. The first is a process developed by Shell, known as Silicalock⁽⁴⁾. This process was designed for use in gas wells and was successfully tested in the Groningen gas field.

In this process, silicon tetrachloride is injected in a high pressure nitrogen stream into the formation. The silicon tetrachloride reacts with the residual water in

the formation and produces silica oxide cement and hydrochloric acid. The silica gel, cements the sand grains together consolidating the sand. Since the residual water is trapped next to the grains, the cementing process consolidates the sand grains without drastically reducing the pore space and thus the permeability.

The Silicalock process is a relatively quick and simple process. The process is a one phase dynamic treatment consisting of one chemical. Since only gas is injected, the formation will not be damaged due to liquid blocking or incompatible liquids being placed in the producing rock. Also, the single chemical dynamic treatment eliminates curing time, complex chemicals, and placement problems. Other advantages to this process include minimum permeability reduction and sufficient strength build-up.

A large percent of clays in the formation sand, can cause problems with the Silicalock process. Due to the water held by the clay, the silica tends to plate out on the clay particles. This plating can cause a significant reduction in productivity. On the other hand, this phenomenon will tend to stabilize fines in sands with a small percentage of clays.

The second sand consolidation technique was developed by Aslesen, Short, and Terwilliger, then with Gulf Research and Development Company⁽⁵⁾. This technique, called Solder Glass, is a more complex silica cementing system, involving several steps.

The first step in the process is to inject heated air into the formation which starts a forward combustion in the reservoir. This combustion is used to dry up and clean the formation sand. Next the Solder Glass solution is injected into the dry formation. This solution contains silica, lead oxide, zinc oxide, and boric oxide, all in a water base. The solution adheres to the sand grains due to the wetting property of the grains. Unheated air is then injected to displace the silica solution. Finally heated air is injected in order to evaporate the water, melt the solder glass, and finally to devitrify the amorphous silica material.

This process of devitrifying this particular silica material leaves an extremely stable silica cement on the sand grains. It is reported to be stable at temperatures up to 1200° F which would make the consolidation useful in thermal processes such as fire floods. Also, being an inorganic cement, it is impervious to chemical attack, with the exception of hydrofloric acid. Another advantage

with this method is that it is reported to improve both porosity and permeability⁽⁵⁾. This results from cleaning the wellbore area by the initial combustion process. The combustion will dehydrate any clays contacted thus reducing their volume. Also these dehydrated clays outside the area of silica devitrification, are less likely to migrate as are hydrated clays.

One of the major disadvantages with this process, is that it is both expensive and time consuming. The process generally takes five to seven days. Also, the process is designed for only one perforation, in order to control proper injection placement. Thus, thick formations will require multiple treatments, which have to be done separately. Also, a fairly high permeability sand is needed for the Solder Glass process.

Gravel Resin Slurries

High gravel content resin slurries are a modification of the in-situ sand consolidation systems. Here the sand grains are coated with resin at the surface and are then pumped into the formation through the perforations and allowed to set. The excess sand is then drilled out of the casing. This type of sand control has many advantages as well as disadvantages.

Because all of the coated gravel is placed outside the casing (after drillout), there is no productivity impairment inside the casing causing turbulent flow. This makes this process useful for consolidating upper zones in multizoned wells.

Since the sand and chemicals are mixed at the surface, all sand grains are contacted by all chemicals, thus good consolidation is achieved. Another advantage is that excess resin is not pumped into the formation. This accounts for no reduction in well productivity. The permeability of the cemented sand grains is roughly 10 darcies⁽¹⁾ which is typically higher than the formation permeability. Finally the squeezing required to inject the coated sand, is reported to re-stress the formation to some degree which will help stabilize fines migration⁽²⁾.

Several problems exist with this consolidation technique. First of all the placement of the coated gravel is often difficult to achieve over the entire interval. For this reason short intervals are preferable, usually 4 to 20 feet with four shots per foot. Besides the placement problem, the resins used are sensitive to contamination and also to degradation due to age and temperature. Thus re-treatments are often necessary at later dates.

Re-Stressing the Formation

Typically the stress regime of an unconsolidated sand is disturbed during the drilling and completion of a well. Because of this, the unstressed sand has a tendency to flow into the wellbore with the produced fluids. Considerable thought has been given to the idea of controlling this sand flow by re-stressing the sand formation. It has been shown that the stressed sand resists motion better than unstressed sand. Also this stressed sand is supposed to inhibit the movements of fines (2).

Completion Tool Company of Houston has developed an inflatable packer that they claim will re-stress the formation and thus help control sand problems (6). Cement is pumped into the sleeve of this packer which expands to conform to the walls of the wellbore. Pressure is then applied to the packer sleeve which re-stresses the formation. Figure 6 shows a schematic of the Pack/Perf inflatable packer.

Sand Arching

The arching phenomenon of sand was first recorded experimentally by Dr. Karl v. Terzaghi (7) (8) (9) in 1936. His experimentation was conducted using a rectangular box

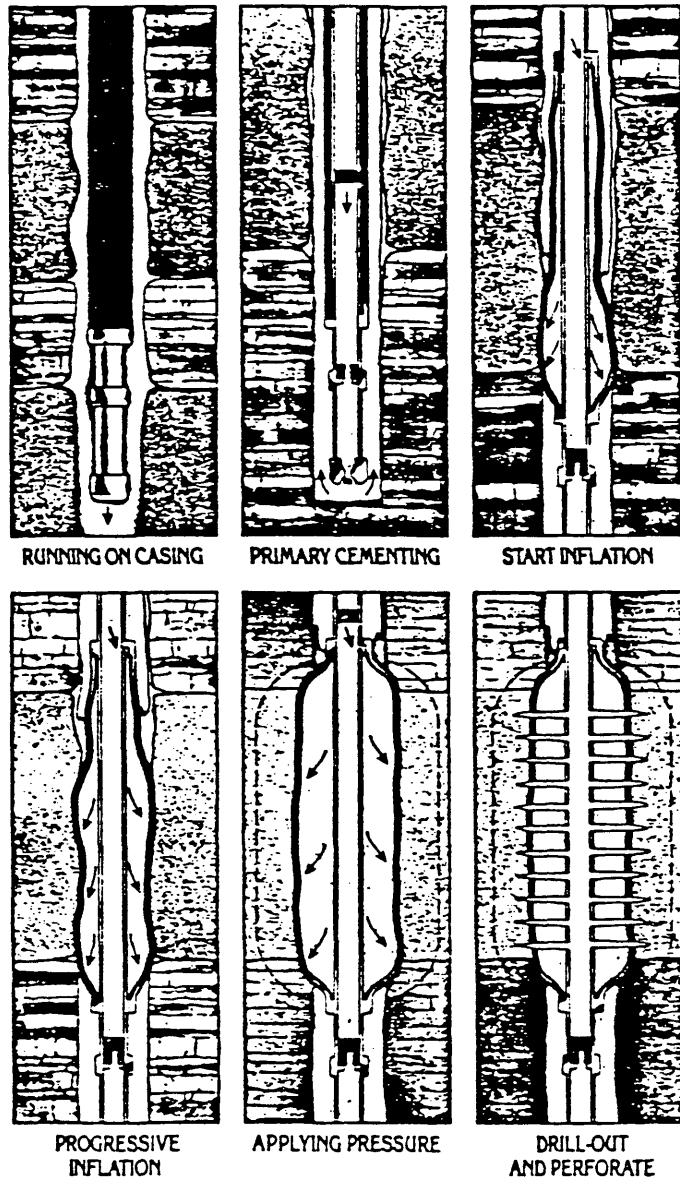


Figure 6

Payzone Packer Illustration
(After Completion Tool Co. (6))

with a trap door in the middle of the bottom plate (Figure 7a). Dry cohesionless sand was packed into the box and then the trap door slowly removed. The trap door was mounted on a scale so that load on the door could be monitored. Before lowering the door, the stress measured was equal to γH per unit area. After slightly lowering the trap door, this measured stress dropped to a fraction of its original value (Figure 7b). The remainder of the stress was transferred to the surrounding bottom plate. Terzaghi justified this redistribution of stress, by assuming the sand had arched across the opening.

In his book⁽⁸⁾ Terzaghi defines sand arching in the following manner:

"If one part of the support of a mass of soil yields while the remainder stays in place the soil adjoining the yielding part moves out of its original position between adjacent stationary masses of soil. The relative movement within the soil is opposed by a shearing resistance within the zone of contact between the yielding and the stationary masses. Since the shearing resistance tends to keep the yielding mass in its original position, it reduces the pressure on the yielding part of the support and increases the pressure on the adjoining stationary part. This transfer of pressure from a yielding mass of soil onto adjoining stationary parts is commonly called the arching effect, and the soil is said to arch over the yielding part of the support. Arching also takes place if one part of a yielding support moves out more than the adjoining parts."

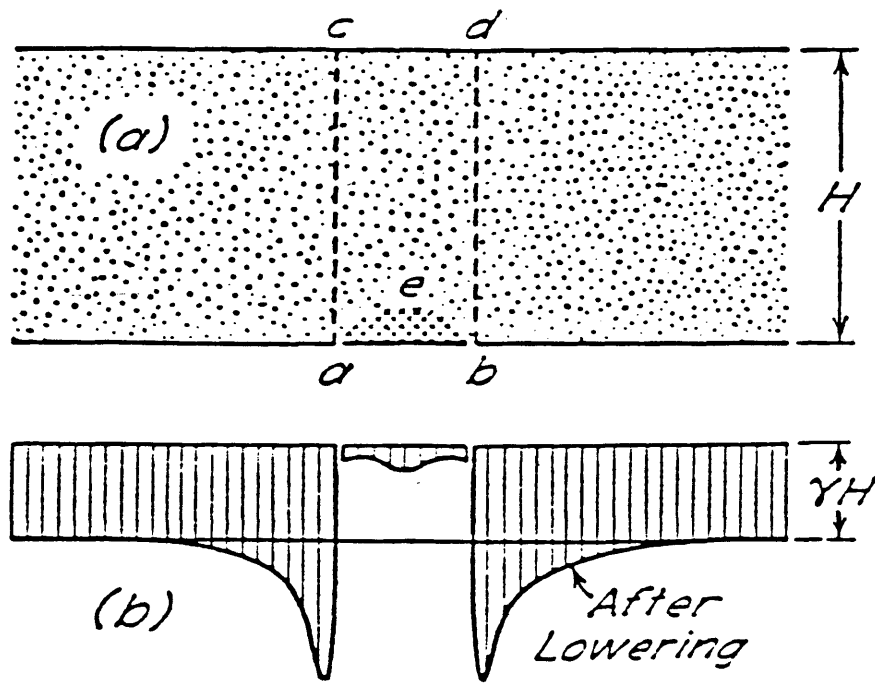


Figure 7
Terzaghi's Trap-Door Apparatus
(After Terzaghi. ⁽⁹⁾)

It might be noted that Terzaghi's work was done with dry sand and with the trap door in the horizontal plane. Using dry sand, Terzaghi's arches had no stability. He reported that as the trap door was continually lowered, the arch would fail and the sand would flow out the opening. The same tests run with wet sand yielded stable or intact arches when the door was removed. Terzaghi concluded that the formation of sand arches was due to the shear resistance within the sand pack. He also stated that some cohesive force was necessary to maintain a stable arch.

Expanding on Terzaghi's work, J. W. McNulty⁽¹⁰⁾ performed arching experiments using a similar trap door set up. He used both angular and rounded sands, with a maximum vertical stress of 110 psig. He found that the stress on the trap door could be decreased to zero by lowering the door a distance of 0.003 times the door's diameter. This was for a sand pack the same thickness as the diameter of the trap-door. If the thickness was increased to twice or four times the diameter, then the trap door need only be lowered 0.0016 times the diameter to relieve the stress.

Following McNulty, the next major research done on sand arching was done by Hall and Harrisberger⁽¹¹⁾, working for Dowell Division of the Dow Chemical Company. The apparatus used to conduct their experiments is shown in Figure 8. Like the work done previously, Hall and Harrisberger's experimentation dealt with arches forming over a horizontal opening. They used both well-rounded sand grains and angular grains, in different sand packs. These sand packs were subjected to confining or vertical stresses of up to 3450 psig. Additionally their tests were run with different fluid saturations. These different initial and flowing saturations along with sand type and stress levels used in their tests are shown in Table 1. These experiments were the first to analyze arching behavior under dynamic conditions.

In defining the mechanism for sand arching, Hall and Harrisberger made two suppositions. First, they stated that arch stability requires some degree of restraint on the grains forming the inner surface of the arch. Secondly, that this stabilized surface permits the remainder of the arch to distribute and support the load over the opening.

From their experimentation, Hall and Harrisberger concluded the following:

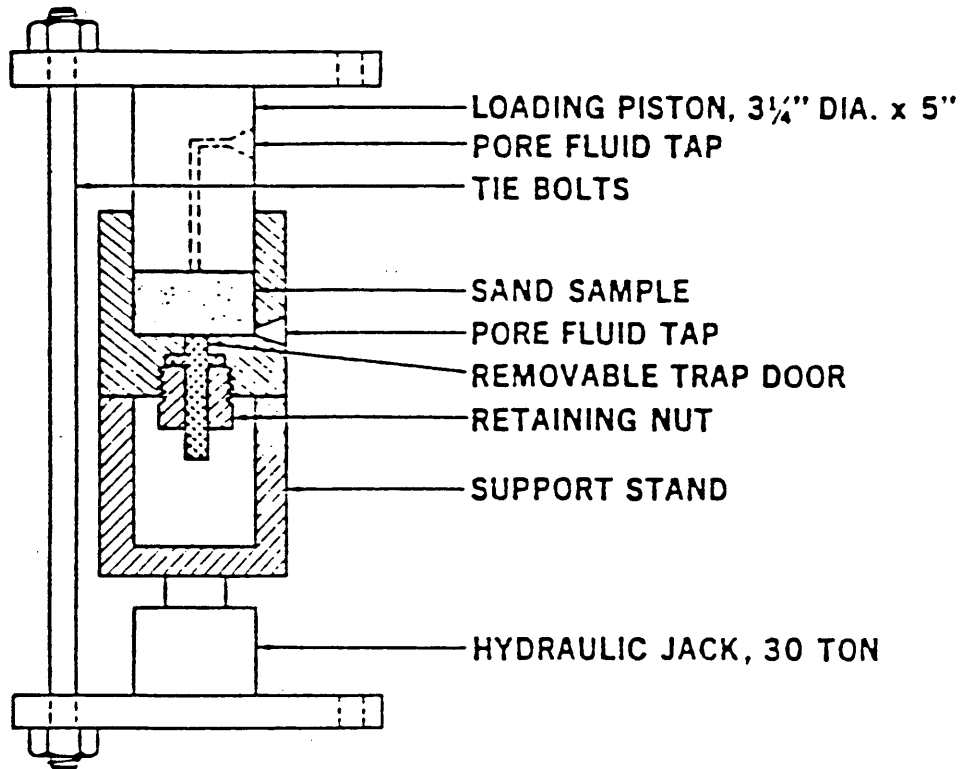


Figure 8

Hall and Harrisberger's Arching Apparatus
 (After Hall and Harrisberger. ⁽¹¹⁾)

Table 1
Hall and Harrisbergers' ⁽¹¹⁾ Data

Test No.	Sand	Step	Initial Saturation	Flow	Load*	Results
1	10-20 Tex. C.Co loose**		Air	None	0	No arch
2	10-20 Tex. C.Co		Air	None	0	Arched: failed when tapped
3	10-20 Tex. C.Co	a.	Air	None	500	Arched
		b.		Air out	500	Held
		c.		Air out faster	500	Failed
4	10-20 Tex. C.Co		Air	None	2,000	Failed: crushed
5	20-40 Ottawa loose**		Air	None	0	No arch
6	20-40 Ottawa		Air	None	0	No arch
7	20-40 Ottawa	a.	Air	None	500	No arch
8	80-100 Ottawa (Same steps)	b.		Air in	500	Arch formed
		c.		Air in slower	500	Failed
		d.		Air in faster	500	Reformed
		e.		Same	2,000	Held
		f.		Air in slower	2,000	Failed
9	20-40 Ottawa		Water-moistened	None	2,000	Arched
10	20-40 Ottawa Oil-wettable-	a.	Kerosene	None	1,000	No arch
		b.		Air in	1,000	Arch formed
		c.		None	1,000	Held
11	20-40 Ottawa	a.	Kerosene at residual water	None	1,000	Arched
		b.		Kerosene out	1,000	Held
		c.		Water out	1,000	Failed
12	20-40 Ottawa Oil-wettable-	a.	Water at residual mineral oil	None	1,000	Arched
		b.		Water out	1,000	Held
		c.		Mineral oil out	1,000	Failed
13	20-40 Ottawa		Water-moistened	None	3,450††	Arch held
14	8-12 Tex. C.Co		Air	None	1,950††	Failed: crushed suddenly
15	8-12 Tex. C.Co		Water-moistened	None	2,100††	Failed stepwise
16	Miocene		Air	None	1,700††	Failed, slow fall-out
17	Miocene		Water-moistened	None	3,450††	Failed, no fall-out

*Average vertical stress, ps.

**Prepared in with no tamping; all other tests were compacted by vibrator.

†Sand treated to be preferentially oil-wettable; all other tests used naturally water-wettable sands.

††Arch formed at 500 ps.; load increased to failure of apparatus limit of 3,450 ps.

- 1) Loosely packed sand will not arch.
- 2) Two conditions must exist for arch stability:
 - a) dilatancy of sand pack, and
 - b) cohesiveness or some other grain restraint.
- 3) Arch failure under load occurs at lower stress levels for angular sands. This is probably due to grain crushing.
- 4) Grain crushing causes arch failure. This crushing of grains will propagate through the sand pack at failure.
- 5) Arches would not form with 100% kerosene saturation.
- 6) Oil-water-sand interfacial tension provided sufficient cohesion to stabilize an arch.
- 7) Arch failure occurred when the wetting phase reached funicular saturation.
- 8) Arches were stable to flow of non-wetting phase at residual saturations of the wetting phase.

In 1972, Nathan Stein and D. W. Hilchie presented a method for estimating the maximum sand-free production rate from a friable sand reservoir, without the use of sand control devices⁽¹²⁾. This method had three underlying assumptions.

- 1) Formation strength can be estimated using density and acoustic log data.
- 2) Formation face can be stabilized by forming sand arches around each perforation.
- 3) Critical production rates from specific sand intervals in a given area can be estimated from one test well, in which reservoir pressure drawdown is increased until sand problems occur.

In their paper, Stein and Hilchie⁽¹²⁾ agreed with Hall and Harrisberger⁽¹¹⁾ that arch formation is contingent on cohesive and frictional resistance forces between sand grains. The cohesive forces were defined as both mineral cementation and capillary forces generated from interstitial water in the hydrocarbon-producing formation. They also stated that arch stability would be greater with depth, due to the greater shear strength of the sand grains.

The procedure brought forth from their work started by logging a test well. From the density and acoustic logs, an estimated value for the dynamic shear modulus of the formation is obtained⁽¹²⁾. Next this test well is produced at increasing rates, until sand problems occur. Using these two pieces of data, new wells are logged and

then their maximum sand-free production rate calculated based on a ratio of dynamic shear moduli set equal to the ratio of reservoir drawdown.

$$\frac{(P_R - P_W)}{(P_R - P_W)_T} = \frac{(E_S)}{(E_S)_T} \quad (1)$$

where P_R = reservoir pressure,
 P_W = wellbore bottom-hole flowing pressure,
 E_S = dynamic shear elastic modulus, and
 T = subscript denoting test well.

D. B. Tippie and C. A. Kohlhaas studied the effect of flowrate on arch stability in a small test cell⁽¹³⁾. This cell (Figure 9) had a 4 inch simulated casing section on which the arches could form. A hole in the plexiglass casing allowed for production of fluids through a simulated perforation. Tippie and Kohlhaas used 20/40 Gopher State frac sand with a mineral spirits/water fluid system. The sand was packed water wet and then desaturated with mineral spirits to residual water. Their arching experiments were run with an overburden pressure of 260 psi.

The vertical casing section of their apparatus added several improvements to arching experimentation as related to the petroleum industry. In the first place, arches occur around perforations in casings, so this simulates

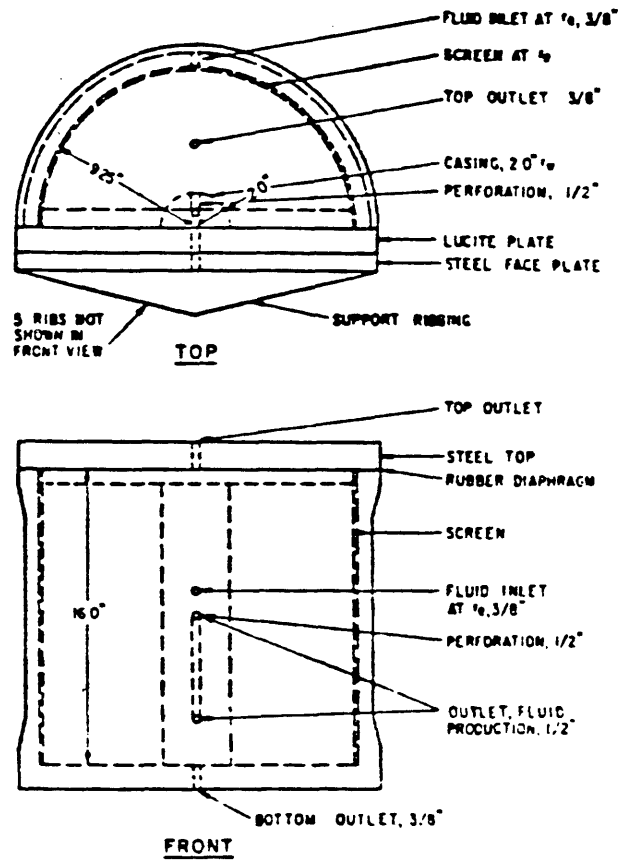


Figure 9

Tippie and Kohlhaas' Arching Apparatus
 (After Tippie and Kohlhaas. ⁽¹³⁾)

real conditions. Experimentation done in the past was done from a soil mechanic view, and thus looked at arching on horizontal surfaces. Tippie and Kohlhaas' cell design studied arches forming on a vertical and rounded surface. Secondly, their cell design made it possible to visually see the cavity/arch shape.

Tippie and Kohlhaas ran tests flowing mineral spirits through the sand pack with a residual water saturation. They increased the rate in a stepping fashion until arch failure occurred. This experimentation brought out the following conclusions:

- 1) Gradual increase of flowrate permits a higher sand-free production rate than sudden increases to high rates.
- 2) Fines migration contributes to arch instability and failure.
- 3) Initial arch size is a function of producing rate. Arch size increases with increasing rate.
- 4) As arch size increases, terminal arch velocity decreases. Thus smaller arches are more stable.
- 5) Arch growth is an increasing function of production rate and initial arch size.

In a second paper published by Tippie and Kohlhaas⁽¹⁴⁾, they also concluded:

- 6) Not only flowrate but flowrate history has an effect on the maximum sand-free production rate for an unconsolidated sand reservoir.
- 7) Flowrates are limited by a maximum possible arch size, which for a well is when arches interfere with one another.

From this last conclusion, they suggest that a spiral perforation pattern is probably the best, and that perforation density is a critical factor.

Stein, Odeh, and Jones⁽¹⁵⁾ presented a method for estimating the maximum sand-free production rate from a friable sand. This work expanded on previous work done by Stein and Hilchie⁽¹²⁾. This new technique accounted for different completion geometries in different wells. The technique is based on the assumption that the maximum pressure gradient at an arch face is proportional to the sand strength. Their technique required the following data:

- 1) Density and sonic log data for all concerned wells.
- 2) Permeability of formations.
- 3) Formation fluid properties.
- 4) Production rate in test well near the critical rate.

This data is plugged into equation 2, to estimate the maximum sand-free production rate for a given well.

$$Q = \frac{Q_T B_T \mu_T k A N (E_S)}{B \mu k_T A_T N_T (E_S)_T} \quad (2)$$

where Q = maximum sand-free flowrate,
 B = formation volume factor,
 μ = viscosity
 k = permeability
 A = area
 N = number of perforations,
 E_S = dynamic shear modulus, and
 T = subscript denoting test well.

Joseph J. Melvan⁽¹⁶⁾ ⁽¹⁸⁾ and Michael P. Cleary⁽¹⁷⁾ ⁽¹⁸⁾ studied the effects of overburden stress and fluid properties on the formation and stability of sand arches respectively. This research was done on the large sand cell (Figure 10) owned by the Petroleum Engineering Department of the Colorado School of Mines. This cell was specifically designed to study the arching phenomenon of sand around perforations in a casing. The cell has an effective sand pack size of 52.75 inches long with a 16 inch diameter. The cell has a 4 inch casing simulated on

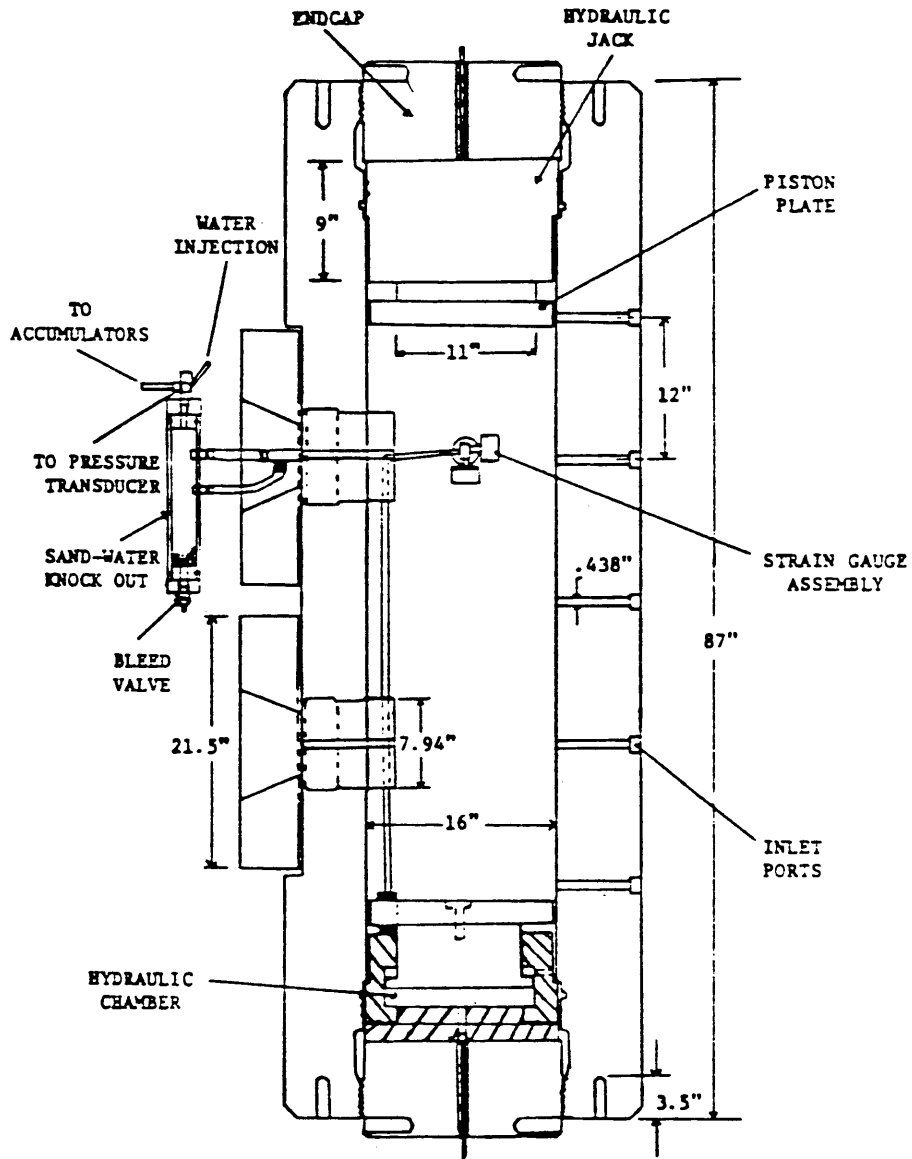


Figure 10

Colorado School of Mines Sand Cell
 (After Melvan.⁽¹⁶⁾)

one side with an outlet hole through the casing. Hydraulic jacks located on each end of the cell are capable of stressing the sand in excess of 3000 psig. Additionally, three strain gauges were mounted inside the cell to measure triaxial stress within the sand pack.

Melvan and Cleary used Gopher State 20/40 frac sand to conduct their experiments. This sand was packed water wet and then desaturated with either mineral spirits or kerosene. Tests were run at vertical stresses of 250, 750, 1500, 2250, and 3000 psig.

Melvan and Cleary made the following conclusions from their work:

- 1) Sand-free production can be obtained from an unconsolidated sand through stable sand arches.
- 2) Arch size is a function of the confining stress. The arch size decreases as the stress increases.
- 3) Arch stability increases with increasing vertical stress.
- 4) Higher sand-free production rates are obtained with a more cohesive sand pack.
- 5) Arches are more stable when the horizontal stress is greater than the vertical stress.

- 6) There are two types of arch instability:
 - a) arch restructuring, and
 - b) final arch failure.
- 7) Only in highly cohesive sand packs (kerosene/water), do arches exhibit both types of instability.
- 8) Arch failure occurs when the dilatant energy of the sand pack is expended.
- 9) Cavity growth is a function of rate and dilatant stress shift.
- 10) Dilatant sand pack behavior was observed above 1100 psig vertical stress.

Donald C. Woods⁽¹⁹⁾ used the same sand cell at the Colorado School of Mines to study the effect that sand size has on the stability of sand arches. Woods ran tests on sand packs consisting of different mixtures of 20/40 and 80/100 mesh frac sands. He used kerosene as his non-wetting, flowing phase. As a result of his work, Woods concluded:

- 1) Sand size has no effect on arch formation and stability.
- 2) Initial cavity formation is a function of cohesive forces, bridging characteristics, and stress redistribution created by arching.

- 3) Cavities result in a negative skin factor.
- 4) The flowrate at arch failure is an increasing function of vertical stress.

Rolf Bratli and Rasmus Risnes⁽²⁰⁾ reported a study of sand arching using 20/40 and 80/100 mesh Ottawa sands. They flowed air and oil vertically through their sand packs in a test cell shown in Figure 11. The confining stress applied to the sand grains was 725 psig.

Bratli and Risnes' observations were similar to previous observations. As with Melvan and Cleary⁽¹⁸⁾, they also identified two types of arch failure. The first being the collapse of the inner shell of the arch during periods of growth and the second the final failure of the arch.

Assuming a spherical model for their arch, and also utilizing the Coulomb failure criterion for a porous material, they developed an arch stability criterion.

In continuing arching research, Gbolahan Lasaki⁽²¹⁾ studied the arching phenomenon using three different natural sands. These sands were reported to contain roughly 1% (by weight) clay and were similar in grain size distribution. Fresh water was used as the residual saturation with kerosene being flowed.

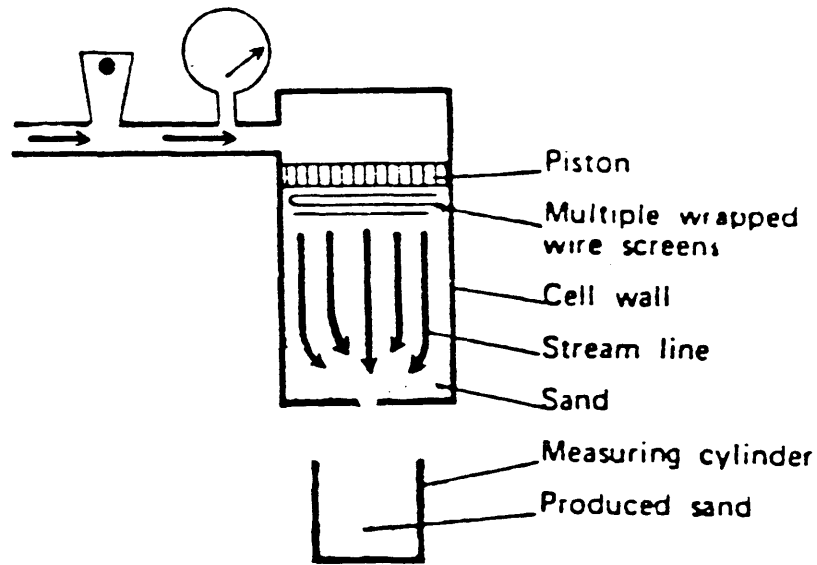


Figure 11

Bratli and Resnes Arching Apparatus
(After Bratli and Resnes. ⁽²⁰⁾)

Based on his results, Lasaki concluded:

- 1) Sand arches form as a result of stress and cohesion in the sand pack.
- 2) Cavities are cleared by fluid drag.
- 3) Cavity size increases with respect to flowrate and pressure drop across the cell.
- 4) Initial cavity size decreases with respect to vertical stress.
- 5) Arch instability is caused by:
 - a) high flowrates,
 - b) high pressure drop across the arch,
 - c) fines accumulating at arch, and
 - d) rate and pressure surges.
- 6) Sand arches will not form with a funicular water saturation.

The most recent experimentation performed on arching was that done by John H. Benton⁽²²⁾ at the Colorado School of Mines. Benton duplicated much of the work done by Melvan⁽¹⁶⁾ using smaller more sensitive strain gauges, that occupied roughly 1/3000 the volume that Melvan's gauges occupied. Benton, in duplicating the previous experimentation used Gopher State 20/40 frac sand and mineral spirits. The stress levels used, coincide with those used in Melvan's⁽¹⁶⁾ research (750, 1500, 2250, and

3000 psig). Benton found these new gauges to be far superior to the old gauges. Because of the reduction in size, the gauges made less of an effect on the stress distribution and flow path within the cell. Also since the new gauges were so much smaller, they could be placed directly behind the sand arches, in order to monitor the arches more closely. Additionally, Benton concluded:

- 1) Arches are effected by flowrate, stress, effective permeability, and cohesion.
 - a) Arch stability increases with increasing vertical stress.
 - b) For a constant vertical stress, arch stability increases with increasing horizontal stress.
 - c) Cavity growth is a function of production rate.
- 2) At higher stress levels, more energy is expended at arch failure.
- 3) Dilatant sand behavior occurs during arch growth.
- 4) Arch permeability decreased with increasing overburden and with the migration of fines.

Rock Mechanics

The relation between stress and strain for an isotropic elastic solid subjected to stress is defined by Hooke's law⁽²³⁾. A solid subjected to a one-dimensional stress will experience a unit elongation or compression in this principle direction. Hooke's law relates the strain, caused by the elongation, and the one-dimensional stress as follows: (23)

$$\epsilon_x = \frac{\sigma_x}{E} \quad (3)$$

where ϵ_x = strain along the principle axis,
 σ_x = principle stress, and
 E = Young's modulus of elasticity.

This one-dimensional stress will also produce strain components in the other two principle axes. These strain components are related to the principle stress by the following equations: (23)

$$\begin{aligned} \epsilon_y &= -\nu \frac{\sigma_x}{E} \\ \epsilon_z &= -\nu \frac{\sigma_x}{E} \end{aligned} \quad (4)$$

where ν = Poisson's ratio.

If this same element is subjected to stress in all three principle axes, the axial strains can be defined as: (23)

$$\begin{aligned}\epsilon_x &= \frac{1}{E} [\sigma_x - \nu (\sigma_y + \sigma_z)] \\ \epsilon_y &= \frac{1}{E} [\sigma_y - \nu (\sigma_x + \sigma_z)] \\ \epsilon_z &= \frac{1}{E} [\sigma_z - \nu (\sigma_x + \sigma_y)]\end{aligned}\quad (5)$$

These equations are a result of superimposing the partial effects of each stress as defined by equations (3) and (4).

Maurice Biot⁽²⁴⁾ expanded on this three-dimensional application of Hooke's law, to include a pore pressure term. Several assumptions went into his mathematical model: (24)

- 1) Isotropic material,
- 2) Reversible stress-strain relations under equilibrium conditions,
- 3) Linear stress-strain relations,
- 4) Small strains,
- 5) Incompressible water in pores,
- 6) Water may contain air bubbles, and
- 7) Water flows according to Darcy's law.

The relation between axial stress and strain including a pore pressure term is: (24)

$$\epsilon_x = \frac{1}{E} [\sigma_x - \nu (\sigma_y + \sigma_z)] + \frac{p}{3H} \quad (6)$$

where p = pore pressure of the fluid, and
 H = proportionality constant.

This proportionality constant H is a measure of soil compressibility for a change in pore pressure. The positive sign in front of the pore pressure term is used because an increase in pore pressure will cause an expansion of the solid. This expansion will cause an increase in the strain on the solid.

Later work by Geertsma⁽²⁵⁾ defined this proportionality constant H in terms of rock compressibilities.

$$H = \frac{(1-\beta)^2}{(1-\phi-\beta)c_r + \phi c_1} + \frac{\beta}{c_r} + \frac{4}{3} G_b \quad (7)$$

where $\beta = c_r/c_b$

c_r = compressibility of rock matrix,

c_b = compressibility of the rock bulk material,

c_1 = compressibility of the pore fluid,

G_b = the shear modulus of the rock bulk material, and

ϕ = porosity.

Solving equation (6) for the principle stress yields:

$$\sigma_x = E\varepsilon_x + \nu (\sigma_y + \sigma_z) - \frac{pE}{3H} \quad (8)$$

Relating this equation to the arching phenomenon of sand, an increase in pore pressure will cause a decrease in stress. It has been shown that arch stability is an increasing function of grain-to-grain stress (22). Thus since pore pressure decreases stress, increased pore pressure should make a sand arch less stable.

Similarly, this inverse function between pore pressure and arch stability can be rationalized using a net effective stress argument. Net effective stress is defined by the following equation: (2)

$$S = P_{ob} - P_p \quad (9)$$

where S = net effective stress,
 P_{ob} = overburden stress, and
 P_p = pore fluid pressure.

Thus fluid pressure acts in a way to reduce the net effective stress on a sand pack. This lower stress level will accommodate a less stable arch.

Equipment Design

Sand Cell

The sand cell is an 87 inch long cylindrical steel cell (Figure 12) manufactured by National Forge Company of Pennsylvania. The cell has an outside diameter (O.D.) of 30 inches and an inside diameter (I.D.) of 16 inches. The cell is constructed with removable hydraulic jacks and end caps on both the top and bottom. With both jacks in place, the remaining internal sand pack length is 52.75 inches.

The cell is equipped with two 8 inch plexiglass ports, each held in place by 21-1/2 inch diameter by 5 inch thick steel face plates. The face plates are mounted to the cell with twelve 1-3/4 inch bolts. Opposite the ports are five 1/2 inch inlet ports. These ports are spaced 12 inches apart. Additionally, there are four 3/4 inch access ports, located on the sides of the cell. These ports are used for the desaturation line, drain line, and for an air bleed line. Finally, the cell is equipped with six instrument access ports. These are located in vertical sets of three, 45° on each side of the ports. The only one being used presently, is for the three triaxially mounted strain gauges located in the middle of the cell behind the producing port.

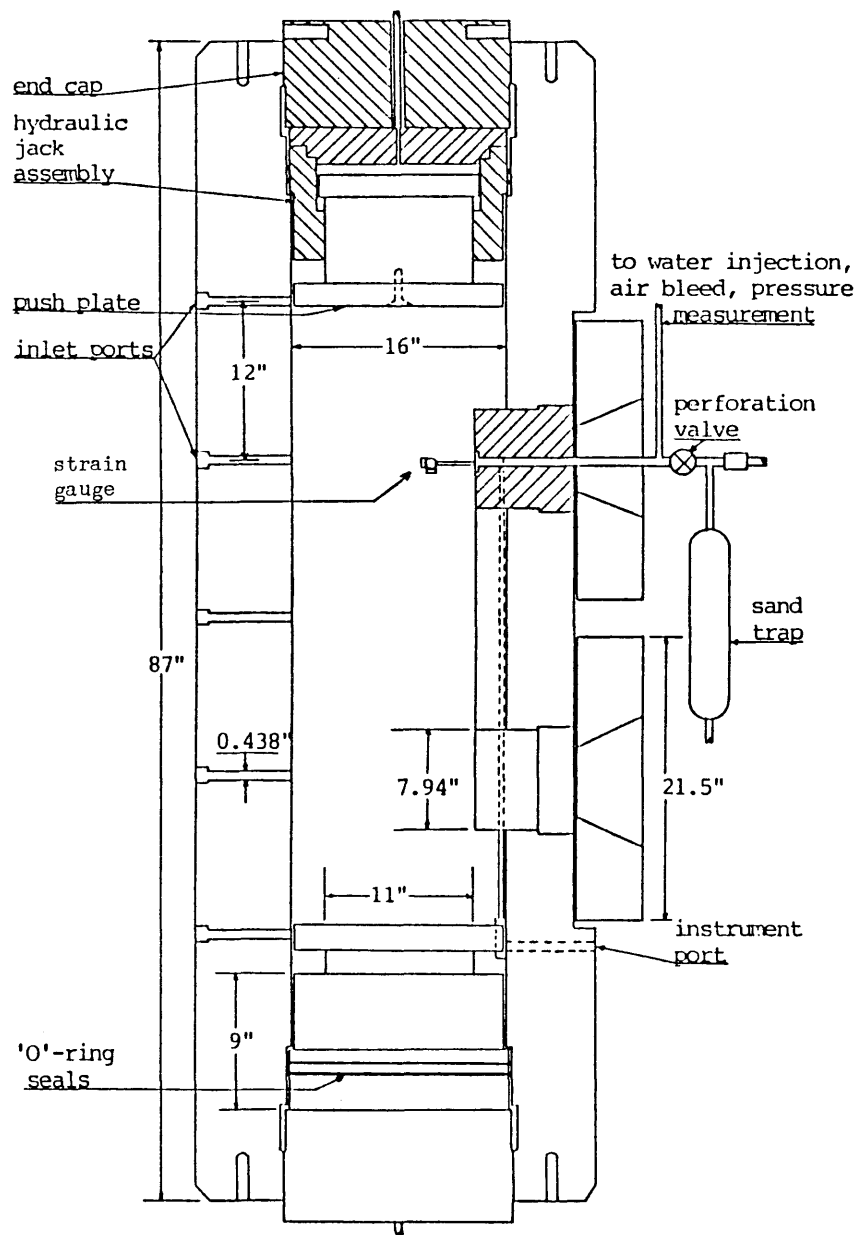


Figure 12
Colorado School of Mines Sand Cell Cross-Section
(After Benton,⁽²²⁾)

The cell is rated to 10,000 psig by the manufacturing company, but has only been hydrostatically tested to 3000 psig with the ports in place. All lines and valves leading to and from the cell likewise have been tested to or rated well above 3000 psig.

Plexiglass Ports

The plexiglass ports (Figure 13) set into the cell, were machined to specification by Plastics Design and Manufacturing of Denver, Colorado. The diameter of the port is 7-15/16 inches when machined, and then expands to 8 inches after being placed in the cell and stressed. This 1/16 inch difference allows for an easier installation of the port. When the port has expanded, due to multiple cycles of stressing the sand against the face of the port, it becomes harder to remove. It requires a hydraulic pump within the cell to push the port back out, whereas it will initially just slide in. An "O"-ring around the port seals the cell.

The inside of the port is machined to simulate a 4 inch casing running longitudinally up the side of the cell. This simulated casing section extends from the inside arc of the port, which matches the inside diameter of the cell. These arcs are illustrated in Figure 13.

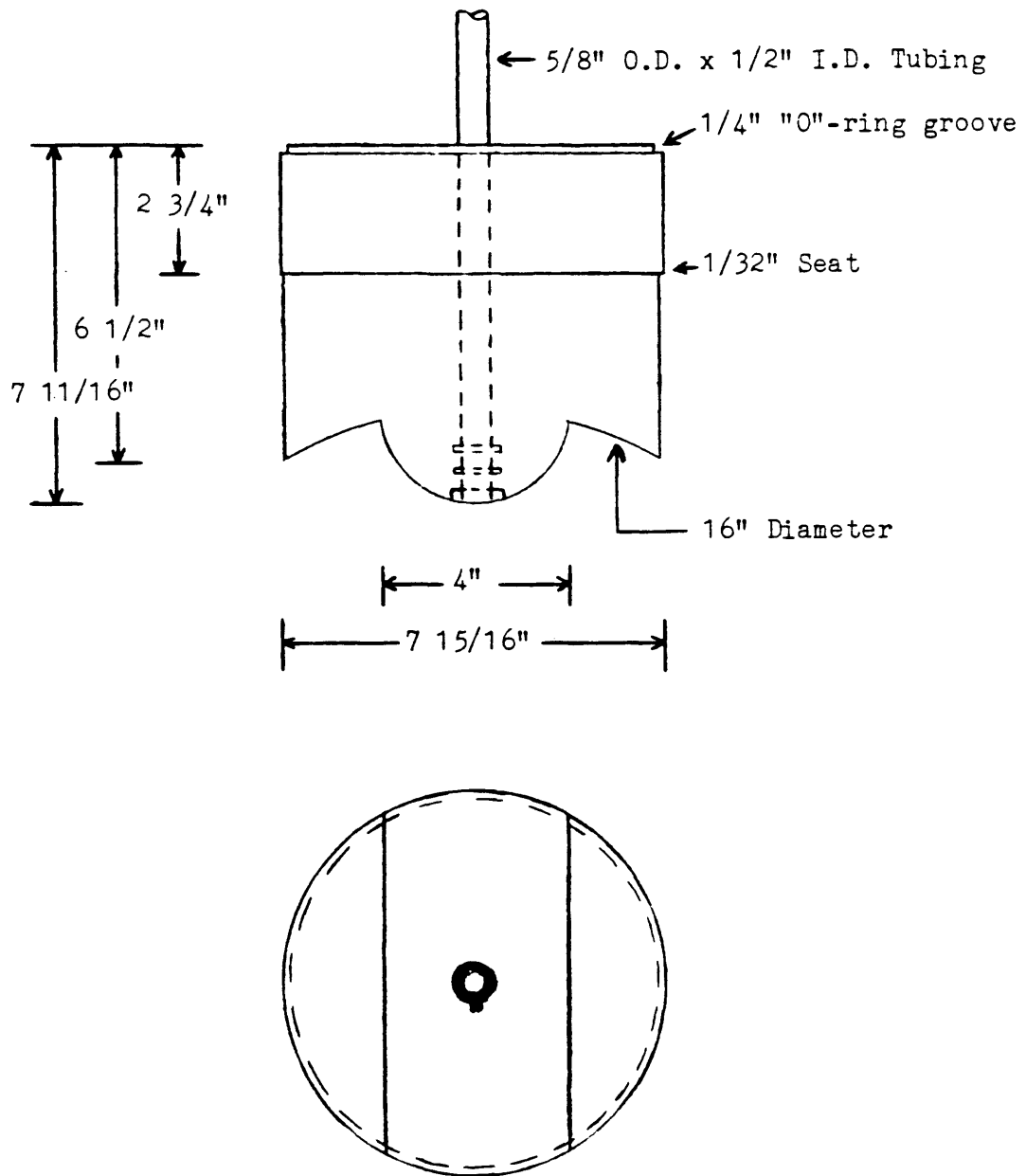


Figure 13

Plexiglass Port Cross-Section

The casing sections of the two ports are connected by another plexiglass piece machined with the same 4 inch diameter.

Of the two ports on the cell, one is left blank, while the other has been drilled and a piece of tubing placed in the hole to simulate a perforation in the casing. This port has a 5/8 inch diameter hole drilled through it with two "O"-ring grooves cut into the hole. This hole is sleeved with a 5/8 inch O.D. x 1/2 inch I.D. x 15 inch long piece of stainless steel tubing. The tubing is shouldered with a 3/4 inch O.D. x 1/2 inch I.D. x 3/8 inch thick washer on the simulated casing end of the port. This shoulder fits into a matching pocket cut into the port. Prior to inserting the tubing, two 5/8 inch I.D. Viton "O"-rings are placed into their cut grooves (Figure 13). These, along with the shouldered washer, seal the inside of the cell.

Hydraulic Jacks

The sand pack within the cell, is stressed using two hydraulic jacks. These jacks are capable of applying a stress of 5000 psig to the ends of the sand pack. This is more than sufficient to apply a grain-to-grain stress of 3000 psig in the middle of the sand pack.

The jacks (Figure 12) are constructed of cylindrically cast steel with an O.D. of 16.28 inches and a length of 9 inches. The internal piston has an O.D. of 12 inches and has a 3.5 inch stroke length. The piston is connected to an 11 inch diameter ram, which is in turn connected to a push plate of dimensions 16 inch O.D. x 1.6 inches thick. The ram and push plate are connected with a 1/2 inch allen head bolt. The push plate is used in order to distribute the force of the ram over the entire area of the sand pack.

A Sprague 150:1 pneumatic/hydraulic pump is used to pressure up and thus extend the jacks. The hydraulic lines leading to both jacks are equipped with check valves and bleed valves to minimize hydraulic pressure leak off during tests. Also incorporated in the hydraulic system (Figure 14), is a 9500 psig relief valve to eliminate the chance of over-pressurizing the system.

Strain Gauges

The grain-to-grain stress within the sand pack is measured by three strain gauges mounted triaxially (Figure 15) in the middle of the cell. As illustrated in Figure 16 the gauges are mounted in the center of the cell, directly behind the producing port. One gauge is in the

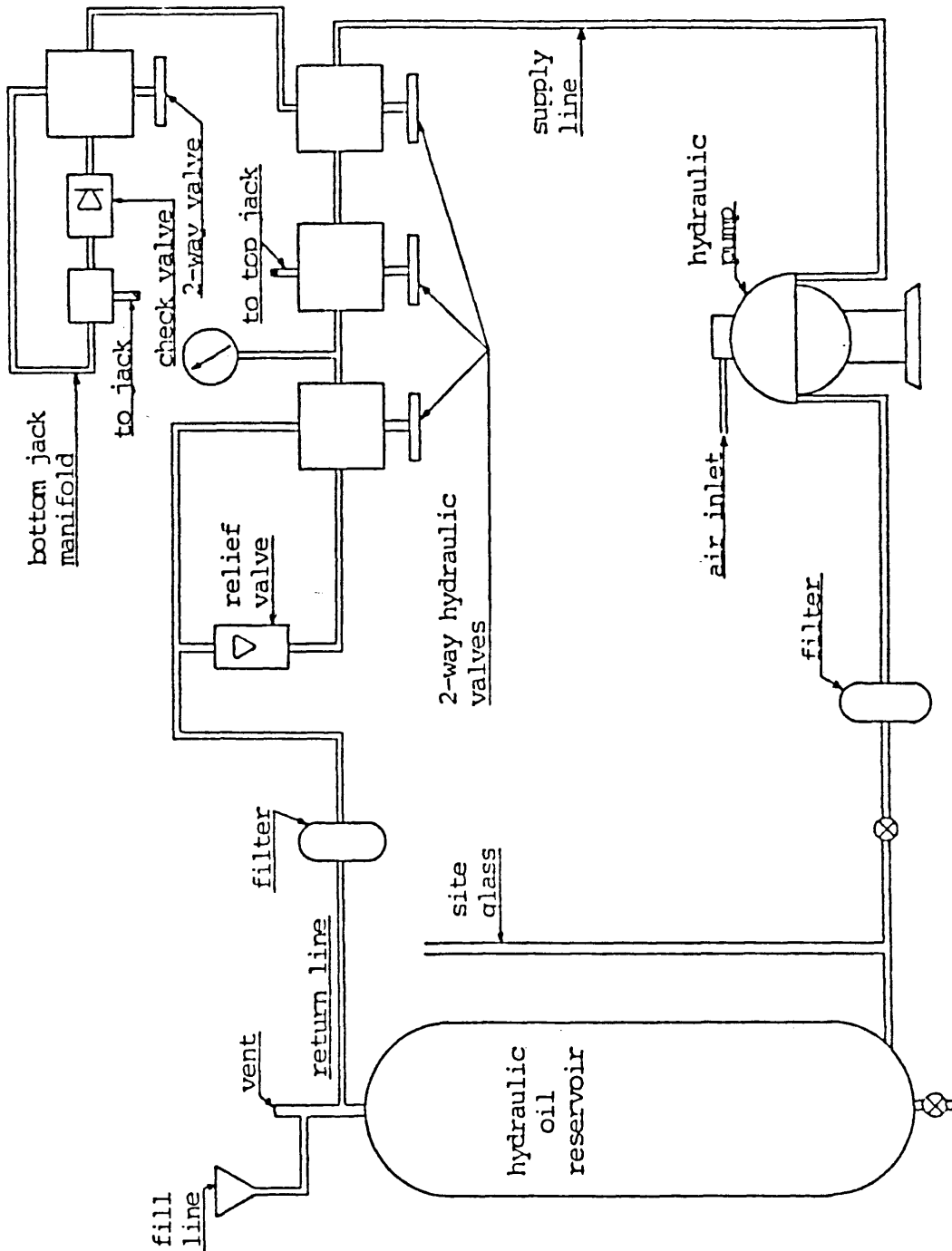


Figure 14
Hydraulic Jack System Diagram (After Benton. (22))

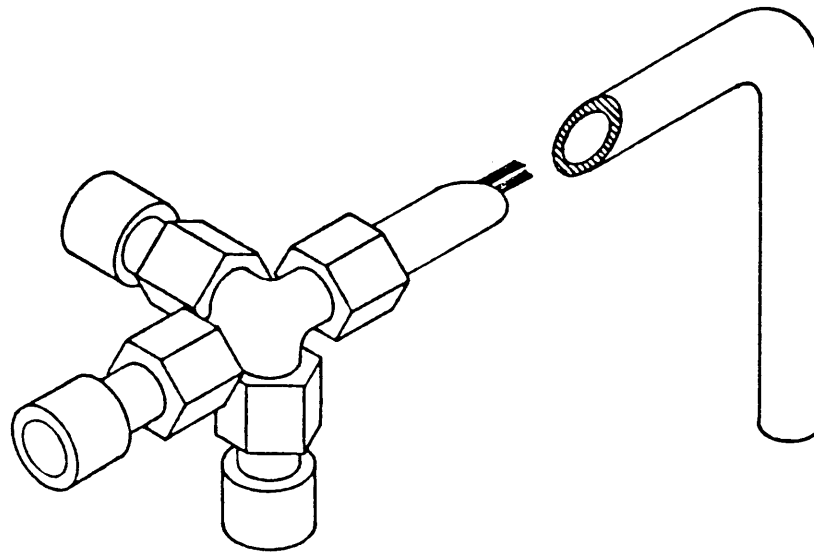


Figure 15
Triaxial Mounting of Strain Gauges
(After Benton. (22))

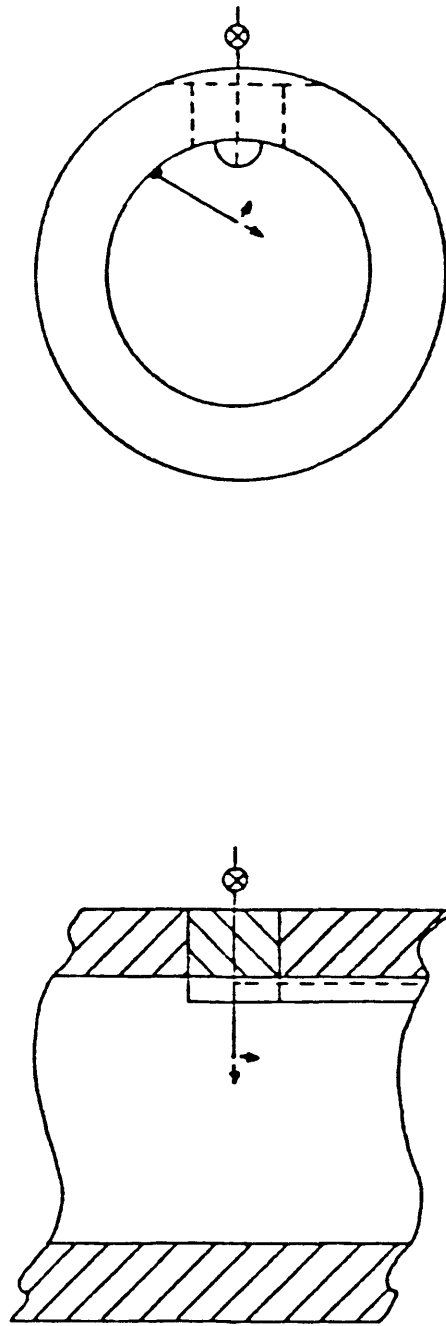


Figure 16
Gauge Positioning, Cross-Sectional View
(After Benton. (22))

vertical plane facing down, and the other two in the horizontal plane facing 45° (Gauge G) and 135° (Gauge H) away from the port.

The strain gauges are welded steel diaphragm type pressure transducers manufactured by Sencotec, Inc. out of Columbus, Ohio. The surface of the gauge measures $1/4$ inch in diameter and its housed measurements are $3/8$ inch O.D. by $5/16$ inch long with a $1/4$ inch O.D. by $5/8$ inch long stainless steel stem. This $1/4$ inch stem allows the gauge to be connected with $1/4$ inch Swagelock fittings (Figure 15). The wires from the three gauges are carried within the Swagelock assembly and $3/8$ inch tubing and exit the sand cell through a lower instrument port.

The gauges are designed to measure stress electrically due to the deflection of the metal diaphragm. In the sand cell this deflection is caused by roughly 60-70 sand grains on the diaphragm surface and not a uniform pressure as they were designed to measure. Consequently the gauges had to be calibrated using the test cell shown in Figure 17.

For calibration, the gauges were mounted one at a time in the test cell on top of a $1/2$ inch steel plate and then packed with wet 20/40 frac sand. A rubber disk was placed on top of the sand and then a 4 inch steel piston

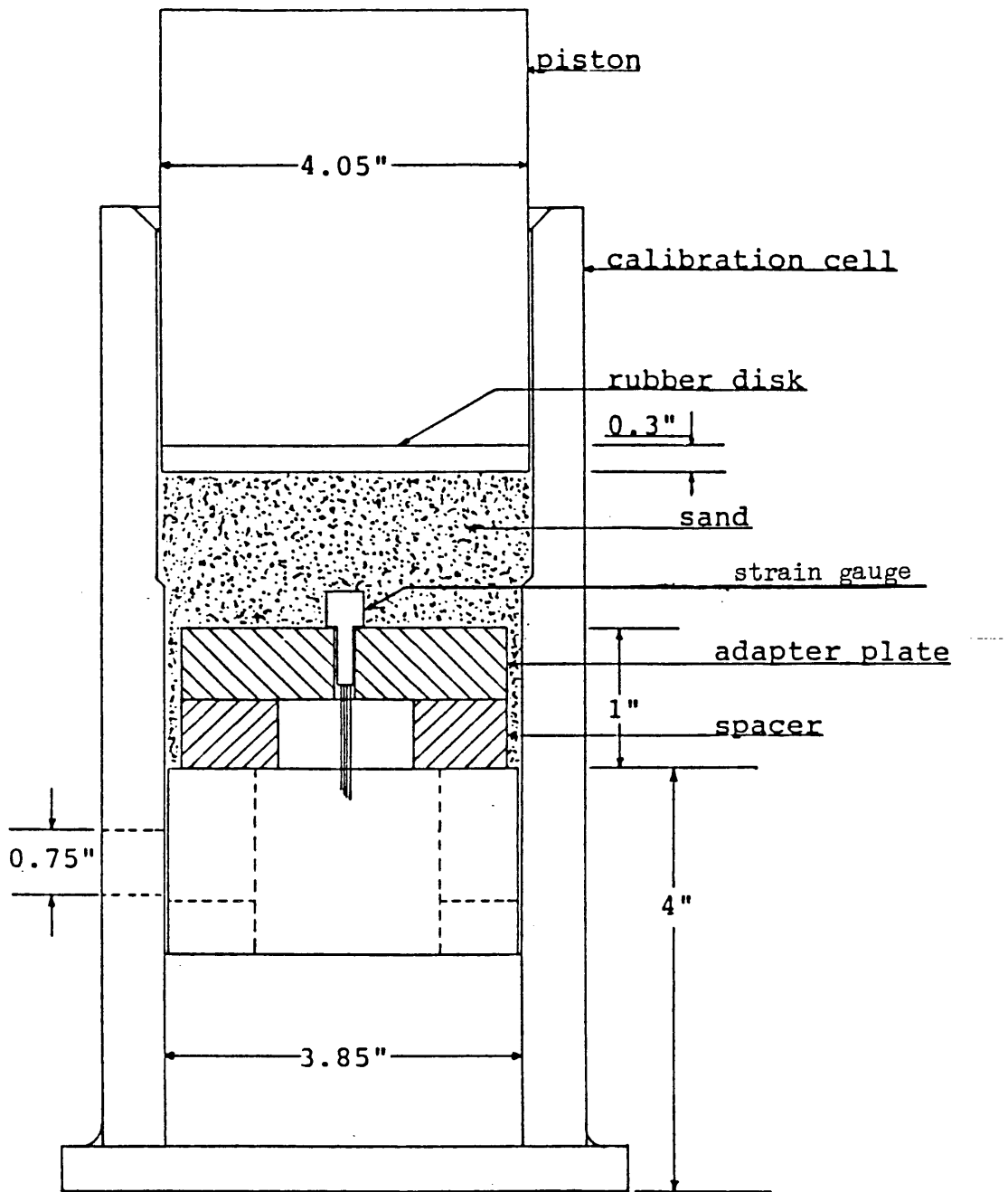


Figure 17

Gauge Calibration Test Cell
(After Benton. (22))

placed on top. The entire cell was then set on top of a hydraulic jack and placed in a retaining vise. The sand pack was then stressed repeatedly to 4000 psig as measured by gauge on the hydraulic line, and the gauge deflection was recorded on a Honeywell Electronik 196 chart recorder. After numerous cycles to 4000 psig to ensure a stabilized sand pack, calibration measurements were taken in 500 psig increments up to 3000 psig. These calibrations were run on each gauge, with sand packs varying from 1/4 inch to 3/4 inch over the strain gauge surface. The resulting calibration curves are shown as Figures 18, 19, and 20.

Flow Equipment

A schematic of the flow lines and equipment is shown in Figure 21. A 3000 psig Cat pump is used to pump mineral spirits throughout the system. This low rate, high pressure pump supplied sufficient rate to form and break down the sand arches at fluid pressures up to 900 psig. Above 900 psig, the pump rate was too unstable to achieve constant rates and thus data was not run above this fluid pressure. This Cat pump replaced the Wallace and Tiernan pump used in previous experimentation⁽²²⁾, which was not designed to handle fluid pressure. In addition to the

STRAIN GAUGE CALIBRATION

Gauge #58899 (Track F)

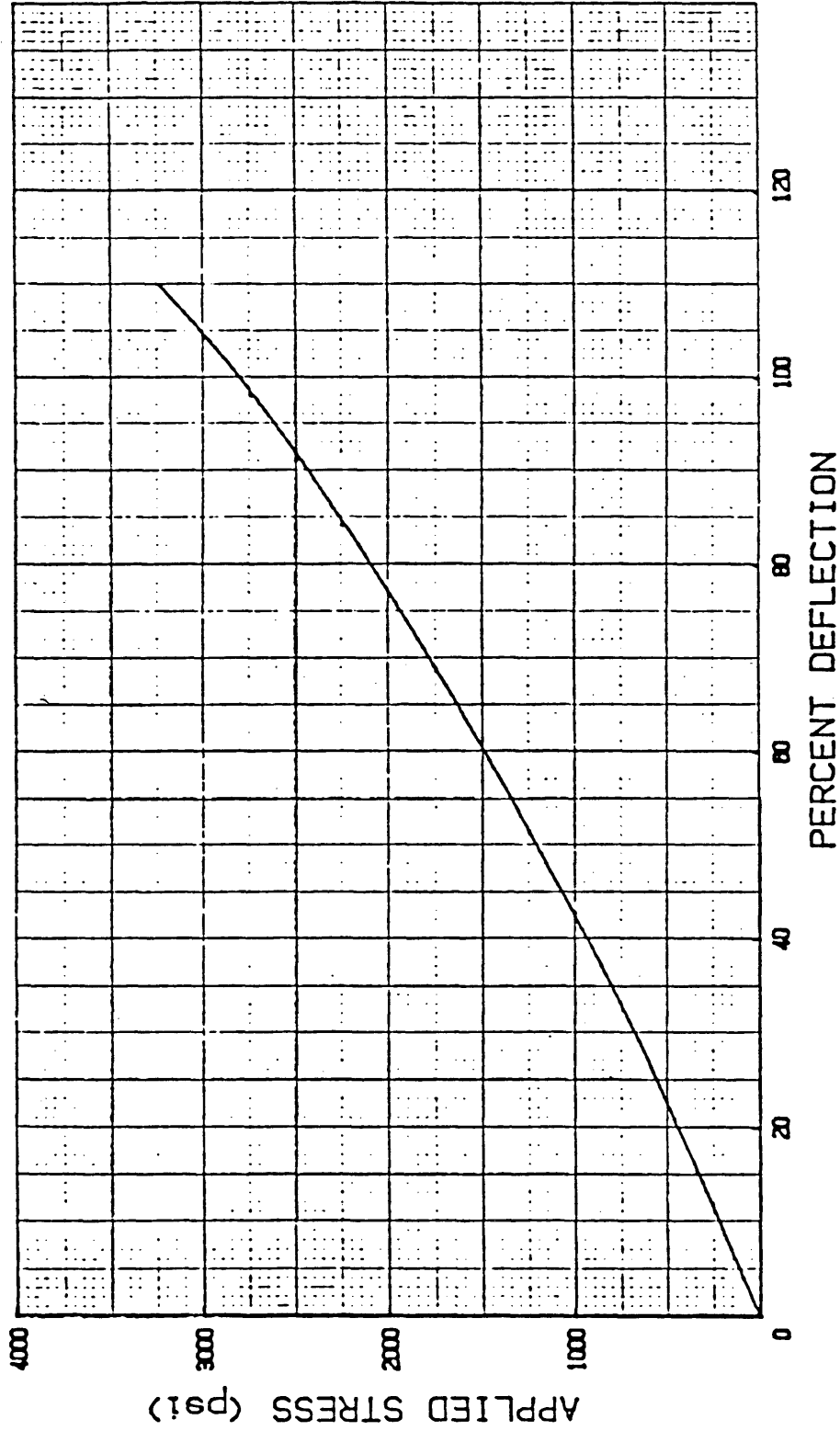


Figure 18 Strain Gauge Calibration Curves (After Benton. (22))

STRAIN GAUGE CALIBRATION

Gauge #58896 (Track G)

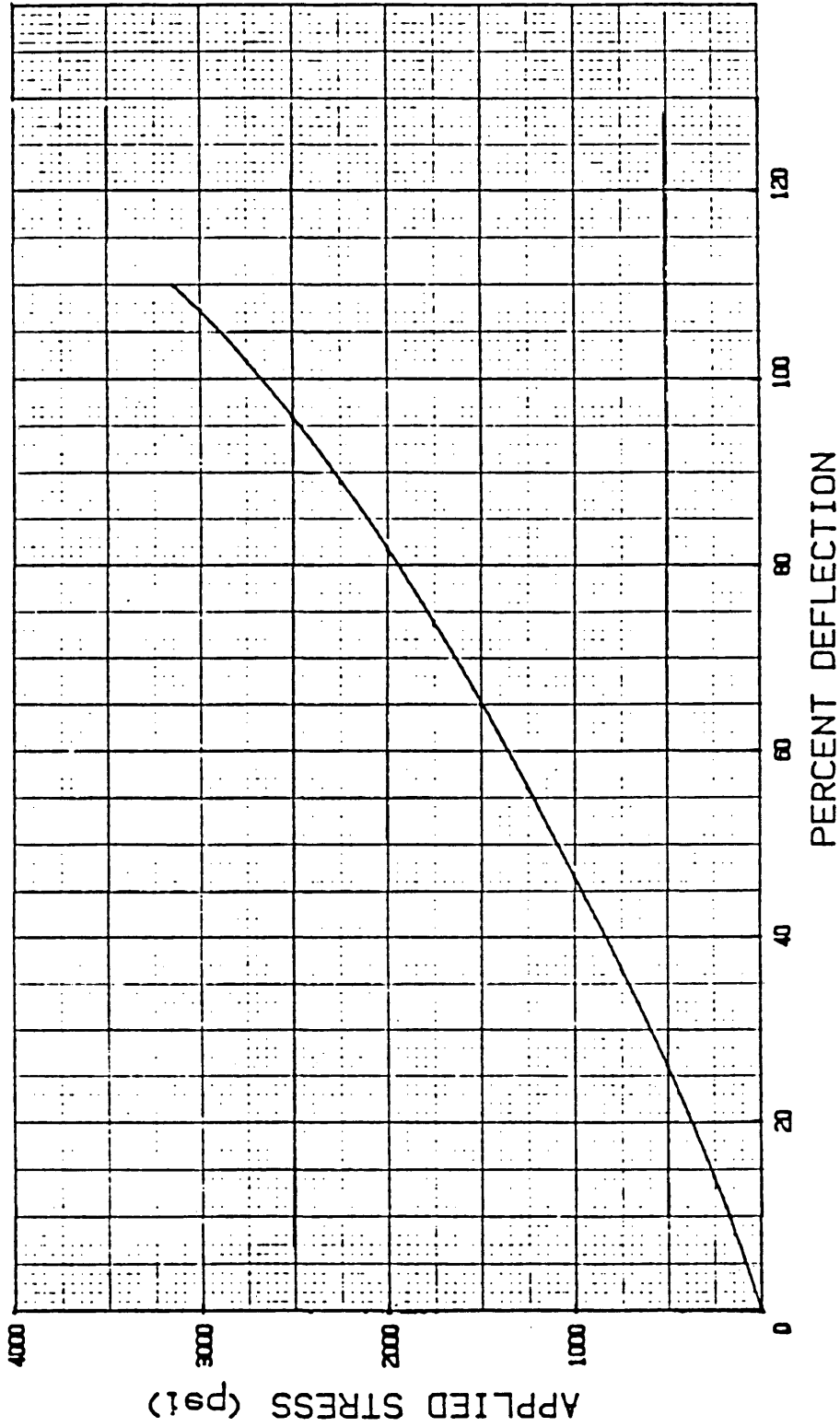


Figure 19 Strain Gauge Calibration Curve (After Benton. (22))

STRAIN GAUGE CALIBRATION

Gauge #58898 (Track H)

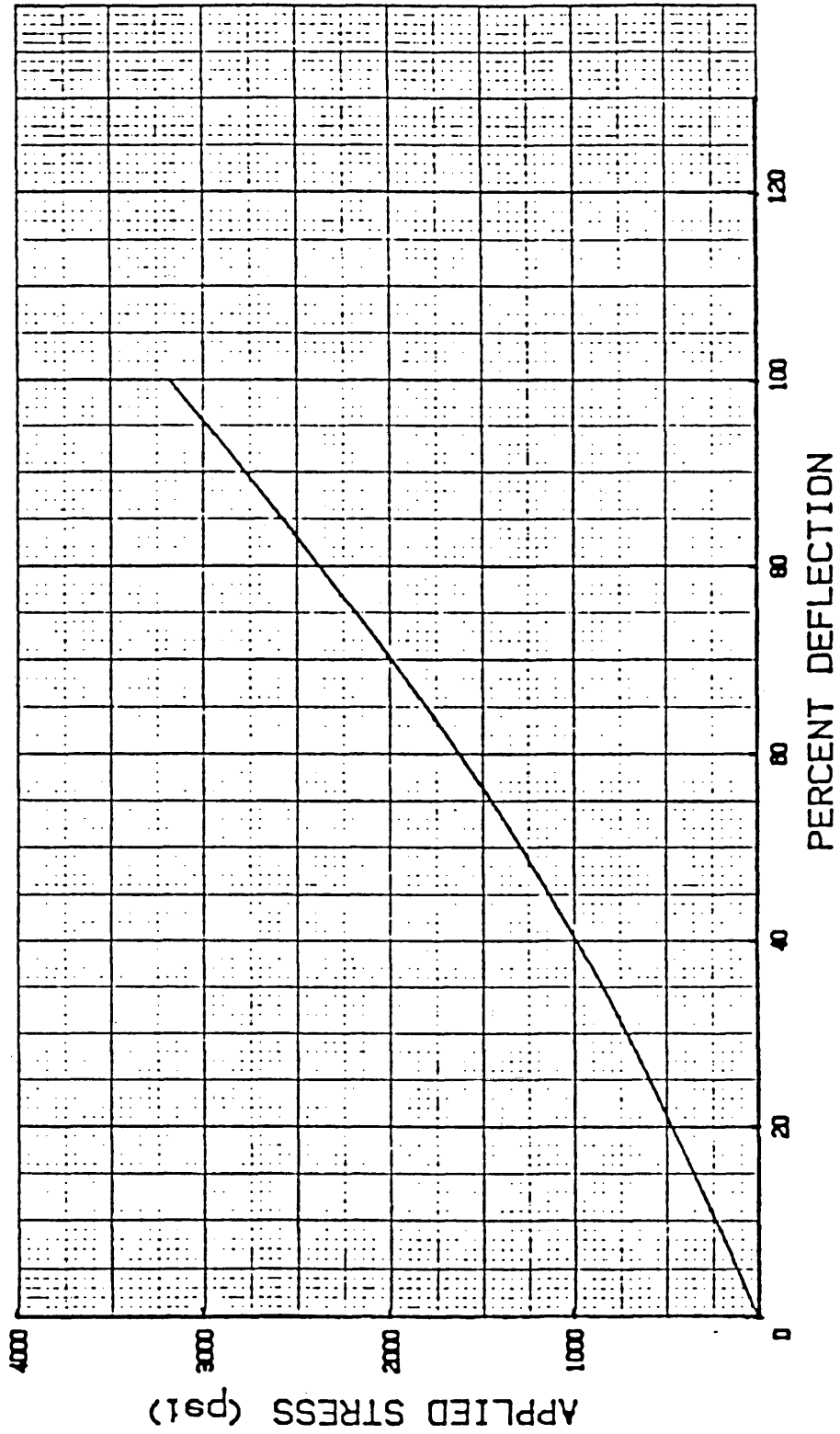


Figure 20 Strain Gauge Calibration Curve (After Benton. (22))

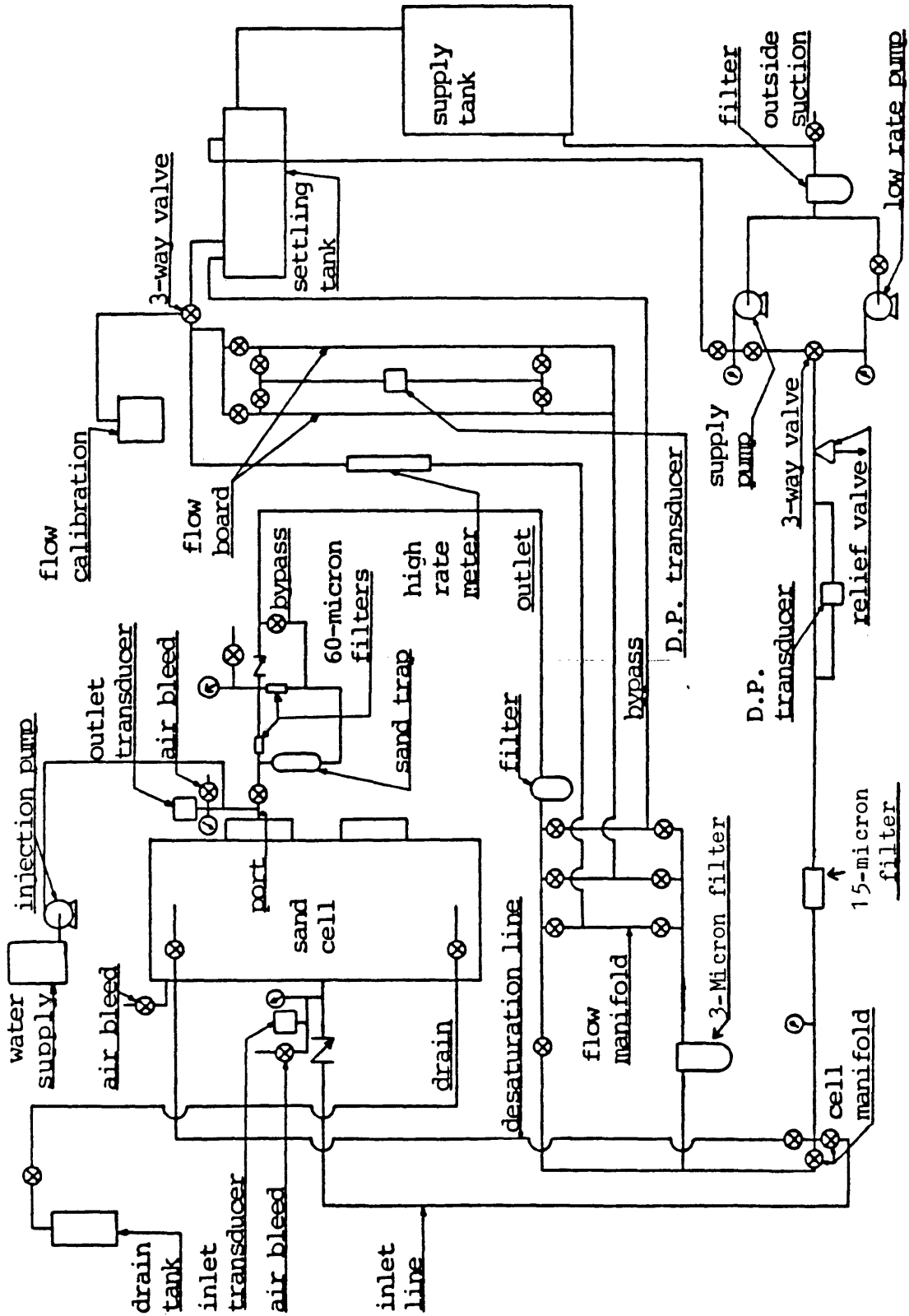


Figure 21
Flow Equipment Schematic (After Benton (22))

high pressure Cat pump, a progressive-cavity Moyno pump was used to transfer mineral spirits from supply drums to the holding tanks.

The flow lines consist of stainless steel tubing rated to well over 3000 psig. All valves and other apparatus connected to the flow line have been hydraulically tested to 3000 psig. With the exception of the few following changes, the flow set-up is the same as was used in previous tests run by Mr. John Benton⁽²²⁾. A check valve was added to the cell inlet in order to prevent sand from flowing back into the line prior to and after running experiments. The flow-rater and surge dampeners were removed from the flow system due to their low pressure rating. A 15-micron filter was installed where the dampeners had been, in order to filter out fines entering the cell. Also the 60-micron filters on the sand trap were replaced with better Nupro filters that use replaceable filter cartridges. 60-micron cartridges were used.

The flowrates run through the cell, were measured using a graduated cylinder and stopwatch. This was done by diverting flow just prior to entering the settling tank, and collecting the flow in the cylinder.

Pressure Transducers

Pressure transducers were mounted on both the inlet and outlet of the cell, in order to monitor fluid pore pressure as well as the pressure drop across the cell. The instruments used were 3000 psig transducers manufactured by Data Instruments Inc., out of Lexington, MA. The signals put out by the pressure transducers were recorded on a Honeywell Elektronik 196 chart recorder.

Water Injection System

The water injection system is illustrated on the flow schematic (Figure 21). This system utilizes a high pressure Wallace and Tiernan metering pump to inject 200 cc of water into the port side of the cell, just prior to running a test. This water re-establishes the pendular water saturation necessary for arch stabilization. The water system consists of the pump, graduated water reservoir, and the necessary lines and fittings to connect the system to the outlet side of the cell, just upstream the outlet valve.

Experimental Procedure

With the cell secured in an upside-down position (ports facing North), the inside of the cell is cleaned and the strain gauge assembly installed. Using the electric hoist, the bottom jack is lowered into place, making sure that the notch in the push plate slips over the strain gauge assembly. The jack must be cleaned initially and well greased. Again using the hoist, the end cap is set into place and then screwed down using 1 inch steel bars.

Using the floor winches, the cell is then turned to its upright position and secured. Once secured in the upright position, the inlet and outlet lines as well as the desaturation and drain line are hooked up. After attaching all lines, the cell is ready to be packed with sand.

Before the sand is placed into the cell, it is washed to remove the fines and any other impurities. The washing is done with a high velocity venture type nozzle on the end of a water hose. Using this washing technique, it was found that roughly four gallons of sand could be washed at a time in a five gallon bucket. The water has sufficient velocity to agitate the sand and float off the fines.

This washed sand is then placed into the cell along with enough free water to cover the sand. In order to get a tighter sand pack, a 1/2 inch galvanized pipe is used to tamp each bucket of sand that is placed into the cell. This cleaning and packing is continued until the sand reaches a level 5-7/8 inches below the jack seat. At this point the sand is leveled and the excess water removed. With the cell packed with sand, the top jack and end cap are installed.

The cell is then desaturated with mineral spirits. This process takes four to five hours, with the pump set at its minimum rate (3.0 BPD). The desaturation is complete when the draining water cut is less than one percent. After the desaturation, the cell is left shut-in overnight and then desaturated again the following morning. This second desaturation removes more of the water that was bypassed due to fingering, and had migrated to the bottom of the cell overnight.

Prior to running a test, the sand pack is cycled to 3000 psig to build the grain-to-grain stress in the middle of the cell. This is accomplished by pressuring up the two hydraulic jacks, and thus extend the rams and push plates against the sand pack. After fifteen minutes the pressure is bled off. Three cycles to 3000 psig are

made for each test, and then two more to the stress level that the test is being run at (3000, 2250, 1500, or 750 psig).

After the sand has been stressed the final time, and after all flow lines have been filled, water is injected into the port side of the cell. 200 cc of water is used to re-establish the pendular water saturation in the area of the simulated casing. After water injection, the pump is turned on and pressure is built up in the cell and flow lines. The cell is shut-in at the desired fluid pressure (900, 450, or 200 psig), and the flow board is then pressured up by partially closing the needle valve on the flow board.

To initiate the test, flow is diverted to the inlet of the cell and the outlet valve is opened. The needle valve on the flow board is used to adjust the fluid pressure to the desired level. Generally an arch will form (evidenced by the cavity) upon initial flow through the cell. Once the flowrate and pressure stabilize, a rate is taken and the chart readings recorded. These readings consist of inlet and outlet pressure and the three stress readings. Also visual observations such as the cavity size are noted.

At this time the rate is increased by increasing the pump speed. Data is recorded and rates increased until the arch fails. Arch failure for this set of experiments is defined as a significant drop in the vertical stress as well as in one of the horizontal stresses (σ_{H2}), and either complete flow of sand or growth of the cavity above the port.

If the cavity grows above the port and a significant pressure drop occurs, this is called the failure point because any further data would have different arch conditions. The pump rate is turned up one turn at a time until the cavity reaches a length of roughly 2 inches, and then turned up by half turns until failure.

After recording the data at the failure point, the fluid and hydraulic pressure are bled off the cell. By pumping fluid into the cell with all outlet lines closed, the jacks can be pumped out to their original position. At this point the fluid pressure is bled off again and the top end cap and jack removed.

To prepare for the next test, the sand pack has to be dug out to a level below the port and then re-packed. Also the outlet sand trap has to be cleaned out.

A detailed outline of the experimental procedure is listed in the appendix.

Discussion of Results

Data Collection

The sand used for this experiment was 20/40 mesh Gopher State frac sand. This sand yields a sand pack with 34 percent porosity and an absolute permeability of roughly 50 darcies. These parameters were measured by flowing water through tubular sand packs of various lengths. The hydrocarbon fluid used to saturate the sand was mineral spirits with properties shown in Table 2. Data was taken at three different fluid pressure levels. These pressure levels were 900, 450, and 200 psig. At each of these pressure levels, tests were run at vertical stresses of 3000, 2250, 1500, and 750 psig. These stress levels were chosen in hopes of comparing the data to that previously done by John Benton(22). His experimentation was done at these stress levels, and with essentially atmospheric fluid pressure. The use of 20/40 frac sand and mineral spirits also duplicate his work.

As a result of Benton's work(22), he concluded that a given pack of sand should not be used more than six times. He felt that the sand pack deteriorated over these runs and that the build-up of fines within the sand caused

Table 2

Fluid Properties of Mineral Spirits

Specific Gravity	0.796 @ 60°F
	0.790 @ 72°F
	0.787 @ 86°F
API Gravity	46.28 @ 60°F
	47.65 @ 72°F
	48.33 @ 86°F
Saybolt Viscosity	0.334 cp @ 72°F
	0.175 cp @ 86°F

erroneous results in subsequent tests. Consequently, five sand packs were used to run twenty-five tests, with no more than six tests being run on a given pack. For the fourth sand pack, on which six tests were run on, sand samples were taken after each run in order to investigate Benton's theory about fines buildup. This sand analysis will be discussed later in this section.

The first three sand packs were used to collect data at 900 and 450 psig fluid pressure. This raw laboratory data, along with the data from the other packs, is shown in Table 3. Using these three sand packs, a total of seventeen tests were run. Of these seventeen tests, two were aborted for the following reasons. Test #16 was run at a fluid pressure of 900 psig and at a stress level of 750 psig. Upon initiating flow through the cell, a very wide arch formed and stabilized as usual. This wide arch grew vertically as the flowrate was increased. Eventually the flowrate was increased to the point that the fluid pressure could not be held down to 900 psig so the test had to be abandoned. Although the cavity did extend above the top of the port at a lower flowrate, this could not be defined as a typical failure because no stress drop accompanied the cavity growth.

Table 3
Raw Laboratory Data

Test #	Inlet Pressure (psig)	Outlet Pressure (psig)	Flowrate (BPD)	Measured Stress			Cavity Length (inches)	Comments
				σ_v (F) (psig)	σ_{H1} (H) (psig)	σ_{H2} (G) (psig)		
1	0	0	0.00	3000	750	300	0.00	
	870	870	0.00	3750	1300	900	0.00	
	900	900	1.18	3750	1260	900	1.00	Initiate flow
	930	930	2.52	3750	1300	900	1.00	
	900	900	3.41	3750	1260	900	1.50	
	930	930	6.07	3000	1450	750	3.00 +	Cavity above port.
	870	860	6.43	3000	1400	750	3.00 +	
	870	860	6.89	2950	1400	750	3.00 +	
	0	0	0.00	2550	900	230		
	2	0	0	0.00	3000	750	650	0.00
920		900	2.61	3650	1250	1100	0.00	Initiate flow
915		895	2.63	3750	1250	1100	0.00	
915		900	2.94	3750	1250	1100	1.00	Cavity formed
885		870	3.49	3750	1250	1100	1.50	
915		900	4.51	3750	1250	1100	1.50	
895		885	5.01	3760	1250	1100	2.00	
880		860	5.28	3750	1200	1060	2.00	
895		880	5.55	3760	1200	1100	2.00	
915		900	5.79	3760	1230	1100	2.00	
910		895	6.00	3760	1230	1100	2.00	Slightly wider arch
900		890	6.33	3760	1230	1100	2.00	
915		900	6.68	3760	1240	1100	2.00	
900		885	6.97	2550	1370	600	----	Complete failure
0	0	0.00	2150	800	175			

Table 3 (continued)

Test #	Inlet Pressure (psig)	Outlet Pressure (psig)	Flowrate (BPD)	Measured Stress			Cavity Length (inches)	Comments
				σ_v (F) (psig)	σ_{H1} (H) (psig)	σ_{H2} (G) (psig)		
3	0	0	0.00	3000	500	300	0.00	Initial stress
	900	900	2.97	3550	1050	900	0.50	
	905	910	3.27	3550	1050	900	0.50	Pressure transducer problems
	905	900	3.64	3550	1050	900	0.75	
	900	905	4.17	3550	1050	900	0.75	
	905	900	4.78	3550	1050	900	0.75	
	900	895	5.41	3550	1050	900	1.50	
	900	895	5.90	3550	1050	900	1.50	
	900	895	6.26	3540	1050	900	1.50	
	903	898	6.60	3540	1050	900	2.00	
	900	890	6.92	3530	1050	900	2.00	
	895	890	5.47	3550	1060	910	2.00	Pressure problems
	900	895	6.61	1220	1250	700	----	Complete failure
	0	0	0.00	700	650	150		
	4	0	0	0.00	3100	600	400	0.00
450		440	1.36	3450	820	650	0.00	
460		460	1.47	3450	820	650	0.00	
460		450	2.45	3450	820	650	0.25	
450		445	2.66	3450	820	650	0.25	
465		455	2.87	3450	820	650	0.25	
430		420	4.32	3450	820	650	0.67	
465		450	5.56	3450	820	650	1.25	
470		460	6.44	3440	820	640	2.00	
440		430	6.97	3350	800	580	3.00	Slight stress drop

Table 3 (continued)

Test #	Inlet Pressure (psig)	Outlet Pressure (psig)	Flowrate (BPD)	Measured Stress			Cavity Length (inches)	Comments
				σ_v (F)	σ_{H1} (H)	σ_{H2} (G)		
4 Cont.	450	435	7.46	3350	800	600	3.00	
	460	440	7.97	3350	800	600	3.00	
	470	450	8.23	3350	800	600	3.00	
	465	445	8.51	3000	800	550	----	Complete failure
5	0	0	0.00	2700	600	320		
	0	0	0.00	3000	900	700	0.00	
	480	480	2.96	3700	1180	950	0.50	
	480	480	3.73	3700	1200	900	1.00	
	480	475	4.40	3700	1180	880	1.25	Pressure problems
	460	450	4.85	3600	1180	800	1.75	Cleaned 60-micron filters
	450	435	5.79	3600	1180	800	1.75	
	460	445	6.80	3650	1180	800	1.75	
	460	445	7.22	3650	1180	800	1.75	
	450	440	7.84	3650	1180	800	1.75	
	480	460	8.28	3150	1130	650	----	Complete failure
6 New Pack	0	0	0.00	2950	900	440		
	0	0	0.00	1500	450	320	0.00	
	895	895	2.45	1900	1010	830	1.00	
	900	895	3.12	1900	1010	830	1.25	
	885	870	4.38	1920	1000	810	1.25	
	945	940	5.11	1950	1040	850	2.00	
	910	900	5.77	1920	1010	830	2.00	
	900	890	6.20	1350	1150	610	----	Complete failure
	0	0	0.00	900	550	100		

Table 3 (continued)

Test #	Inlet Pressure (psig)	Outlet Pressure (psig)	Flowrate (BPD)	Measured Stress			Cavity Length (inches)	Comments
				σ_v (F) (psig)	σ_{H1} (H) (psig)	σ_{H2} (G) (psig)		
7	0	0	0.00	1500	350	260	0.00	
	900	900	2.66	1880	900	750	1.00	
	900	895	3.59	1850	920	770	1.25	
	880	875	4.25	1850	900	760	1.25	
	890	880	5.08	1860	910	760	2.00	
	870	865	5.35	1800	940	750	3.00	
	900	885	5.98	1750	950	750	3.00 +	
	900	885	6.25	1350	870	530	----	Complete failure
	0	0	0.00	1070	450	160	----	
	8	0	0	0.00	1500	880	650	0.00
450		450	0.00	1700	1110	880	0.00	
450		450	3.00	1710	1160	600	0.75	
460		455	3.70	1660	1160	595	1.25	
455		455	4.44	1600	1180	530	2.00	
460		455	4.90	1550	1180	530	2.00	
460		460	5.26	1550	1180	540	2.00	
470		470	5.72	1570	1180	540	2.00	Shut in to clean filter
450		450	5.65	1570	1200	500	2.50	
450		450	6.05	1550	1200	500	2.50	
460	455	6.49	1570	1200	500	2.50		
440	435	6.97	1550	1200	490	2.50		
455	445	7.42	1550	1200	490	2.50		
450	440	7.90	1040	1400	560	----	Complete failure	
0	0	0.00	870	1180	75	----		

Table 3 (continued)

Test #	Inlet Pressure (psig)	Outlet Pressure (psig)	Flowrate (BPD)	Measured Stress			Cavity Length (inches)	Comments
				σ_V (F) (psig)	σ_{H1} (H) (psig)	σ_{H2} (G) (psig)		
9	0	0	0.00	1500	800	440	0.00	
	450	450	0.00	1660	1020	650	0.00	
	445	435	2.95	1680	1040	580	1.00	
	460	450	3.59	1600	1040	580	1.25	
	465	445	4.35	1600	1040	570	1.75	
	470	455	5.07	1640	1050	570	1.75	
	445	430	5.94	1580	1040	550	2.00	
	465	445	6.35	1580	1040	550	2.00	
	455	435	6.88	1580	1040	550	2.00	
	440	420	7.34	1580	1040	550	2.50	
	470	445	7.57	1580	1050	540	2.50	Clean outlet filter
	450	430	7.79	1550	1050	530	2.50	
	485	465	7.97	1450	1070	480	----	Complete failure
	0	0	0.00	1340	880	260		
10	0	0	0.00	750	350	200	0.00	
	450	450	0.00	930	570	410	0.00	
	435	435	3.01	930	570	390	1.75	
	435	435	3.36	930	560	390	2.00	
	445	450	3.76	930	580	390	2.00	
	445	445	4.15	930	580	390	2.00	
	445	440	4.55	920	580	390	2.00	
	450	450	4.94	880	580	390	2.00	
	435	430	5.39	880	580	390	2.00	
	455	445	5.81	890	580	390	2.00	

Table 3 (continued)

Test #	Inlet Pressure (psig)	Outlet Pressure (psig)	Flowrate (BPD)	Measured Stress			Cavity Length (inches)	Comments
				σ_v (F) (psig)	σ_{H1} (H) (psig)	σ_{H2} (G) (psig)		
10 Cont.	445	440	6.33	890	580	390	2.00	
	440	430	6.85	890	580	390	2.00	
	455	445	7.52	860	600	360	3.00 +	Stabilized above port
	0	0	0.00	700	390	180		
11	0	0	0.00	770	200	110	0.00	
	450	445	2.94	950	450	330	1.50	
	450	445	3.76	940	450	330	1.75	
	445	440	4.56	930	450	330	2.25	
	450	445	5.42	940	450	330	2.50	
	455	445	5.79	930	450	330	2.50	
	460	450	6.33	940	450	330	2.50	
	450	445	6.78	930	450	330	2.50	
	465	450	7.30	940	450	330	2.50	
	460	445	7.93	940	450	320	2.75	
	455	440	8.22	910	450	300	3.00 +	Grew above port.
	0	0	0.00	670	230	105		

Table 3 (continued)

Test #	Inlet Pressure (psia)	Outlet Pressure (psia)	Flowrate (BPD)	Measured Stress			Cavity Length (inches)	Comments
				σ_v (F) (psia)	σ_{H1} (H) (psia)	σ_{H2} (C) (psia)		
12 New Pack	0	0	0.00	2250	610	570	0.00	
	900	895	2.85	2800	1180	970	0.75	
	900	895	3.49	2790	1180	950	1.00	
	895	880	4.28	2750	1180	920	1.50	
	895	880	5.10	2750	1180	920	1.75	
	900	890	5.91	2730	1180	920	2.00	
	900	885	6.38	2700	1180	920	2.00	
	900	885	6.63	2650	1180	900	2.50	
	900	880	6.80	2650	1180	900	2.50	
	905	885	7.14	2600	1180	890	3.00 +	
	900	880	7.64	2600	1180	890	3.00 +	
	900	880	8.15	2450	1250	830	----	Complete failure
13	0	0	0.00	2050	750	360	----	
	0	0	0.00	2250	820	560	0.00	
	900	890	2.93	2610	1400	990	1.00	
	900	895	3.61	2590	1400	990	1.00	
	905	895	4.46	2550	1430	980	1.25	
	895	885	5.27	2450	1410	940	1.75	
	910	895	5.95	2380	1430	920	2.50	
	905	895	6.47	2400	1430	920	2.50	
	900	885	6.75	2380	1430	910	2.50	
	905	895	7.22	2150	1460	850	----	Complete failure
	0	0	0.00	1800	980	420	----	

Table 3 (continued)

Test #	Inlet Pressure (psig)	Outlet Pressure (psig)	Flowrate (BPD)	Measured Stress			Cavity Length (inches)	Comments
				σ_v (F) (psig)	σ_{H1} (H) (psig)	σ_{H2} (C) (psig)		
14	0	0	0.00	2300	650	510	0.00	
	450	450	0.00	2350	880	710	0.00	
	455	435	3.06	2300	880	570	1.00	
	455	440	3.83	2250	875	550	1.25	
	450	430	4.52	2230	870	550	1.75	
	450	430	5.36	2150	830	510	2.50	
	450	420	6.38	1870	850	440	3.00	Small failure-Not above the port.
	445	415	7.42	1870	850	440	3.00	
	450	420	8.62	1160	880	350	----	Complete failure
	0	0	0.00	840	650	110		
15	0	0	0.00	2250	680	610	0.00	
	450	450	0.00	2400	900	800	0.00	
	445	440	3.04	2500	900	740	1.00	
	445	445	3.75	2400	900	710	1.25	
	460	460	4.55	2400	900	710	1.25	
	460	450	5.43	2490	900	710	1.50	
	465	450	6.40	2370	920	700	1.75	
	465	450	7.35	2450	910	700	2.00	
	470	455	8.06	2250	900	570	----	Complete failure
	0	0	0.00	2050	670	360		

Table 3 (continued)

Test #	Inlet Pressure (psig)	Outlet Pressure (psig)	Flowrate (BPD)	Measured Stress			Cavity Length (inches)	Comments
				σ_v (F) (psig)	σ_{H1} (H) (psig)	σ_{H2} (G) (psig)		
16	0	0	0.00	750	180	105	0.00	
	900	900	0.00	1150	780	650	0.00	
	895	895	2.94	1120	780	630	1.75	2x wide
	900	900	2.98	1120	800	650	2.00	
	900	895	3.50	1110	800	650	2.50	
	910	905	3.75	1120	800	650	2.50	
	900	890	4.08	1110	790	630	2.50	
	905	900	4.45	1110	800	650	2.50	
	900	890	4.91	1110	790	630	2.75	
	915	900	5.26	1110	800	640	2.75	
	900	880	5.69	1110	790	630	2.75	
	900	880	6.07	1110	780	630	2.75	
	900	890	6.51	1110	780	630	2.75	
	910	885	8.26	1110	780	630	3.00 +	Cavity above port.
---	---	9.50	1110	780	630	3.00 +	Pressure problems.	
17	0	0	0.00	700	260	140		
	0	0	0.00	2995	610	490	0.00	
	15	0	1.97	2930	600	320	0.50	
	30	10	3.03	2900	580	300	0.67	
	100 +		4.00					Abort test due to pressure problems.
								Installed new filters for the next sand pack.

Table 3 (continued)

Test #	Inlet Pressure (psia)	Outlet Pressure (psia)	Flowrate (BPD)	Measured Stress				Cavity Length (inches)	Comments
				σ_v (F) (psia)	σ_{H1} (H) (psia)	σ_{H2} (G) (psia)			
18	0	0	0.00	3000	450	425	0.00		
	200	200	0.00	3120	550	500	0.00		
	210	205	3.02	3060	550	510	0.67		
	210	200	4.08	3050	550	510	1.25		
	200	180	5.41	3025	535	500	1.50		
	195	175	6.38	3025	535	500	1.75		
	205	180	7.39	2950	510	500	2.25		
	205	175	8.70	2880	490	500	2.75		
	205	165	9.26	2750	450	500	2.87		
	205	175	9.80	2600	430	520	3.00 +		
	200	170	10.25	2350	400	560	-----	Complete failure	
	0	0	0.00	2180	250	350			
	19	0	0	0.00	2250	460	430	0.00	
		200	200	0.00	2300	550	500	0.00	
195		180	3.11	2320	550	480	0.75		
200		185	4.20	2300	540	460	1.50		
200		180	5.43	2290	540	445	1.87		
210		180	6.33	2290	535	445	2.00		
210		175	7.44	2200	520	400	3.00		
210		170	7.96	2200	520	400	3.00		
200		160	8.50	2200	520	400	3.00		
210		175	8.98	2190	520	390	3.00		
200		155	9.50	2010	525	370	-----	Complete failure	
0		0	0.00	1930	450	290			

Table 3 (continued)

Test #	Inlet Pressure (psig)	Outlet Pressure (psig)	Flowrate (BPD)	Measured Stress			Cavity Length (inches)	Comments
				σ_V (F) (psig)	σ_{H1} (H) (psig)	σ_{H2} (C) (psig)		
20	0	0	0.00	1500	250	180	0.00	
	200	200	0.00	1550	350	250	0.00	
	210	195	3.01	1560	350	260	0.25	
	195	175	4.22	1560	320	250	1.00	
	205	175	5.50	1560	320	250	1.33	
	205	175	6.30	1550	320	240	2.00	
	210	180	7.41	1550	320	240	2.25	
	210	175	7.84	1550	320	240	2.25	
	200	165	8.35	1420	325	220	----	Complete failure
	0	0	0.00	1350	250	135		
	21	0	0	0.00	750	160	150	0.00
200		200	0.00	800	260	230	0.00	
195		180	3.07	800	260	230	0.67	
210		185	4.56	800	260	230	1.50	
210		180	5.43	800	260	230	1.75	
210		180	6.29	795	260	225	2.00	
210		175	7.36	790	260	225	2.00	
210		175	8.06	790	260	225	2.50	
215		175	8.57	790	260	225	2.50	
210		165	9.24	750	260	220	3.00 +	Cavity above port.
215		165	9.89	750	260	220	3.00 +	
220	170	10.20	630	285	190	----	Complete failure	
0	0	0.00	580	180	120			

Table 3 (continued)

Test #	Inlet Pressure (psig)	Outlet Pressure (psig)	Flourate (BPD)	Measured Stress				Cavity Length (inches)	Comments
				σ_v (F) (psig)	σ_{H1} (H) (psig)	σ_{H2} (G) (psig)	σ_{H2} (G) (psig)		
22	0	0	0.00	750	195	155	155	0.00	
	200	200	0.00	810	300	225	225	0.00	
	205	190	3.00	810	295	215	215	1.00	
	195	175	4.56	790	295	200	200	2.25	
	200	180	5.35	790	295	200	200	2.25	
	210	182	6.34	770	295	200	200	3.00	
	210	170	7.44	750	295	200	200	3.00 +	Cavity above port, but no stress drop.
	215	170	8.11	750	295	200	200	3.00 +	
	220	170	8.83	750	295	200	200	3.00 +	
	220	170	8.83	690	305	165	165	----	Complete failure
	0	0	0.00	590	200	125	125	----	
	23	0	0	0.00	1500	200	165	165	0.00
200		200	0.00	1525	300	250	250	0.00	
210		195	2.97	1550	310	250	250	0.67	
200		180	4.43	1525	310	245	245	1.75	
205		180	5.79	1510	310	240	240	2.00	
210		185	6.72	1510	310	240	240	2.25	
215		180	7.79	1500	300	225	225	3.00 +	
210		170	8.38	1490	300	220	220	3.00 +	
200		160	8.88	1370	305	200	200	----	Complete failure
0		0	0.00	1350	205	145	145	----	

Table 3 (continued)

Test #	Inlet Pressure (psig)	Outlet Pressure (psig)	Flowrate (BPD)	Measured Stress			Cavity Length (inches)	Comments	
				σ_v (F) (psig)	σ_{H1} (H) (psig)	σ_{H2} (G) (psig)			
24	0	0	0.00	2250	500	320	0.00		
	200	200	2.07	2310	600	380	0.50		
	195	180	3.02	2290	600	380	0.67		
	190	175	4.31	2290	590	380	0.67		
	200	185	5.81	2280	590	380	1.25		
	210	190	7.07	2280	590	380	1.75		
	205	185	8.10	2275	590	380	2.00		
	195	170	8.45	2240	600	370	2.67		
	200	170	8.79	2240	600	370	3.00 +		
	210	175	9.02	2100	620	310	----	Complete failure	
	25	0	0	0.00	3000	535	480	0.00	
		200	200	0.00	3150	640	560	0.00	
		190	180	2.97	3140	635	560	0.67	
		195	185	4.10	3140	635	560	0.75	
180		170	5.21	3140	620	560	1.00		
185		175	6.30	3140	625	560	1.25		
210		190	7.47	3145	625	560	1.50		
205		185	8.13	3130	625	560	2.00		
210		185	8.60	3015	635	540	3.00 +		
200		170	9.20	3015	635	540	3.00 +		
200	165	9.64	2875	640	500	----	Complete failure		

At this point, the data taken at 900 and 450 psig fluid pressure was compared to that taken by John Benton(22). Little correlation was found so steps to retake part of his data were taken. Test #17 was to be conducted at 3000 psig vertical stress, and atmospheric fluid pressure. It was quickly determined that zero pressure could not be maintained so the test was shut-in. With a flowrate of roughly 4.0 BPD, the inlet cell pressure had climbed to over 100 psig. It was felt that this increasing fluid pressure would render erroneous results. This increase in fluid pressure is also the reason for the lack of comparison with previous data taken by Benton. This will be discussed in further detail later.

Because tests could not be run with zero fluid pressure maintained, it was decided to run tests at 200 psig. Also to help solve the problem of excess pressure build-up, new filters were installed on the outlet of the cell. These new filters are Nupro filters, with replaceable filter cartridges. These cartridges are much cheaper to replace when dirty, than replacing the entire filter as was done previously. Another advantage is that different pore size filter cartridges (7-60 micron) can be used depending on filtration needs.

Sand packs four and five were used to collect data at 200 psig fluid pressure (Table 3). This data along with the data from the first three sand packs is reduced and discussed on the following pages.

Arch Formation and Stability

Upon initiating flow through the sand pack, an arch forms around the perforation in the casing, as evidenced by a cavity. This cavity is a result of the zero stress regime created within the arch. The unstressed sand is washed out of the arch structure due to fluid drag and aided by gravity. The resulting cavity is observed to be ellipsoidal in shape with its major axis being vertical. The cavity is seen to extend from the perforation upward. It is assumed that the arch is symmetrical about the perforation, but that the cavity does not clean out below the perforation due to the force of gravity and not enough fluid velocity. Figure 22 shows a cross-sectional view of this arch model.

As the flowrate is increased, the arch cavity grows upward thus dropping out more sand from the top of the cavity. The majority of the larger cavity growths were accompanied by a slight drop in the vertical sand stress as well as the horizontal stress measured on chart G which is the gauge facing 45° away from the arch. The other

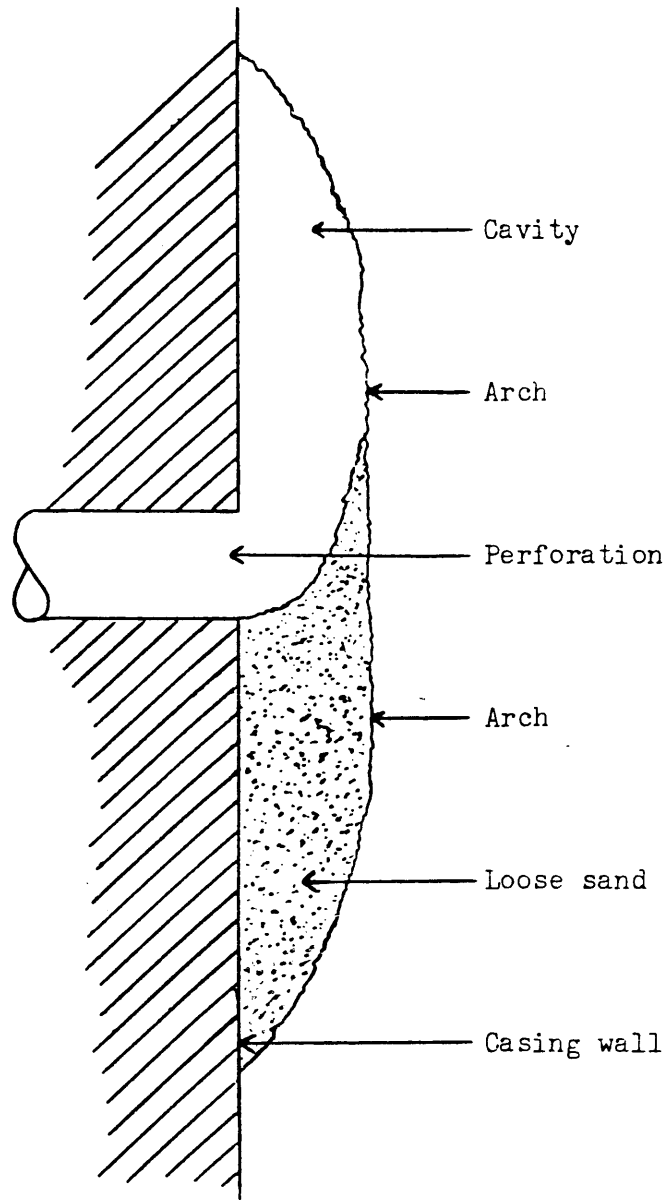


Figure 22

Arch Cross-Sectional View

gauge (H) facing away from the arch (135°) will sometimes record a slight increase. This change in sand stress means that the grains have moved or realigned themselves, thus it is likely that the arch itself changed shape or grew. Based on this assumption, cavity length increase is taken to mean arch growth. Thus as the flowrate of hydrocarbons is increased and the arch grows, additional sand within the arch is relieved of stress and falls out.

In running the tests, the flowrate is stepped up until the arch fails. For most tests, arch failure was observed by a sharp decrease in the vertical and 45° horizontal (G) gauges and an increase in the 135° horizontal gauge (H). This sharp stress drop is accompanied by continuous sand flow out the perforation. For these tests, the stress drop recorded at failure, by the three gauges, was strictly a function of the amount of time that the sand was allowed to flow. Thus no correlation can be made relating stress drop at failure with flowrates or stress levels.

The remaining tests failed in the same manner, but the arch restabilized above the port. This restabilization above the port followed a massive slumping of sand and a sharp stress drop in two of the gauges. Again the

horizontal gauge facing away from the arch would experience an increase in stress. This point was taken to be the failure point because no casing simulator extends above the port and thus the arch boundary conditions have changed. Without an extension of casing, the surface for the arch has changed and thus the data after that point can not be compared with the other data.

As the cavity increases in size, the rate at which the flowrate is increased becomes more and more critical. Thus the pump rate was stepped up one turn (1.0 BPD) at a time until the arch cavity reached a length of roughly 2 inches, and then was stepped up to failure by half turns (0.5 BPD). The problem lies in the fact that sudden rate increase causes surging to occur in the flow system and thus across the arch. It was observed that this surging of pressure and flowrate across the arch often caused premature failure of the arch. These surging effects become more critical as the flowrate approaches the failure point.

Fluid Pore Pressure Effects

Tests were run with varying vertical stresses at three fluid pore pressure levels, 900, 450, and 200 psig. The flowrate at arch failure for each of these tests is

summarized in Table 4. This data is also plotted as failure flowrate versus fluid pressure, seen in Figures 23-27. Figure 23 contains the data plotted on one axis for all four vertical stress levels. Figures 24-27 are the data pertaining to each of the four specific stress levels. From these graphs, it is clearly seen that arch stability is an inverse function of fluid pore pressure. As the pore pressure is increased, the flowrate corresponding to arch failure decreases. This supports the theory of Biot (24), that was discussed earlier in this thesis.

Observing Figure 23, it can be seen that arch stability is a greater function of fluid pore pressure than of vertical stress. For any pore pressure level, the flowrate at arch failure varies roughly 1.5 BPD over the range of vertical stresses. On the other hand, varying the fluid pressure from 200 to 900 psig, caused a reduction in failure flowrate of roughly 3.0 BPD for any vertical stress level.

A least squares analysis (solid line) performed on the data points shown in Figure 23 yields the following equation.

$$Q_F = 9.822 - 0.0036 P_p \quad (10)$$

Table 4
Flowrate at Arch Failure vs.
Fluid Pressure Data

<u>Test #</u>	<u>Vertical Stress (psig)</u>	<u>Fluid Pressure (psig)</u>	<u>Failure Flowrate (BPD)</u>
1	3000	900	6.07
2	3000	900	6.97
3	3000	900	6.61
4	3100	450	8.51
5	3000	450	8.28
18	3000	200	9.80
25	3000	200	9.64
12	2250	900	7.14
13	2250	900	7.22
14	2300	450	8.62
15	2250	450	8.06
19	2250	200	9.50
24	2250	200	9.02
6	1500	900	6.20
7	1500	900	6.25
8	1500	450	7.90
9	1500	450	7.97
20	1500	200	8.35
23	1500	200	8.88
10	750	450	7.52
11	750	450	8.22
21	750	200	9.24
22	750	200	8.83

FLOWRATE AT ARCH FAILURE VS FLUID PRESSURE

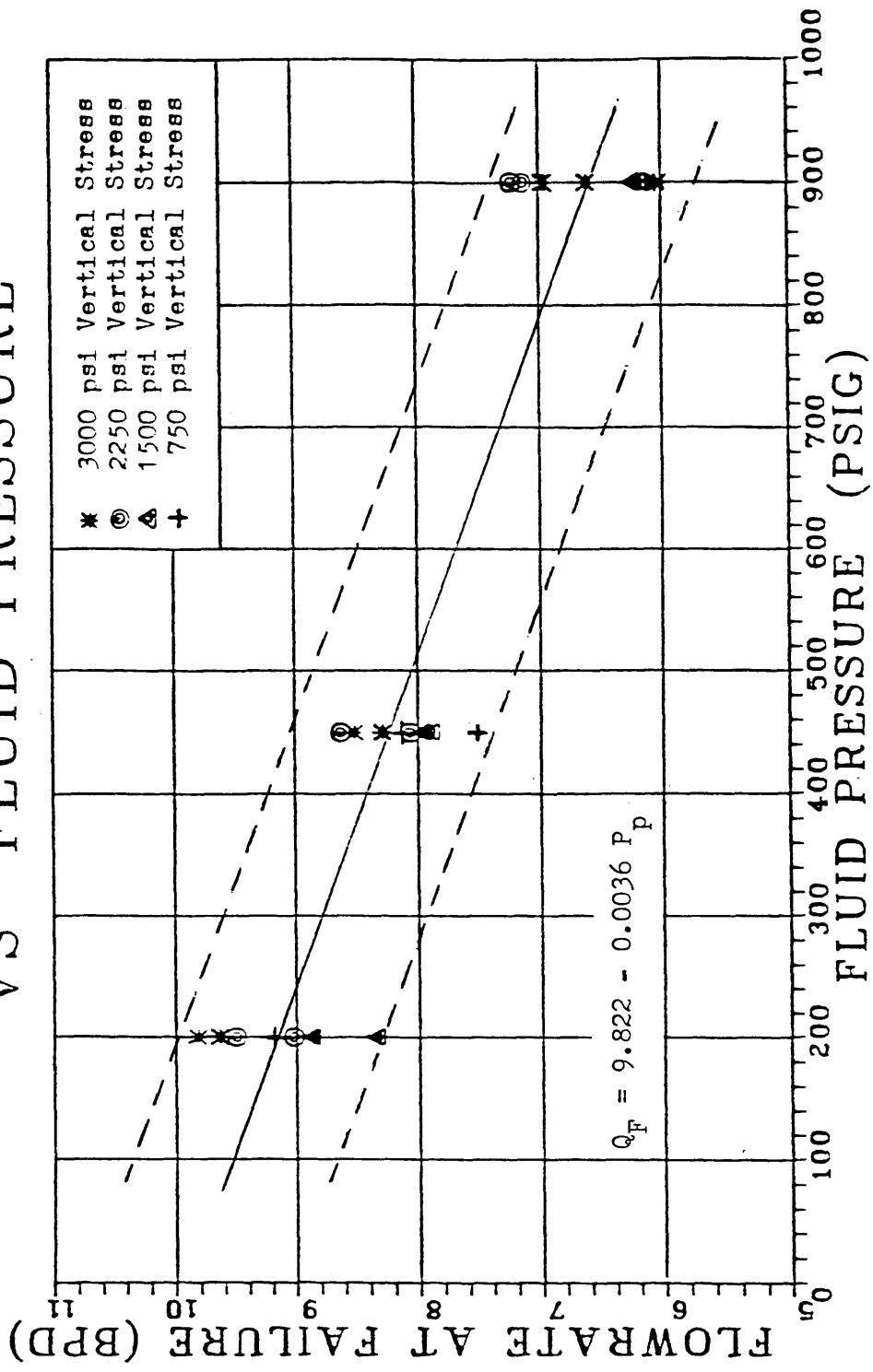


Figure 23

FLOWRATE AT ARCH FAILURE VS FLUID PRESSURE

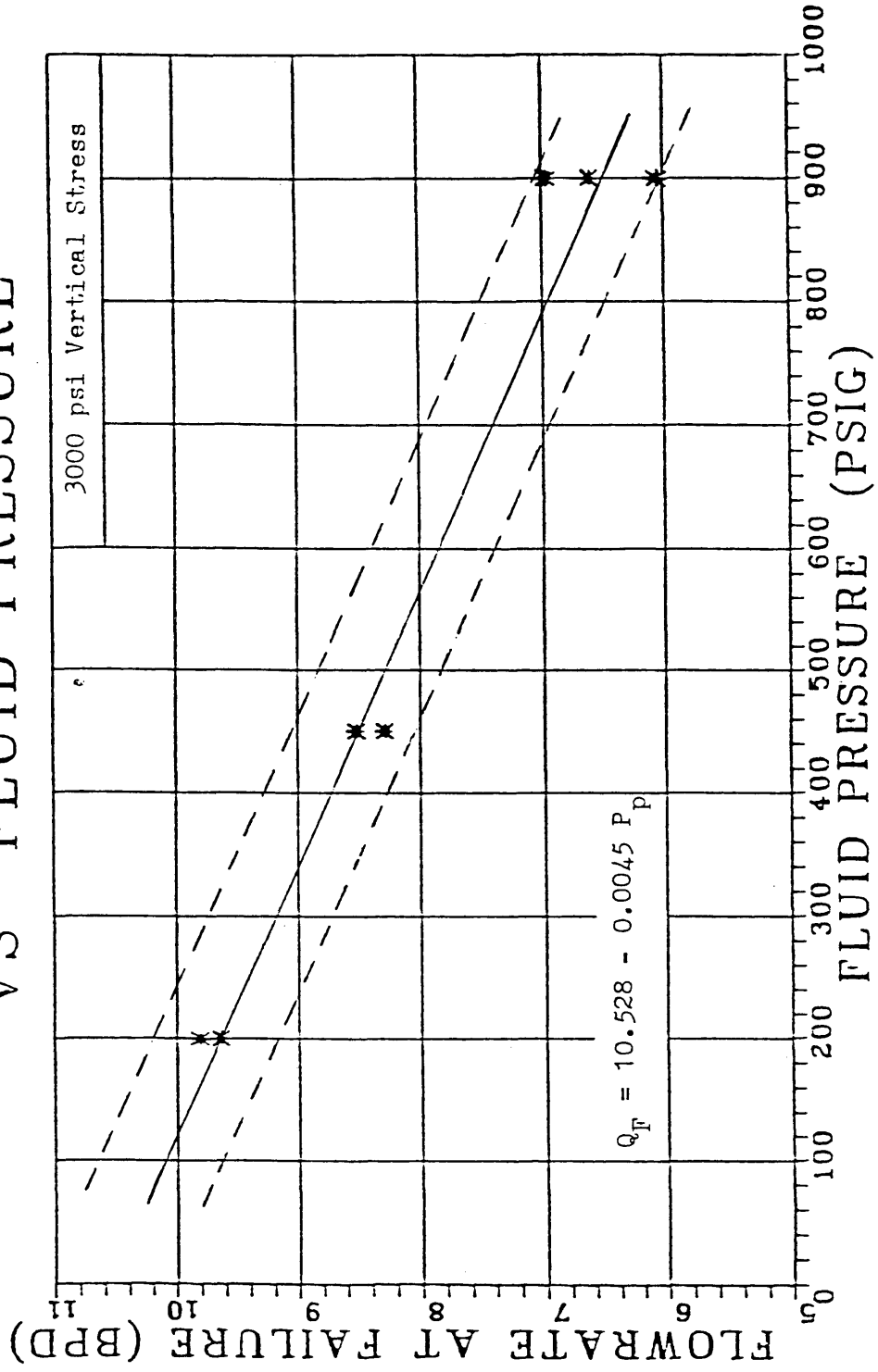


Figure 24

FLOWRATE AT ARCH FAILURE VS FLUID PRESSURE

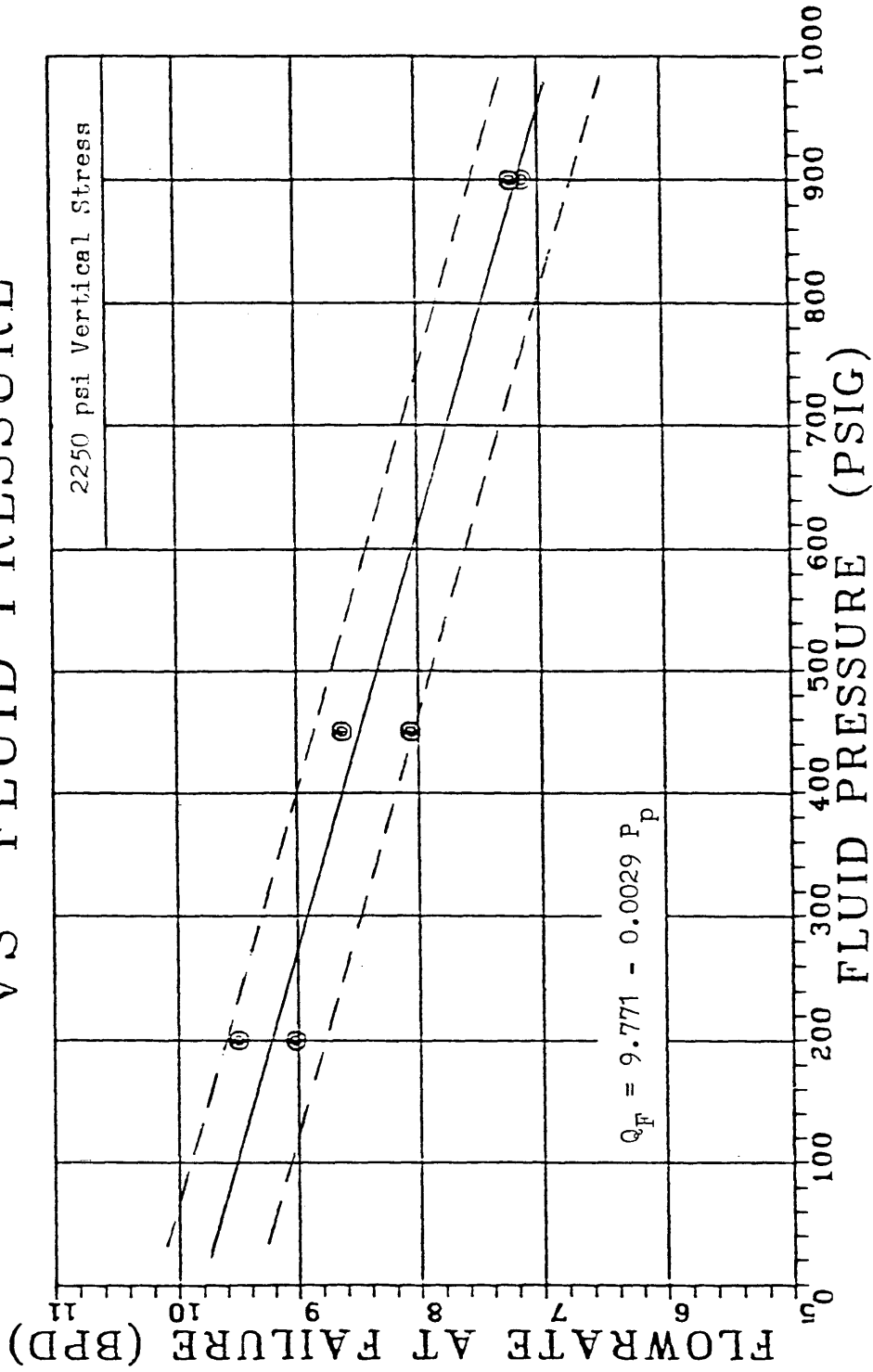


Figure 25

FLOWRATE AT ARCH FAILURE VS FLUID PRESSURE

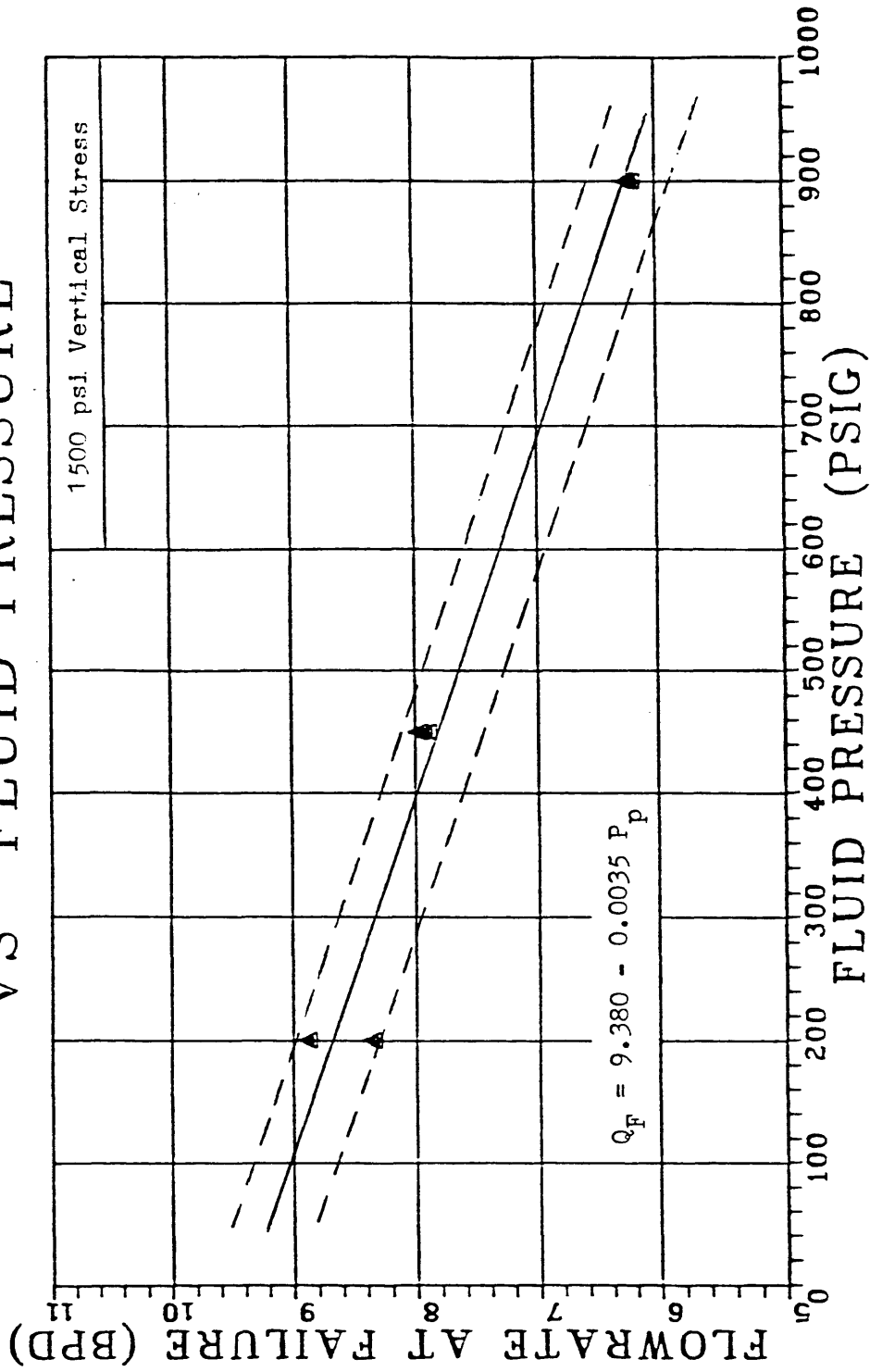


Figure 26

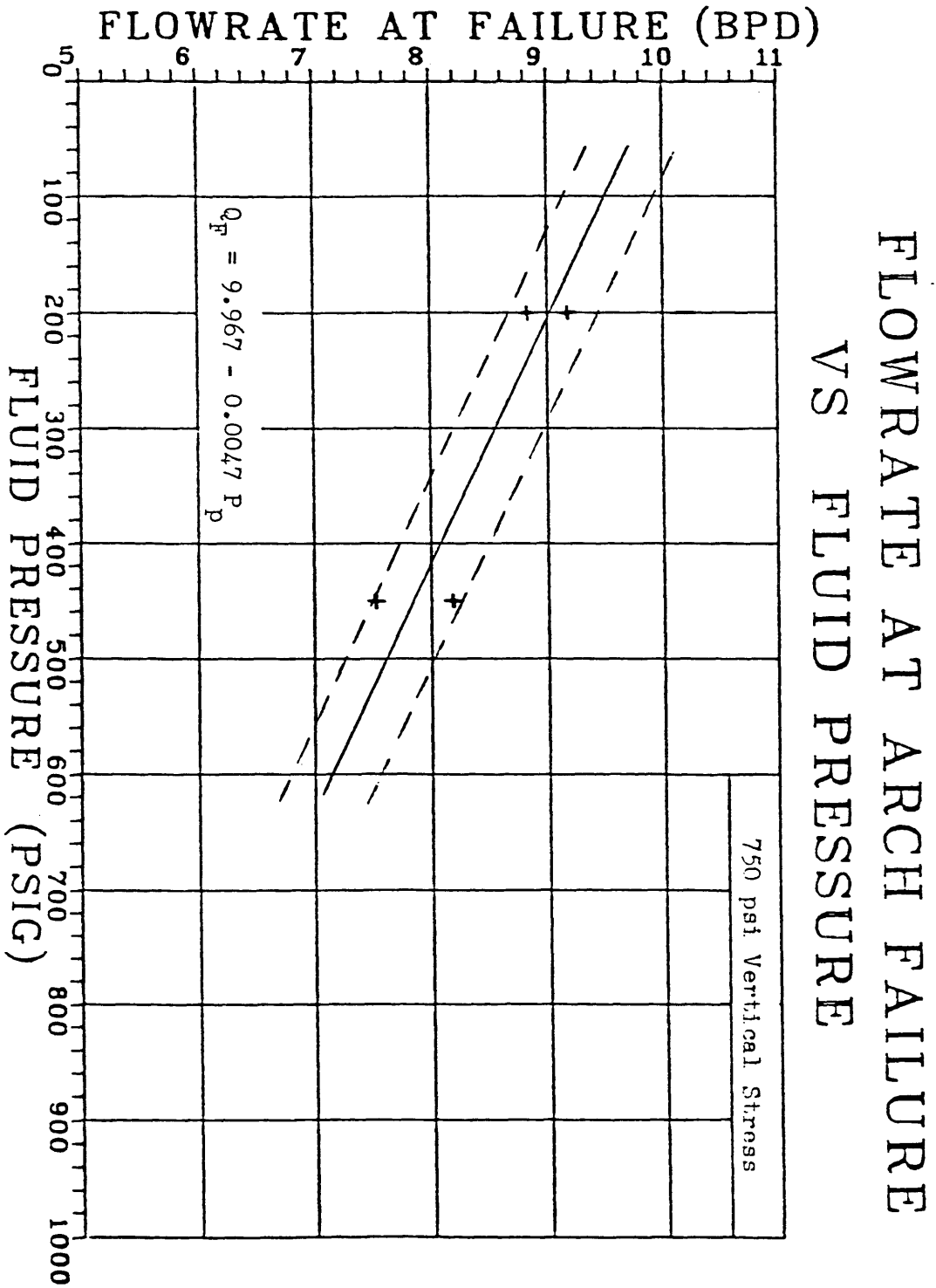


Figure 27

This equation defines the flowrate per perforation at arch failure, for a given fluid pore pressure. The confidence limits (dashed lines) for the equation is plus or minus 1 BPD per perforation. For relatively high vertical stress levels, the actual flowrate corresponding to arch failure will tend to be on the upper side of the confidence limits. Similarly, lower stress levels will cause the flowrate to fall below the calculated value toward the lower side of the confidence limits.

The knowledge that arch stability is a strong function of fluid pore pressure, can help explain the lack of correlation between the presented data and that reported by previous authors(22). Figures 28 and 29 present failure flowrate data versus stress for this author's work and the work done by John Benton(22). Benton's data was taken in the same manner as was this author's, with the exception of having varying fluid pressure. His tests were initiated at atmospheric pressure, and experienced continual pressure increase with increased flowrate. The pore pressure at arch failure for his data ranged from 16 to 205 psig. In contrast, this author's data was taken at constant fluid pressure levels.

FLOWRATE AT ARCH FAILURE VS VERTICAL STRESS

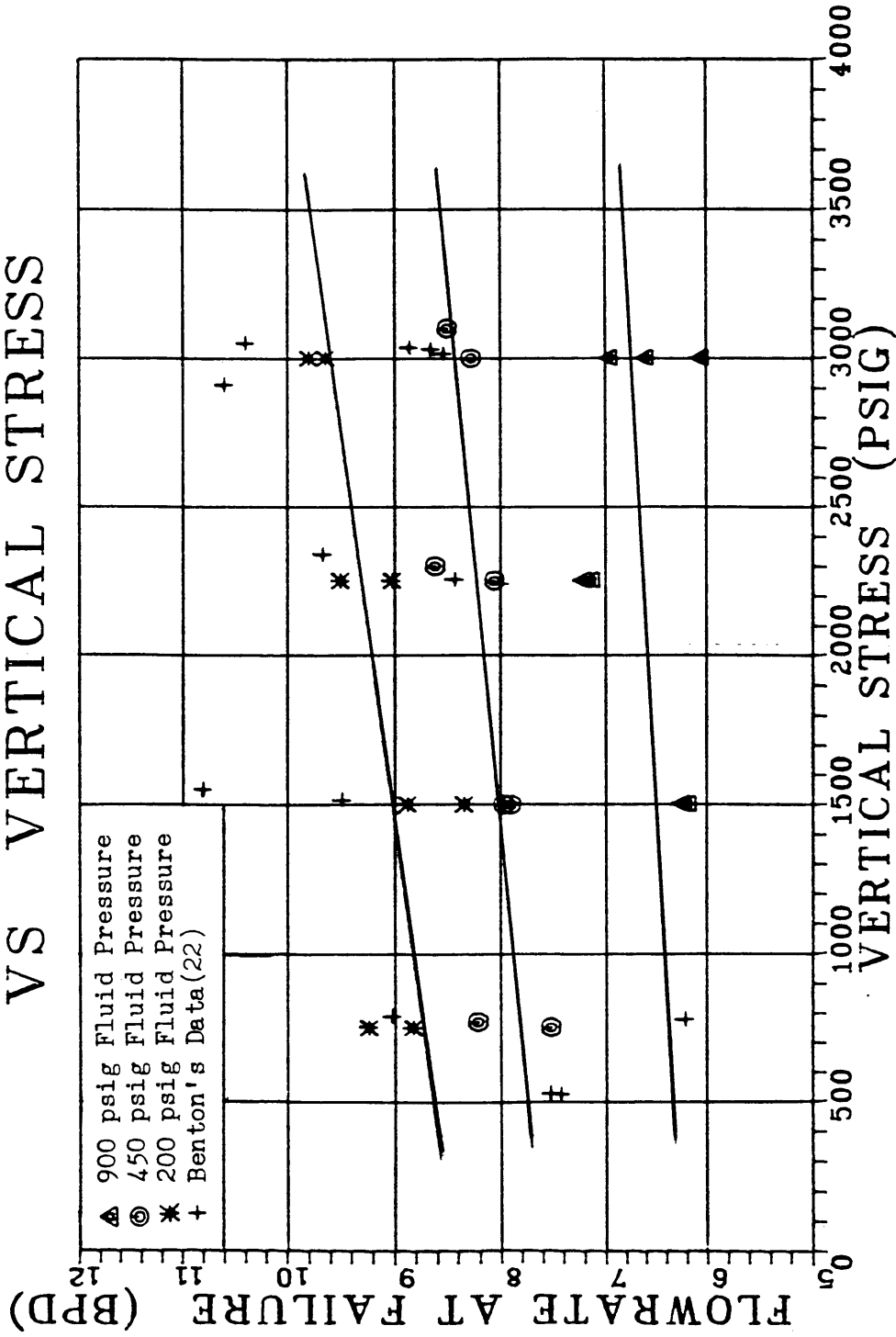


Figure 28

FLOWRATE AT ARCH FAILURE VS HORIZONTAL STRESS

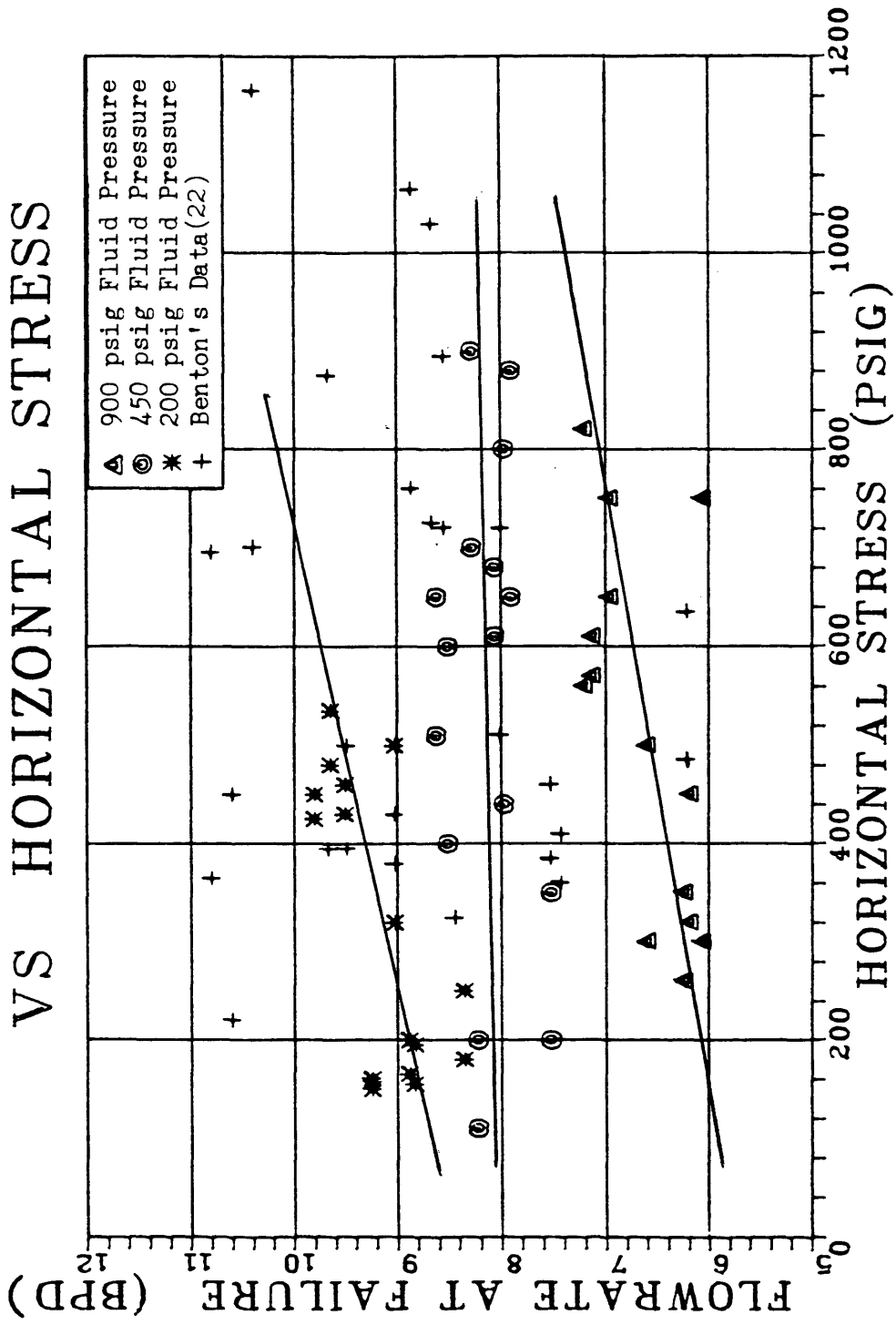


Figure 29

Viewing Figures 28 and 29, it is evident that the data taken at constant pore pressure, is much more consistent than that taken at varying pressure. This author's data falls on three distinct trends corresponding to the three fluid pressure levels used. The data presented by Benton(22) is not as consistent.

Looking at Figure 28, it can be seen that much of Benton's data lies above the data taken at 200 psig pore pressure. This is to be anticipated since arch stability is an inverse function of fluid pore pressure. The points that are interspersed with the high pore pressure data are low due to two reasons. The first reason is that the increasing pore pressure of these tests tend to reduce the arch stability and thus cause the arch to fail at a lower flowrate.

The second and main reason is due to the test procedure. This author's data was taken with flowrate steps of 0.5 BPD at the end of each test. The data taken by Benton(22) was conducted using flowrate steps of up to roughly 3.0 BPD. In conducting the experimentation, this author noticed that large flowrate steps caused premature arch failure at a lower flowrate. This is a result of the surging that occurs across the arch due to the sudden increase in flowrate. This surging becomes more critical

as the flowrate approaches the true failure point for the arch. Thus the large flowrate steps used in the previous work contributed to lower failure flowrates than would be expected.

This emphasizes the importance that experimental procedure has on consistent and accurate results. Part of this author's task was to establish a set procedure for future experimentation to ensure consistent and accurate data. This procedure is outlined in the appendix. It might be noted that flowrate step sizes of 0.5 BPD were used and that the recommended procedure calls for 0.25 BPD steps. The author feels that these smaller steps would be the optimum size for obtaining consistent data. This optimization of flowrate step size along with a consistent experimental procedure should minimize experimental variables which adversely affect data accuracy.

In looking at Benton's data, it might also be noted that he observed dilatant sand behavior during his experimentation. He observed that when the arch grew, the strain gauges recorded a slight increase in stress level. In order for the gauges to record a higher stress, the sand grains would have to expand in a dilatant manner. In conducting tests with constant fluid pore pressure, this dilatant sand behavior was not observed. Thus it seems

likely that what was observed as dilatant sand behavior was probably a misinterpretation of fluid pressure. As arches grow, stress relieved sand is washed out of the cavity and collects in the sand trap. This sand in the trap causes an increase in fluid pressure due to the reduction in permeability within the outlet lines. This increase in fluid pressure causes an increased deflection of the strain gauge surface which will then record a larger stress. This behavior was noticed while experimenting, but the fluid pressure was then adjusted to be held constant. When the fluid pressure was returned to its original value, the stress recording returned to its original level, or slightly less for large arch growths.

Test #16 was conducted at a vertical stress level of 750 psig and with 900 psig fluid pressure. As soon as flow was initiated through the sand pack, an arch formed around the perforation. The cavity associated with the arch was twice as wide and much larger than normal starting cavities. As the flowrate was stepped up, the arch grew in a peculiar fashion remaining twice as wide as all other cavities observed. Eventually with increased flowrate, the cavity extended above the port. This growth was not accompanied by a stress drop so failure could not be concluded. As the flowrate was increased further, fluid

pressure could not be held down to 900 psig due to the flow capabilities of the system. The needle valve on the flow board used to control fluid pressure, could not be opened further to relieve the rising pressure, thus the test had to be shut-in.

In explaining this test, it seems that the arch actually failed upon initiating flow through the sand pack. This initial flow caused a massive slumping of sand that was washed out the perforation. In all other tests, sand slumping or flow within the arch occurred in a vertical manner, falling down from the top of the cavity. In this test sand was observed flowing not only from the top of the cavity, but also slumping in from the sides. As the flow rate was stepped up, each step was accompanied by massive slumping of sand from the sides of the cavity but the overall length of the cavity would only slightly change. Thus with each flowrate increase, the cavity geometry would appear to stay about the same, only large amounts of sand would have been produced. Additionally, sand would also slump into the perforation after the flow-rate had stabilized, showing the unstable nature of the sand. Thus it seems logical to conclude that the arch or sand pack was unstable from the outset.

One question raised by this explanation is why the gauges recorded no stress drop during the test. It might be noted that with the fluid pore pressure greater than the grain-to-grain stress level, the fluid would be carrying the load of the jacks and not the sand grains. Thus the gauges would be reading the fluid pressure and not the sand stress. Since the fluid pressure was kept constant throughout the test, the gauges would show no change.

In conducting this test with a fluid pore pressure greater than the sand stress level, a fluidized bed is simulated. Fluidized beds are known to be very unstable and tend to flow in two manners. The first type of flow is by slumping and the second by massive flow. This slump flow is what was observed within the sand cell.

Stress Effects

Sand arching experiments were conducted at four vertical stress levels, 3000, 2250, 1500, and 750 psig. The results of this data are shown in Table 5. Also included in Table 5 is the reduced data calculated from data in Table 3. Figures 30 through 33 show the flowrate at arch failure versus vertical grain-to-grain stress. Figure 30 contains all of the data while Figures 31 through 33 show the data points corresponding to the three specific fluid pore pressures used.

Table 5
Reduced Data

Test #	Fluid Pressure (psig)	Vertical Stress (psig)	Horizontal Stress H1 (psig)	Horizontal Stress H2 (psig)	Failure Flowrate (BPD)	Pressure Drop @ Failure (psi)	$\Delta P/Q$ @ Failure (psi/BPD)	Net Effective Stress (psig)
1	900	3000	750	300	6.07	10	1.65	2850
2	900	3000	750	650	6.97	15	2.15	2750
3	900	3000	500	300	6.61	10	1.51	2650
6	900	1500	450	320	6.20	10	1.61	1000
7	900	1500	350	260	6.25	15	2.40	980
12	900	2250	610	570	7.14	20	2.80	1890
13	900	2250	820	560	7.22	10	1.39	1710
16	900	750	180	105	-----	--	-----	220
4	450	3100	600	400	8.51	20	2.35	3000
5	450	3000	900	700	8.28	20	2.42	3250
8	450	1500	880	650	7.90	10	1.27	1250
9	450	1500	800	440	7.97	20	2.51	1210
10	450	750	350	200	7.52	10	1.33	480
11	450	770	200	110	8.22	25	3.04	500
14	450	2300	650	510	8.62	30	3.48	1900
15	450	2250	680	610	8.06	15	1.86	1950
18	200	3000	450	425	9.80	30	3.06	2920
19	200	2250	460	430	9.50	40	4.21	2100
20	200	1500	250	180	8.35	35	4.19	1350
21	200	750	160	150	9.24	50	5.41	600
22	200	750	195	155	8.83	50	5.66	610
23	200	1500	200	165	8.88	40	4.55	1325
24	200	2250	500	320	9.02	30	3.33	2110
25	200	3000	535	480	9.64	30	3.11	2950

Table 5 (continued)

Test #	Stress Ratio $\frac{\sigma_V}{\sigma_{H1}}$	Stress Ratio $\frac{\sigma_V}{\sigma_{H2}}$	Stress Drop @ Failure		
			$\Delta\sigma_V$	$\Delta\sigma_{H1}$	$\Delta\sigma_{H2}$
1	4.00	10.00	750	-190	150
2	4.00	4.62	210	-130	500
3	6.00	10.00	2330	-190	210
6	3.33	4.69	570	-140	220
7	4.29	5.77	400	80	220
12	3.69	3.95	150	-70	60
13	2.74	4.02	230	-30	60
16	4.17	7.14	---	---	---
4	5.17	7.75	350	0	50
5	3.33	4.29	500	50	150
8	1.70	2.31	510	-200	-70
9	1.88	3.41	100	-20	50
10	2.14	3.75	30	-20	30
11	3.85	7.00	30	0	20
14	3.54	4.51	710	-30	90
15	3.31	3.69	200	10	130
18	6.67	7.06	250	30	-40
19	4.89	5.23	180	-5	20
20	6.00	8.33	130	-5	20
21	4.69	5.00	40	0	5
22	3.85	4.84	60	-10	35
23	7.50	9.09	120	-5	20
24	4.50	7.03	140	-20	60
25	5.61	6.25	140	-5	40

FLOWRATE AT ARCH FAILURE VS VERTICAL STRESS

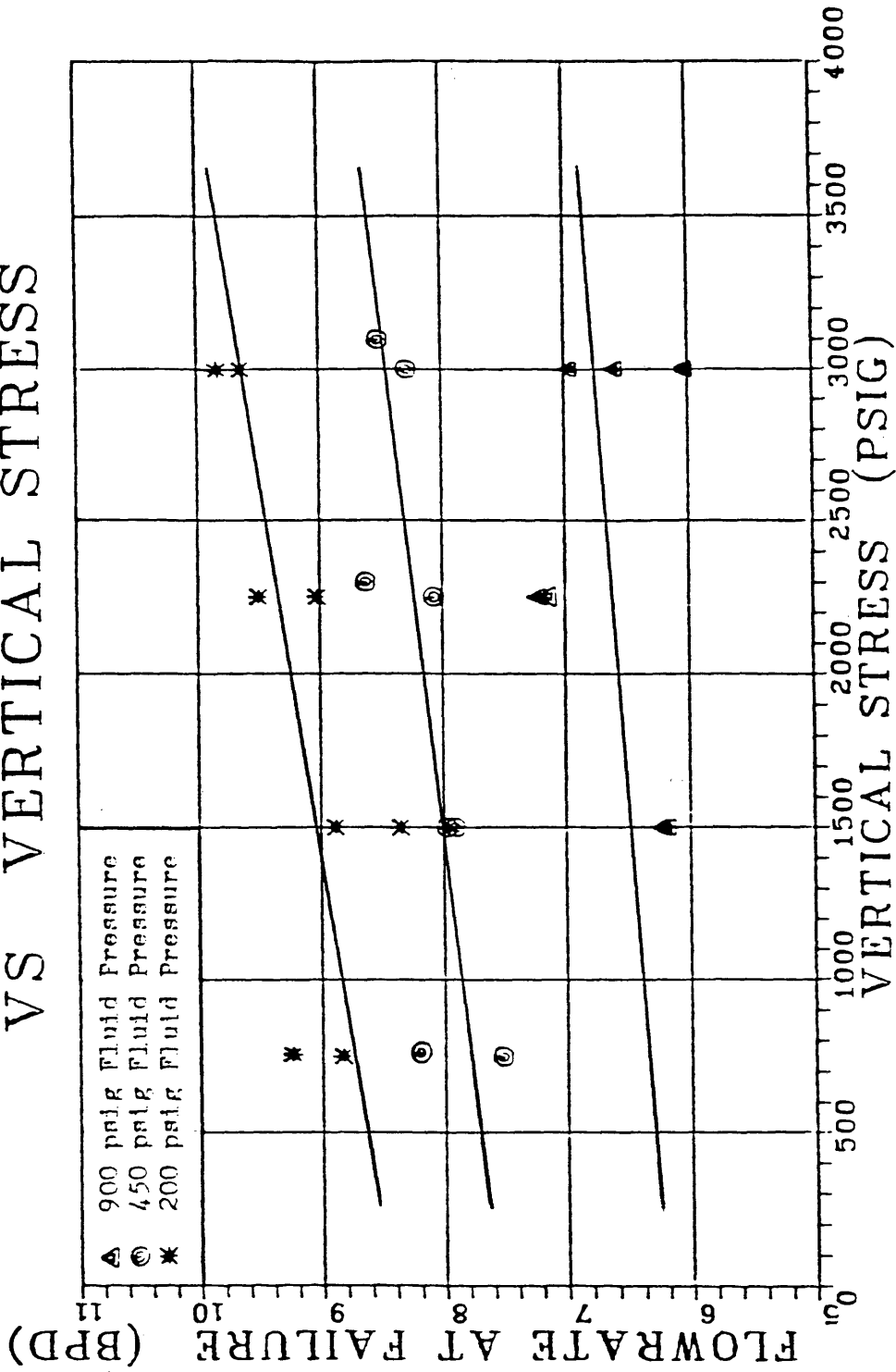


Figure 30

FLOWRATE AT ARCH FAILURE VS VERTICAL STRESS

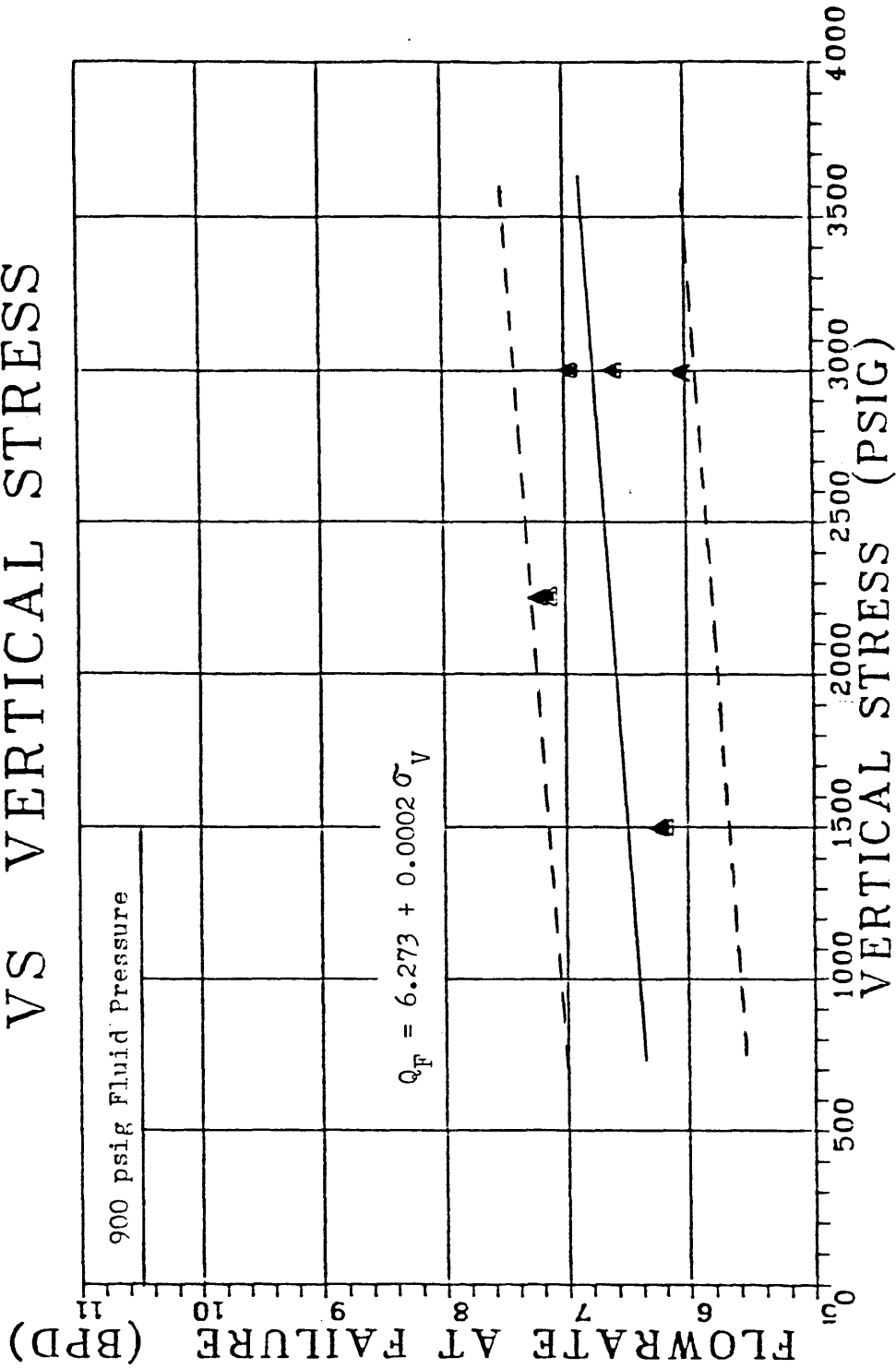


Figure 31

FLOWRATE AT ARCH FAILURE VS VERTICAL STRESS

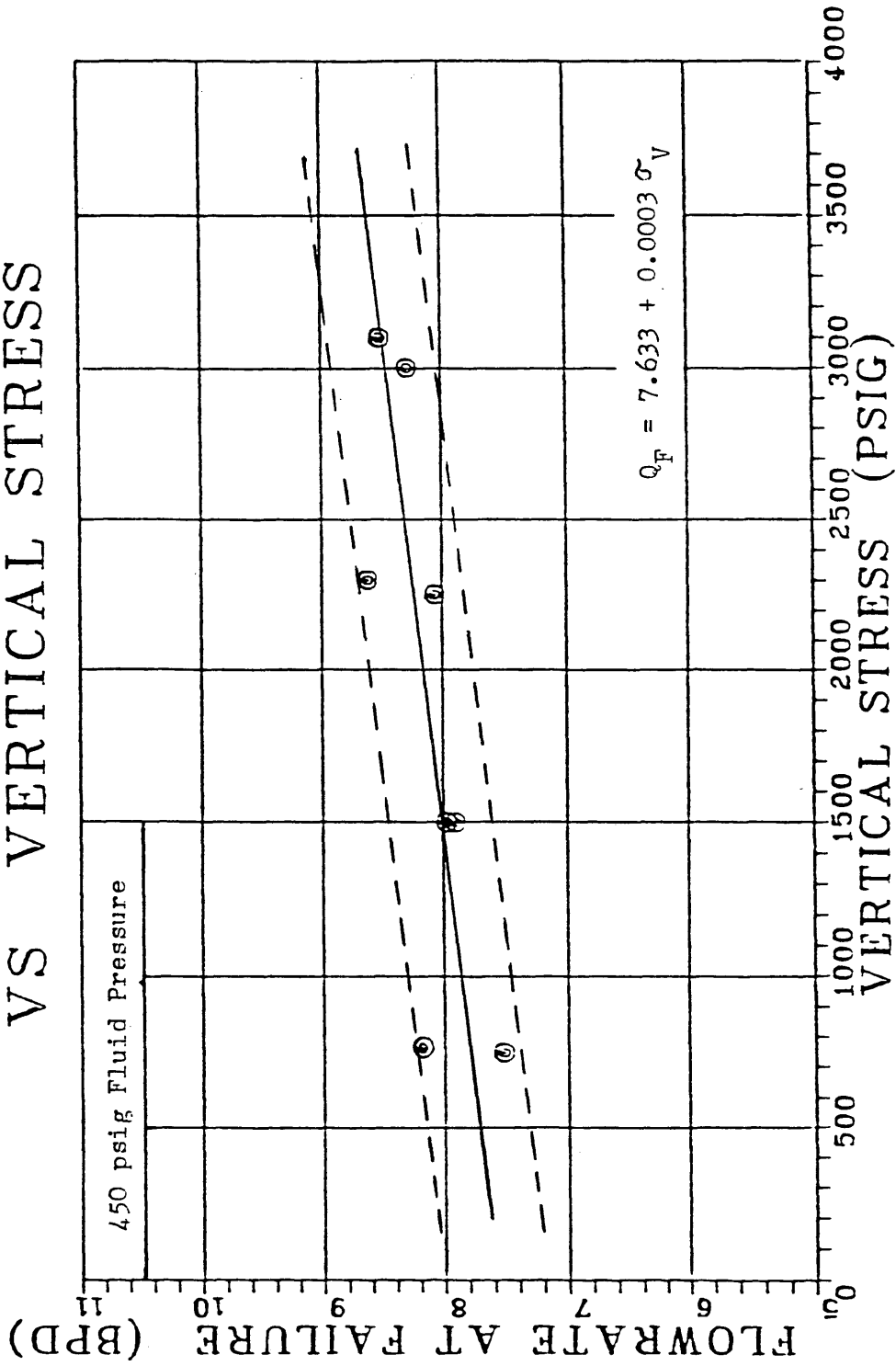


Figure 32

FLOWRATE AT ARCH FAILURE VS VERTICAL STRESS

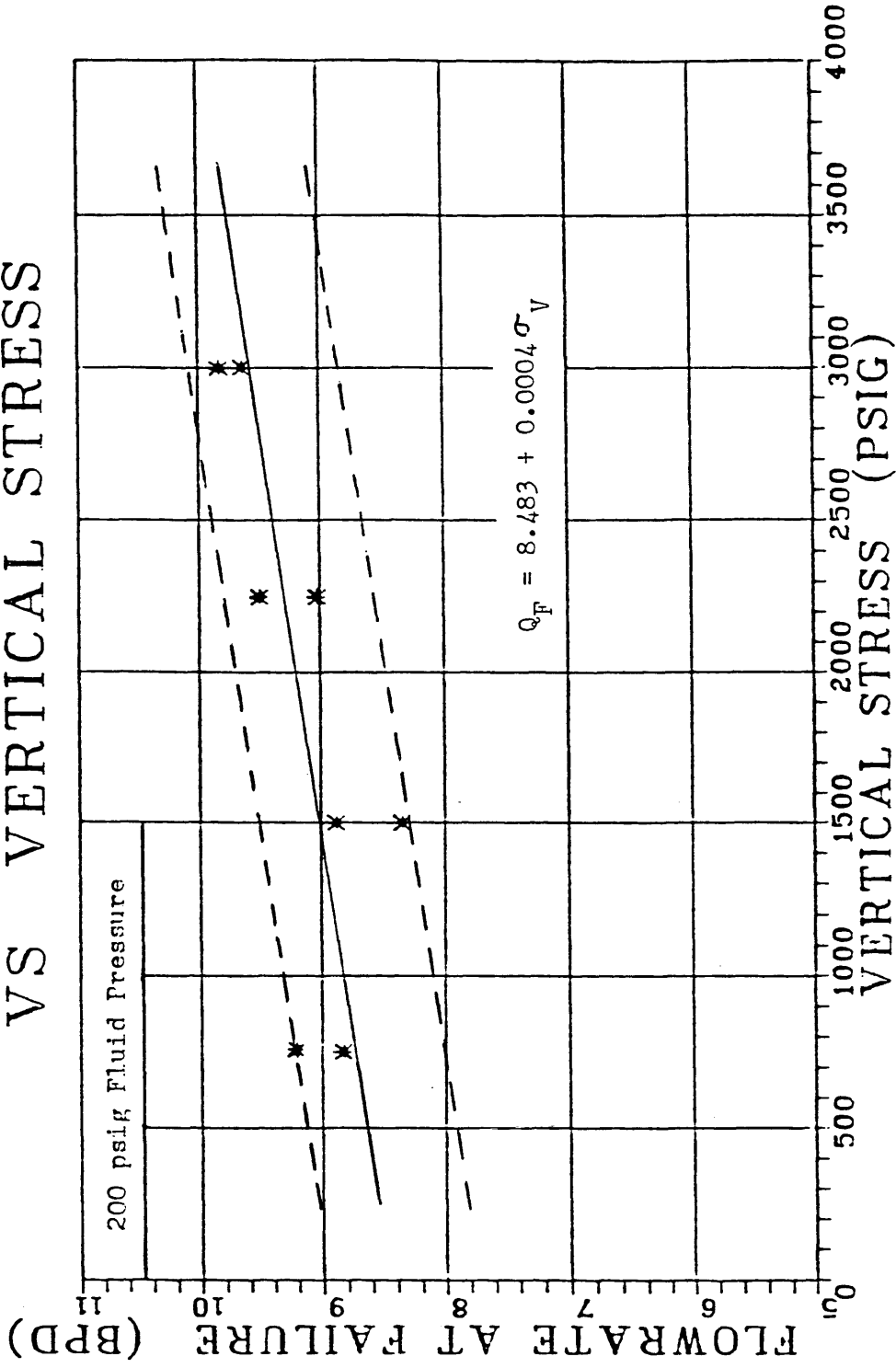


Figure 33

The data for each specific pore pressure shows arch stability to be an increasing function of vertical stress. As the vertical stress is increased, all three sets of data show arch stability increasing. This increase in arch stability is evident by the higher flowrate corresponding to arch failure.

In looking at Figure 30, it might be noted that each pore pressure data set has its own distinct region. This separation or layering of data shows the effect of pore pressure on arch stability as discussed earlier. Again it might be pointed out that for a given vertical stress, the failure flowrate for an arch varies roughly 3.0 BPD over the span of pore pressure from 200 to 900 psig. Similarly the arch failure flowrate at a given pore pressure varies only 1.5 BPD over the span of vertical stress from 750 to 3000 psig. Thus it can be seen that fluid pore pressure has a greater influence on arch stability than does the vertical stress.

This same pattern is noticed in the plots (Figures 34-36) of flowrate at arch failure versus horizontal stress. Figure 34 contains the data for both horizontal gauges while Figures 35 and 36 contain only the data for gauge H and G respectively. It might be noted that the horizontal stress within the cell is a result of the

FLOWRATE AT ARCH FAILURE VS HORIZONTAL STRESS

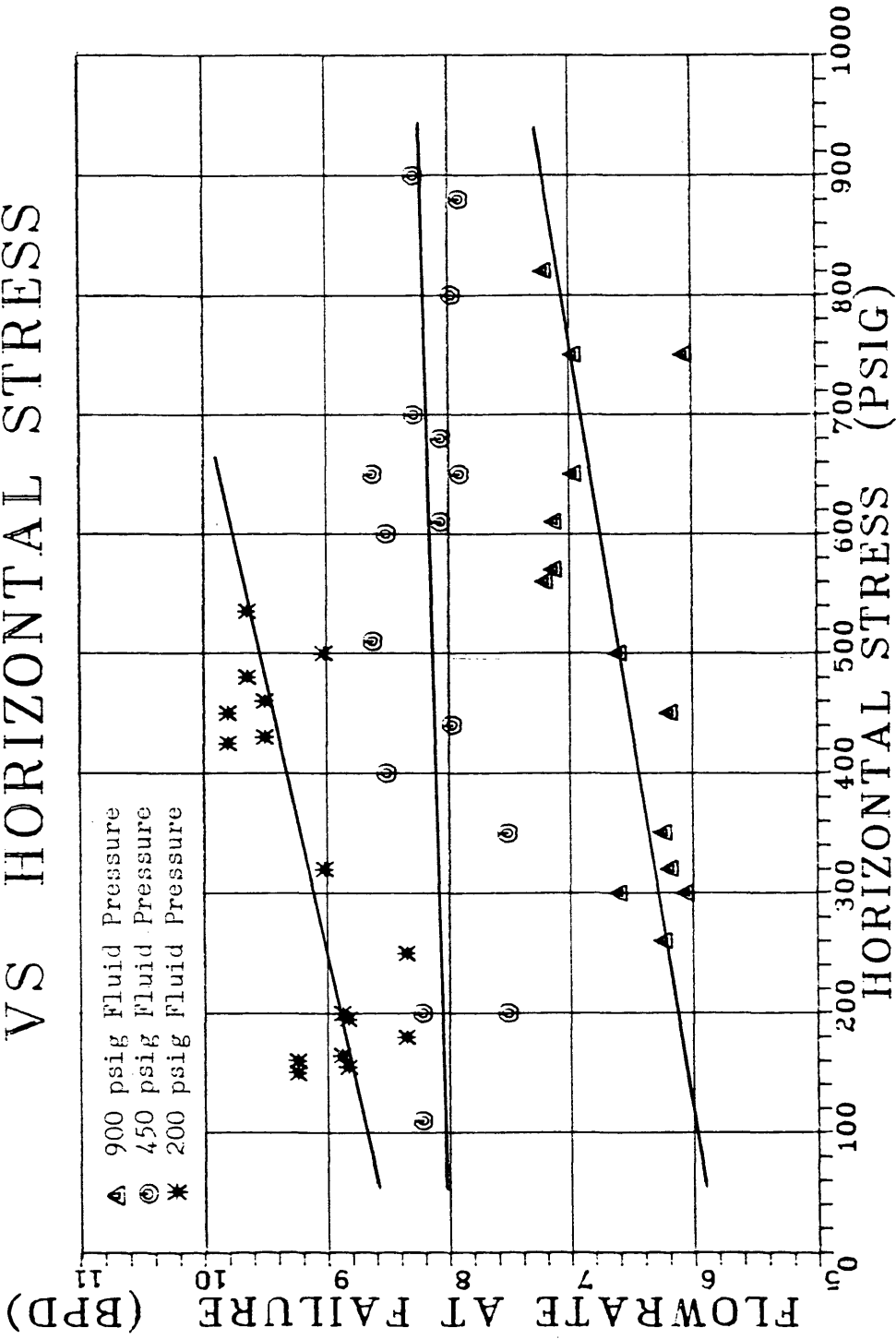


Figure 34

FLOWRATE AT ARCH FAILURE VS HORIZONTAL STRESS

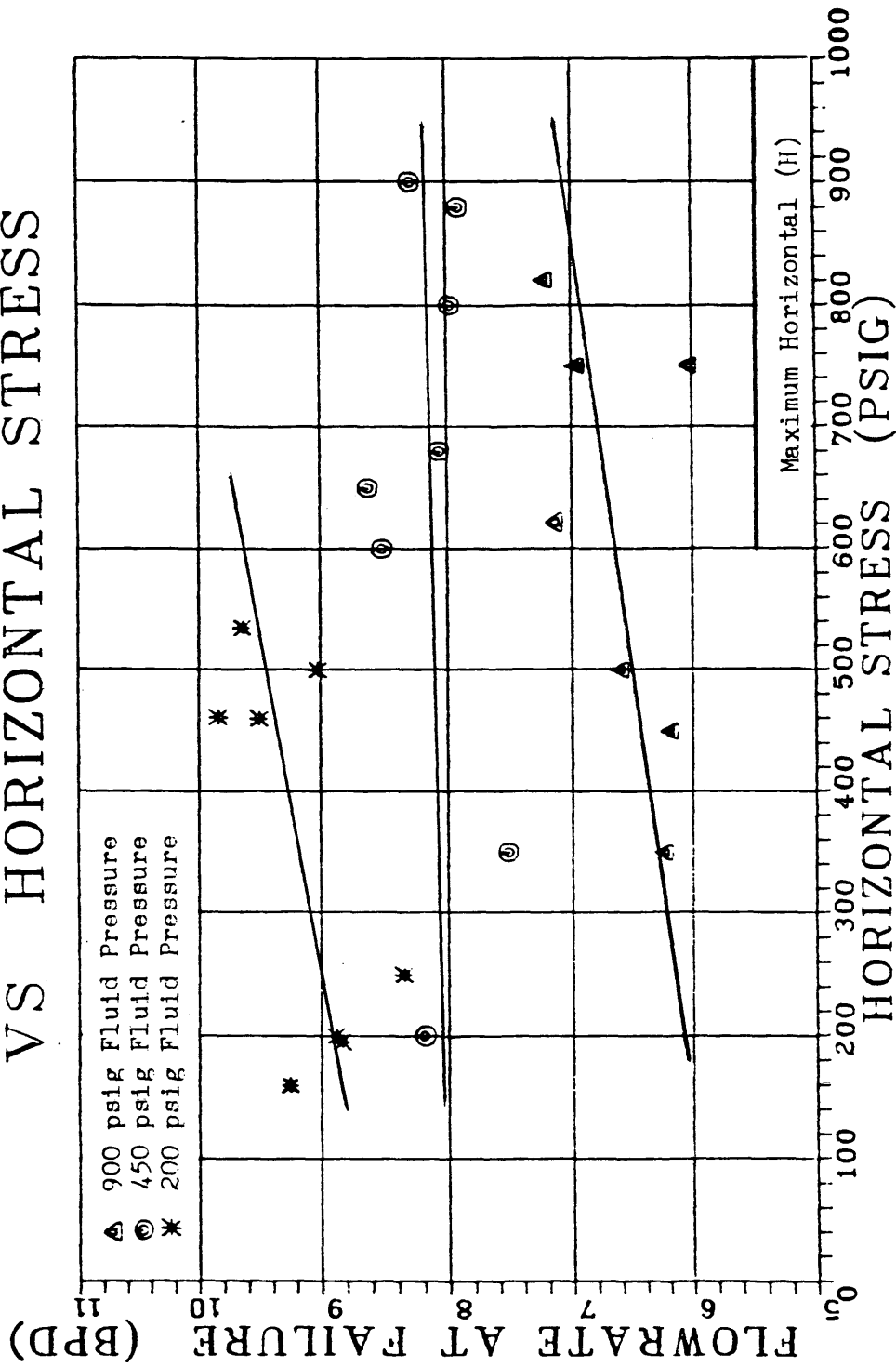


Figure 35

FLOWRATE AT ARCH FAILURE VS HORIZONTAL STRESS

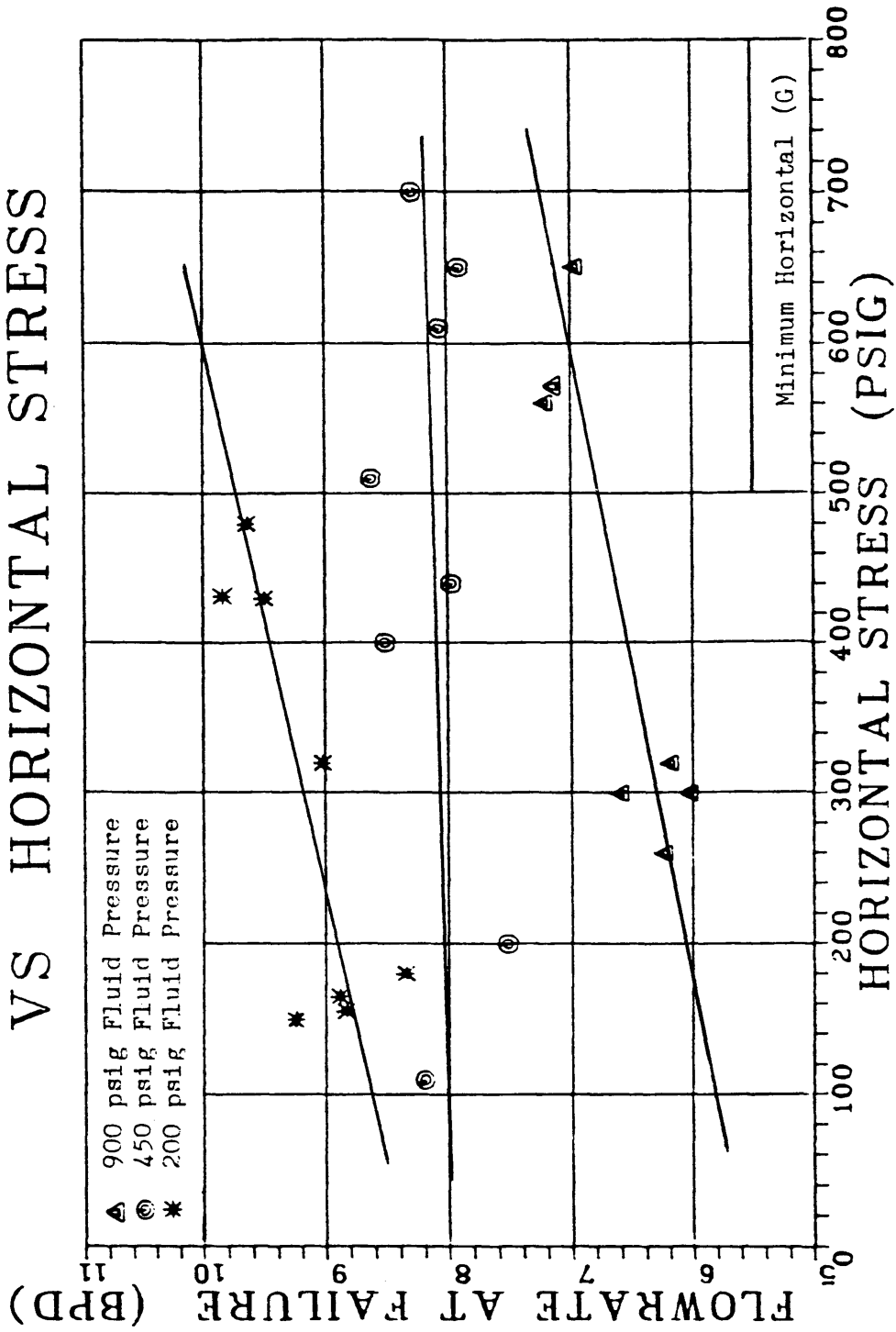


Figure 36

transfer of vertical stress via the walls of the cell. Thus the horizontal stress is directly tied to the vertical stress. Since arch stability has been shown to be a function of vertical or overburden stress, it is to be expected that stability would also increase with increasing horizontal or confining stress. This is due to the two stresses being directly related.

Comparing Figures 35 and 36, it can be seen that both horizontal gauges record consistent stress magnitudes with regard to each other. This is evidenced by the two plots having the same trend. Plotting one horizontal reading against the other (Figure 37), shows just how consistent the two readings are. The gauge facing 45° away from the port (G) measures a stress roughly three-quarters the stress measured by the gauge facing 135° away from the port (H) (Figure 37).

The reason that the two gauges do not measure the same magnitude of stress is due to the unequal transfer of stress within the cell. The inside of the steel sand cell is symmetrical with the exception of the plexiglass ports on one side. Since the gauge pointing more directly towards the port records less stress, it seems probable

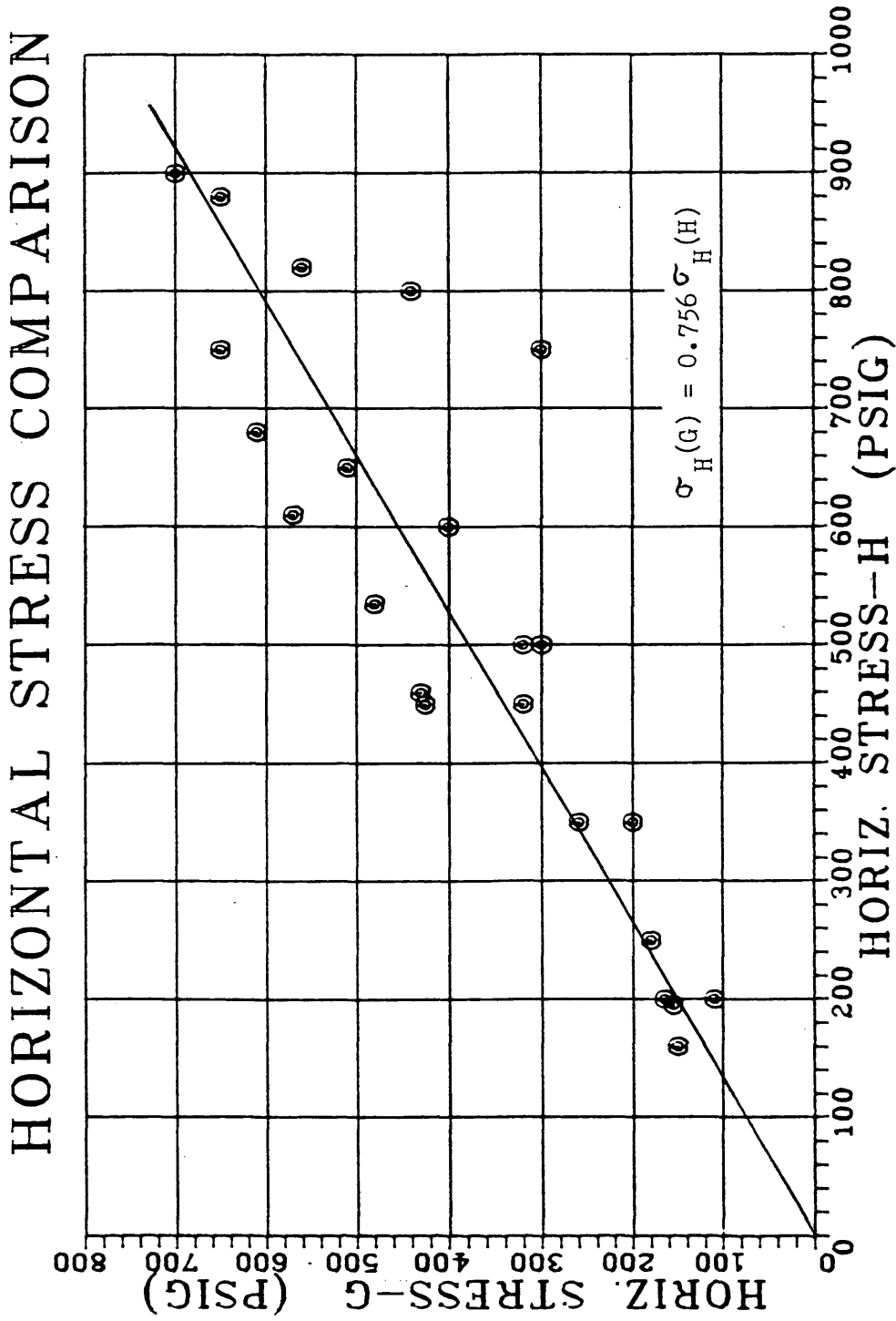


Figure 37

that the plexiglass port does not transfer stress back to the sand pack as well as the walls of the steel vessel. This is due to plexiglass being more ductile than steel.

Although the two horizontal gauges record similar stresses for an applied load, the two gauges respond directly opposite during arch growth and failure. Gauge H (135°) generally experiences a stress increase upon arch growth or failure while gauge G (45°) and the vertical gauge F both record a sharp stress drop. The stress drops in the vertical and horizontal port direction is due to the movement of sand toward the perforation in the simulated casing. When an arch grows or fails, sand shifts horizontally towards the perforation. If the arch holds, only a slight stress drop will be recorded, which is due to the realignment of sand grains forming the larger arch. If the arch fails, a large stress drop will occur as sand is removed from the cell.

As for the reason gauge H experiences a stress increase, this is probably due to some transfer of vertical stress. A better understanding of stress and strain conditions within the cell is needed to fully understand this behavior. In all likelihood, the stress sink on one side of the cell is causing some type of stress influx on the opposite side.

In a past thesis⁽²²⁾, correlations have been made regarding the stress ratio within the sand pack. Figure 38 shows the flowrate at arch failure versus the sand pack stress ratio. This ratio (Table 5) is defined as the vertical stress divided by the horizontal stress. The lines drawn on the graph are least squares analyses on the data corresponding to the three pore pressure levels. It can be seen that these lines have no consistency to them, and thus no correlation can be made. The reason for this poor stress ratio data lies in the inconsistency of the transfer of vertical stress to horizontal. Figures 39 and 40 show the transferred horizontal stress (for gauges H and G respectively) for given vertical stresses. Although the general trend of increasing horizontal stress with increasing vertical stress can be seen, there exists a wide degree of scatter in the data points. This scatter accounts for the poor stress ratio correlation.

Another possible way to correlate the stress data with arch stability is in terms of a net effective stress. The net effective stress is defined as the overburden stress minus the fluid pore pressure (Equation 9). For the experiments conducted in the sand cell, this stress is equal to the vertical stress reading after the fluid pressure has been built up, minus the fluid pressure (Table

FLOWRATE AT ARCH FAILURE VS STRESS RATIO

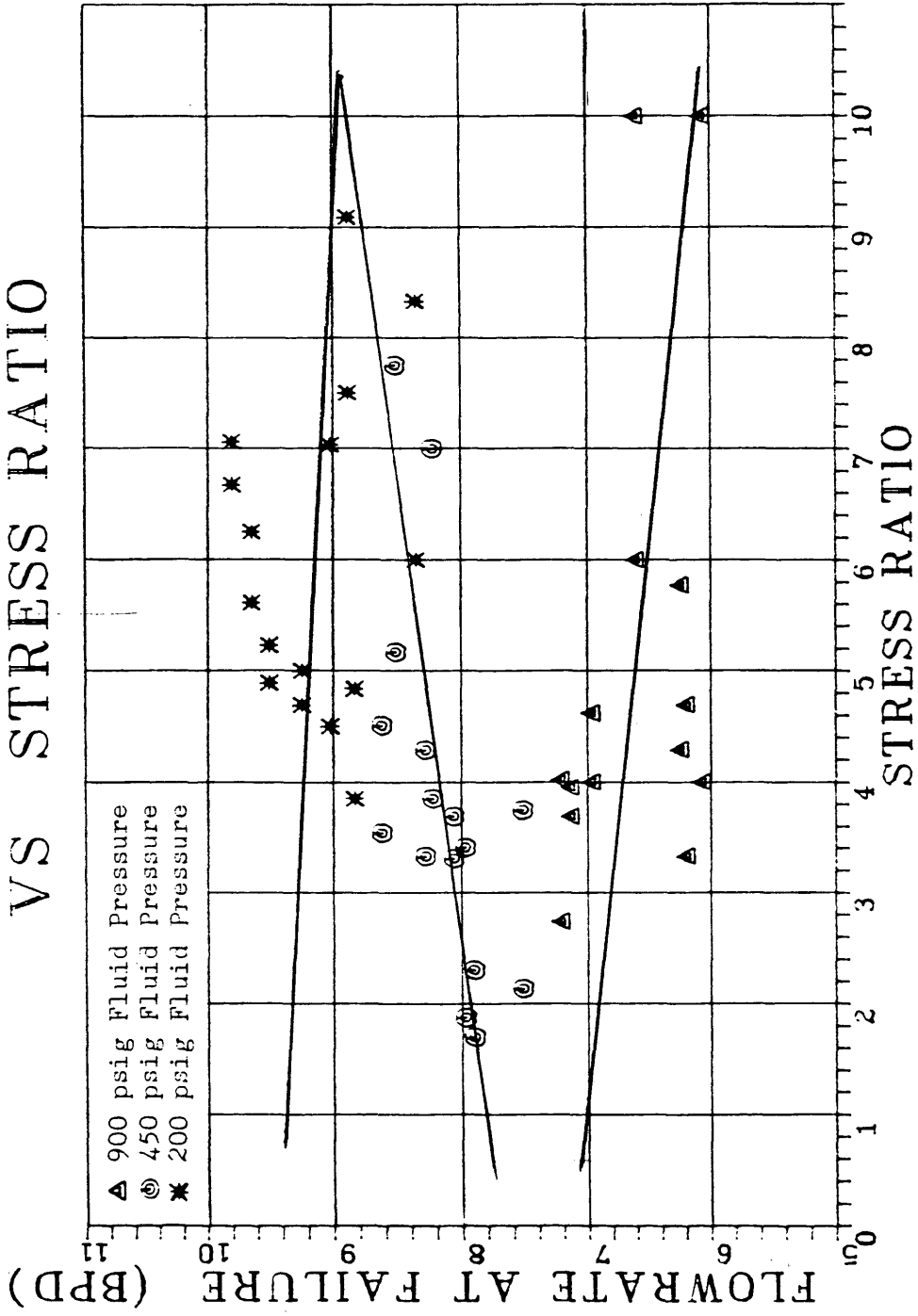


Figure 38

VERTICAL STRESS VS HORIZONTAL STRESS

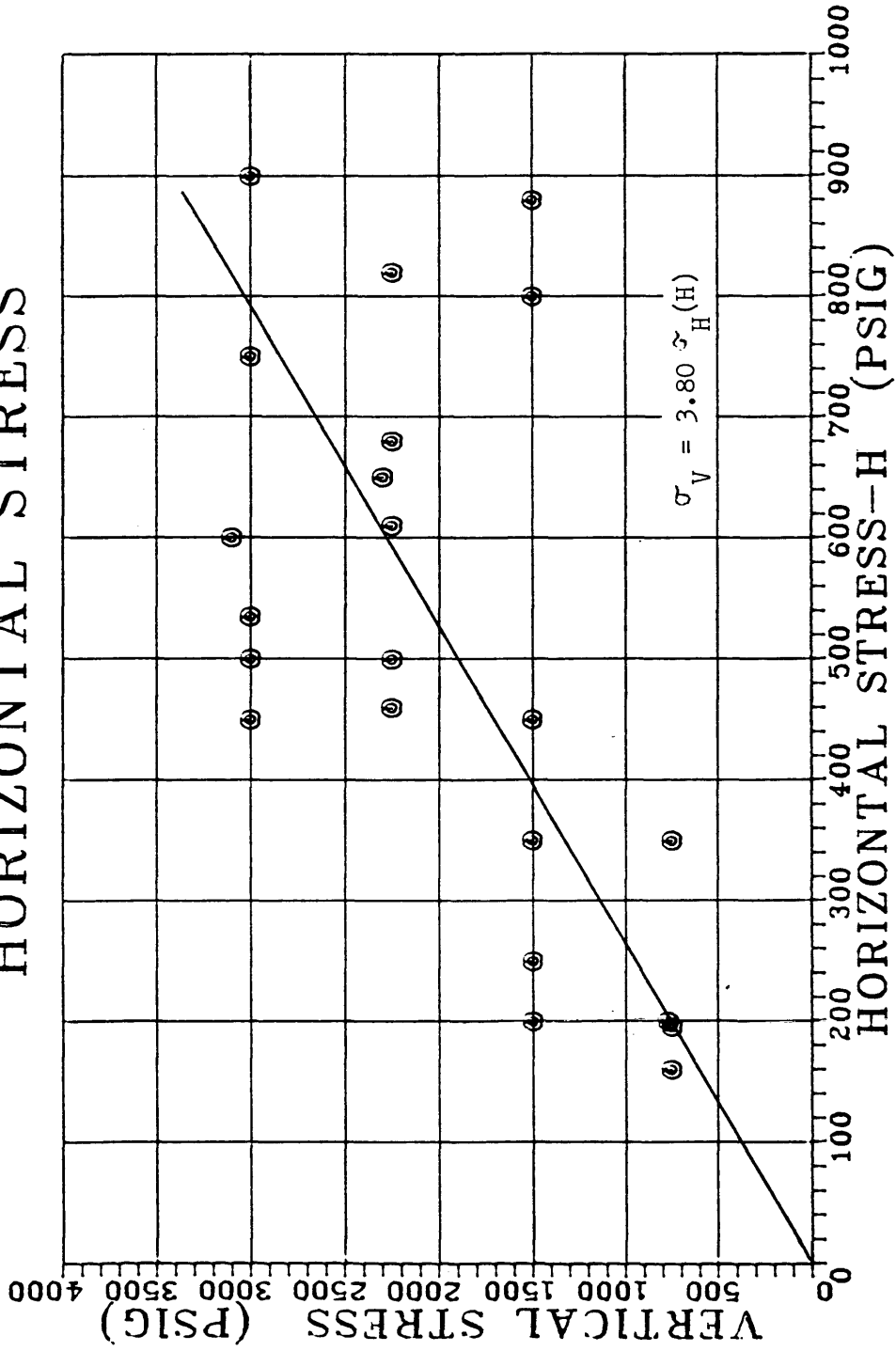


Figure 39

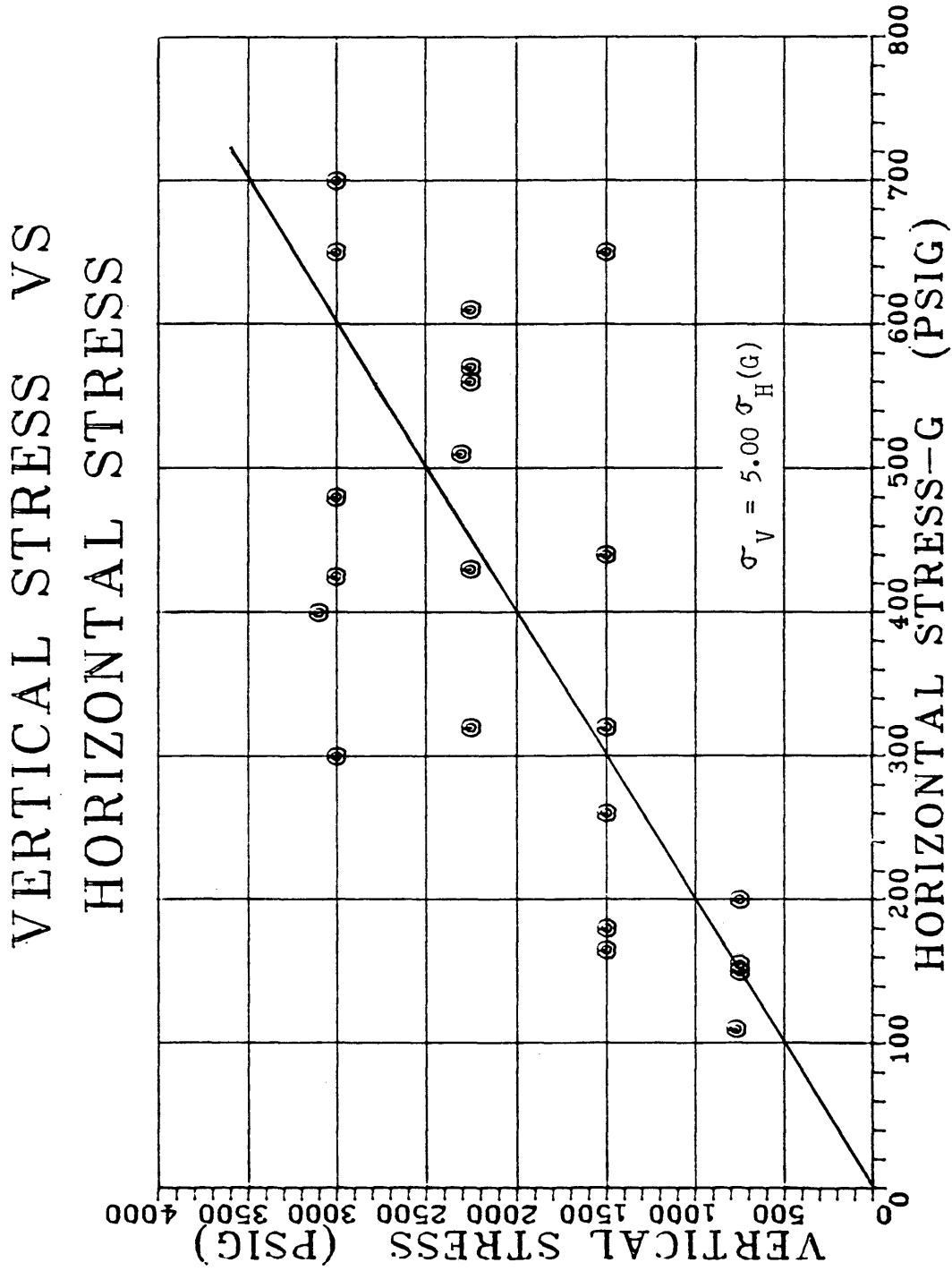


Figure 40

3). These calculated values are listed in Table 5. Figure 41 is a plot of flowrate at arch failure as a function of net effective sand stress. This plot looks almost identical to the plot of flowrate versus vertical stress (Figure 30).

It was hoped that all the data would fall on the same line, as would be predicted by the theory of rock mechanics. This rock mechanics theory states that varying stresses and pore pressures can be related using a net effective stress (2). This concept of net effective stress as defined, does not seem to apply to unconsolidated sands.

Grain Crushing Analysis

Earlier experimentation (22) hypothesized that fines were being generated within the sand pack due to grain crushing. In order to investigate this hypothesis, sand samples were taken after each test for the fourth sand pack. This fourth sand pack was used to take data at 200 psig fluid pore pressure with all four stress levels (3000, 2250, 1500, and 750 psig). Six tests were run, two at 750 psig, two at 1500 psig, and one each at 2250 and 3000 psig. After each test a sand sample was taken from the middle of the cell. Additionally an initial sample was also taken.

FLOWRATE AT ARCH FAILURE VS NET EFFECTIVE STRESS

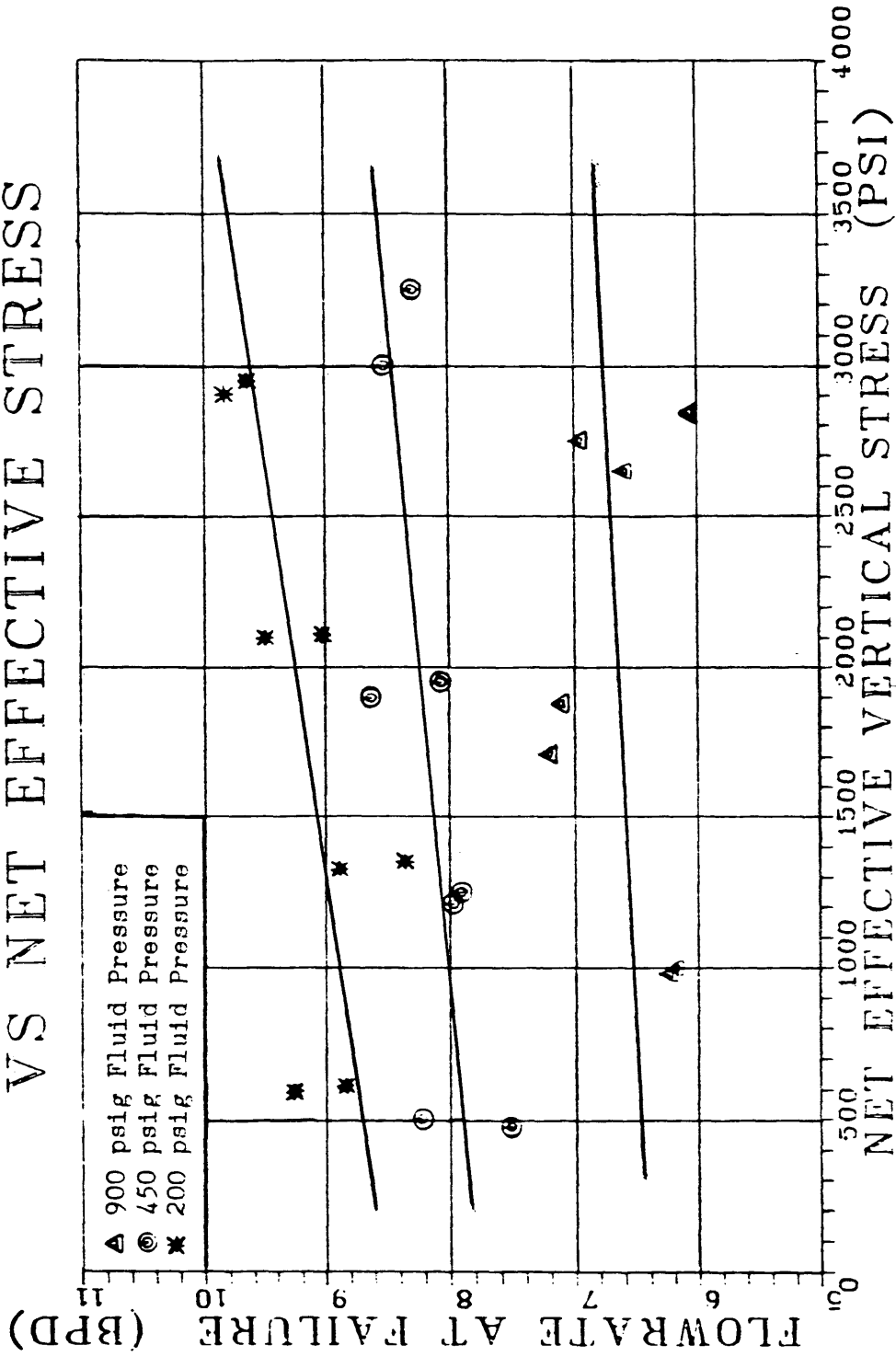


Figure 41

A sieve analysis was conducted on each sample following the API standard procedures for frac sand analysis(26). This analysis calls for sieving a 100 gram sample through a series of sieves for ten minutes on a Ro-tap sieve shaker. Table 6 shows the results of the sieve analysis of each sample. The grain size distributions for the initial and final sand samples are plotted on Figure 42. Figure 43 is an enlargement of the critical section of this distribution seen in Figure 42. From these two plots, it is evident that fines do accumulate in the sand pack over the course of six tests. The means by which the fines are accumulated, is not however, conclusive.

In order to further investigate this influx of fines, a grain crushing test was run on the 20/40 Gopher State frac sand. This crushing test was conducted at 3000 psig and held for two minutes. The load corresponding to this stress level was applied gradually, taking one minute to build to the desired level. This procedure follows the API recommended frac sand crush resistance test(26). The crushed sand was then sieved in the same manner as the other samples. Table 7 shows the sieve analysis for this

Table 6

Sample #	Sand Sample Sieve Analysis											Initial Sand Wt.
	Sieve 16	Sieve 20	Sieve 30	Sieve 35	Sieve 40	Sieve 50	Pan					
	Sieve Wt.	441.6	436.0	412.5	411.4	404.6	392.3	380.05			100.65	
	Sieve + Sand	441.6	437.8	443.7	453.9	422.3	399.7	380.13				
	Sand Wt.	0.0	1.8	31.2	42.5	17.7	7.4	0.08			= 100.68	
	Percent sand	0.00	1.79	30.99	42.21	17.58	7.35	0.08				
	Cum. percent	0.00	1.79	32.78	74.99	92.57	99.92	100.00				
1	Sieve Wt.	441.6	436.1	412.6	411.5	404.7	392.33	380.10			97.78	
	Sieve + Sand	441.6	437.8	442.8	451.6	421.3	400.8	380.51				
	Sand Wt.	0.0	1.7	30.2	40.1	16.6	8.47	0.41			= 97.48	
	Percent Sand	0.00	1.74	30.98	41.14	17.03	8.69	0.42				
	Cum. Percent	0.00	1.74	32.72 ₁	73.86	90.89	99.58	100.00				
2	Sieve Wt.	441.5	436.0	412.7	411.5	404.6	392.31	380.03			97.26--Slightly	
	Sieve + Sand	441.5	439.0	450.7	451.1	417.8	395.61	380.17			Wet	
	Sand Wt.	0.0	3.0	38.0	39.6	13.2	3.3	0.14			= 97.24	
	Percent Sand	0.00	3.09	39.08	40.72	13.57	3.39	0.14				
	Cum. Percent	0.00	3.09	42.16	82.89	96.46	99.86	100.00				
3	Sieve Wt.	441.5	436.1	412.6	411.6	404.6	392.33	380.05			89.30	
	Sieve + Sand	441.5	437.7	441.7	448.8	418.1	399.71	380.52				
	Sand Wt.	0.0	1.6	29.1	37.2	13.5	7.38	0.47			= 89.25	
	Percent Sand	0.00	1.79	32.61	41.68	15.13	8.27	0.53				
	Cum. Percent	0.00	1.79	34.40	76.08	91.20	99.47	100.00				
4	Sieve Wt.	441.5	436.0	412.7	411.6	404.7	392.30	380.05			100.33	
	Sieve + Sand	441.5	437.8	443.7	453.8	420.5	401.2	380.72				
	Sand Wt.	0.0	1.8	31.0	42.2	15.8	8.90	0.67			= 100.37	
	Percent Sand	0.00	1.79	30.89	42.04	15.74	8.87	0.67				
	Cum. Percent	0.00	1.79	32.68	74.72	90.47	99.33	100.00				

Table 6 (continued)

Sample #	Sieve 16	Sieve 20	Sieve 30	Sieve 35	Sieve 40	Sieve 50	Pan	Initial Sand Wt.
5	Sieve Wt.	441.5	412.6	411.6	404.7	392.28	380.05	93.55
	Sieve + Sand	441.5	441.4	450.6	420.0	400.4	380.71	
	Sand Wt.	0.0	28.8	39.0	15.3	8.12	0.66	= 93.68
	Percent Sand	0.00	1.92	30.74	41.63	16.33	8.67	0.70
	Cum. Percent	0.00	1.92	32.66	74.30	90.63	99.30	100.00
6	Sieve Wt.	441.5	412.7	411.6	404.6	392.30	380.07	95.07
	Sieve + Sand	441.5	441.1	450.8	421.0	400.9	381.18	
	Sand Wt.	0.0	28.4	39.2	16.4	8.6	1.11	= 95.21
	Percent Sand	0.00	1.58	29.83	41.17	17.23	9.03	1.17
	Cum. Percent	0.00	1.58	31.40	72.58	89.80	98.83	100.00

GRAIN SIZE DISTRIBUTION 20/40 FRAC SAND

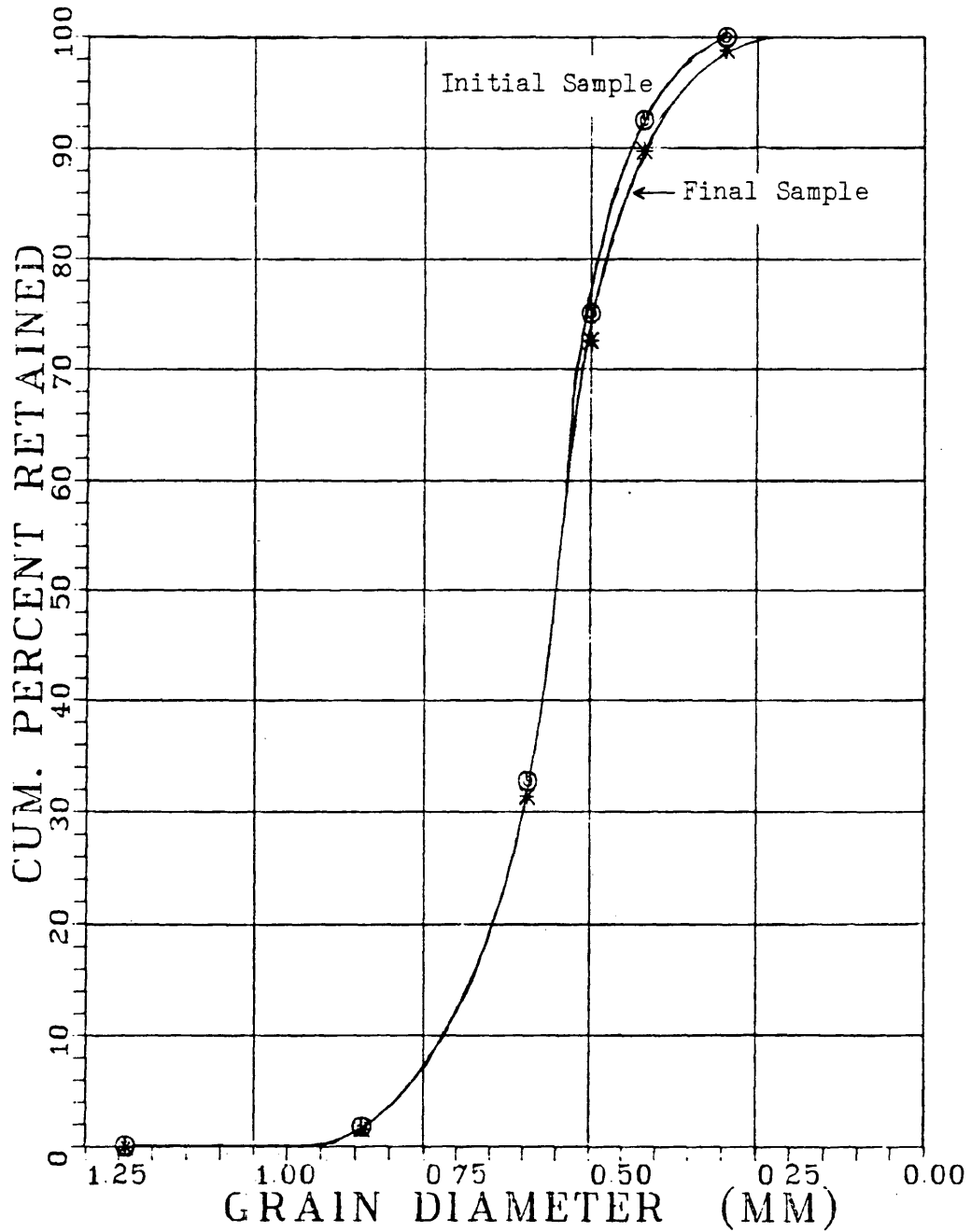


Figure 42

GRAIN SIZE DISTRIBUTION 20/40 FRAC SAND

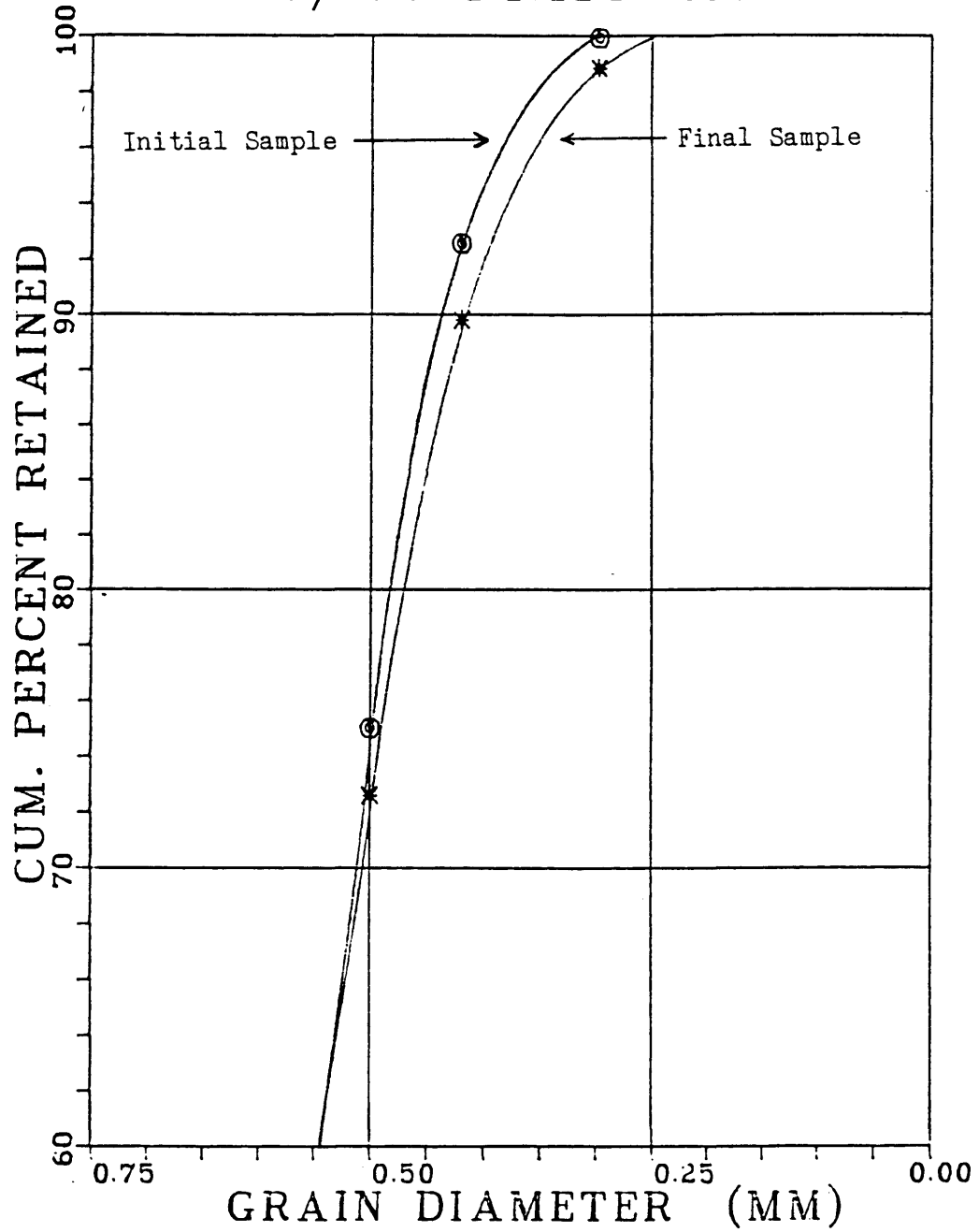


Figure 43
Blow-up of Figure 42

crushed sample as well as for another initial sample. The grain size distributions for these two samples are shown in Figures 44 and 45.

From the crush test it can be seen that 3000 psig applied stress is sufficient to crush a significant amount of 20/40 frac sand. For example, looking at Table 7, it can be seen that 80 percent of the initial sand sample was retained on the #35 sieve, while only 67 percent was retained after the crush test. This shows an increase in fines due to the applied stress. Thus the fines that accumulated during the course of six tests could and probably are due to grain crushing. In comparing the crush test data with that taken from the sand pack, it might be noted that a larger amount of fines were created in the crush test. This greater amount of crushing is due to the lack of fluid around the sand grains in the crush test.

Hall and Harrisberger⁽¹¹⁾ did some research on crushing of frac sands. They ran crush tests on dry sands as well as wet saturated sands at different fluid pore pressures. They showed that wet sands do not crush as readily as dry sands, and also that increased fluid pore pressure greatly reduces grain crushing. Figure 46 shows Mohr's stress envelope's for sands at two different pore

Table 7
Crush Test Sieve Analysis

Sample #	Sieve 16	Sieve 20	Sieve 30	Sieve 35	Sieve 40	Sieve 50	Pan	Initial Sand Wt.
Initial								
Sieve Wt.	441.4	436.0	420.3	411.5	404.6	392.30	380.04	100.02
Sieve + Sand	441.4	438.2	461.4	448.3	419.5	397.28	380.07	
Sand Wt.	0.0	2.2	41.1	36.8	14.9	4.92	0.03	= 99.95
Percent Sand	0.00	2.20	41.12	36.82	14.91	4.92	0.03	
Cum. Percent	0.00	2.20	43.32	80.14	95.05	99.97	100.00	
Crushed								
Sieve Wt.	441.4	435.9	420.2	411.5	404.7	392.30	380.04	40.02
Sieve + Sand	441.4	436.3	430.7	427.6	413.7	396.25	380.15	
Sand Wt.	0.0	0.4	10.5	16.1	9.0	3.95	0.11	= 40.06
Percent Sand	0.00	1.00	26.21	40.19	22.47	9.86	0.27	
Cum. Percent	0.00	1.00	27.21	67.40	89.87	99.73	100.00	

GRAIN SIZE DISTRIBUTION -GRAIN CRUSHING-

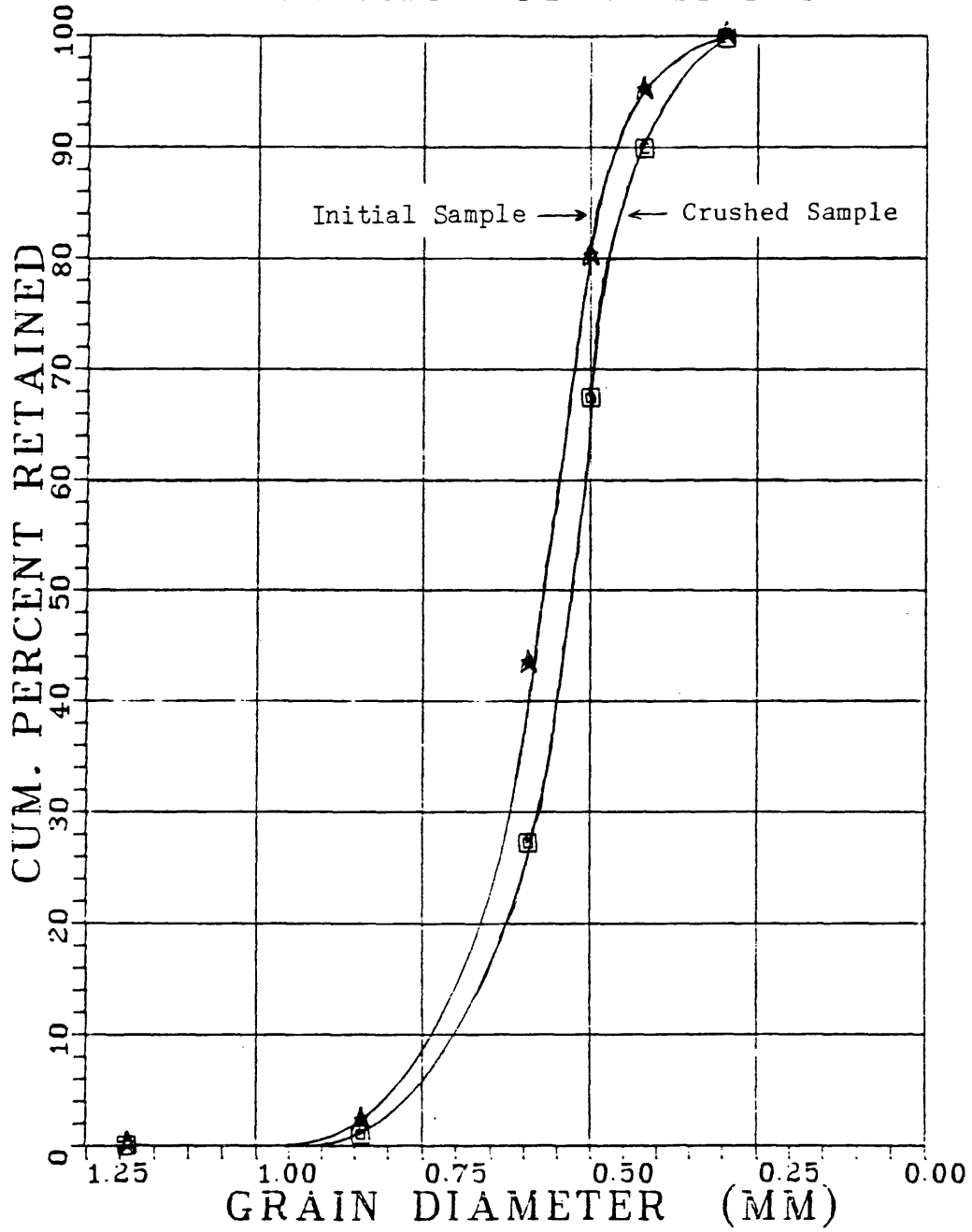


Figure 44

GRAIN SIZE DISTRIBUTION -GRAIN CRUSHING-

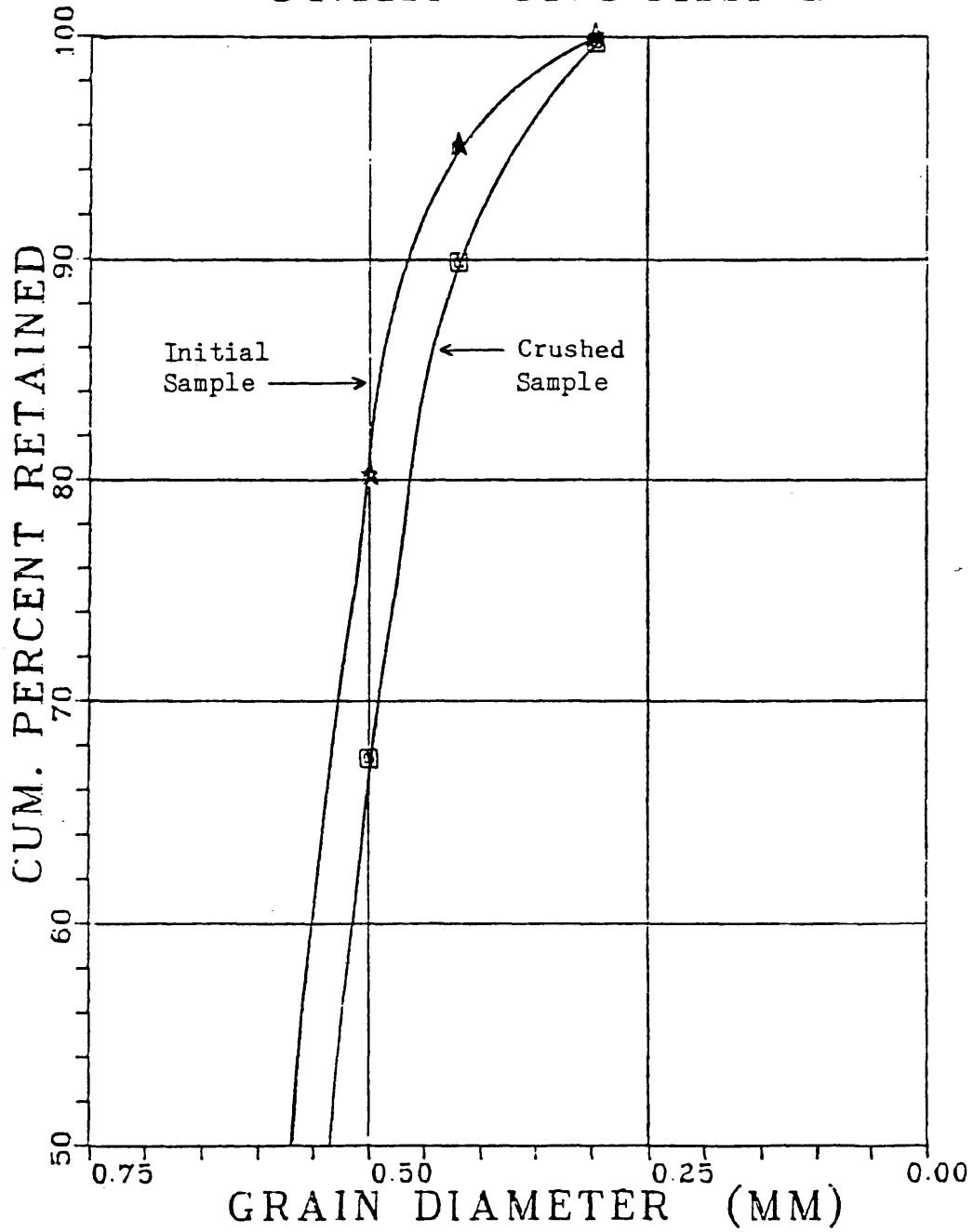


Figure 45
Blow-up of Figure 44

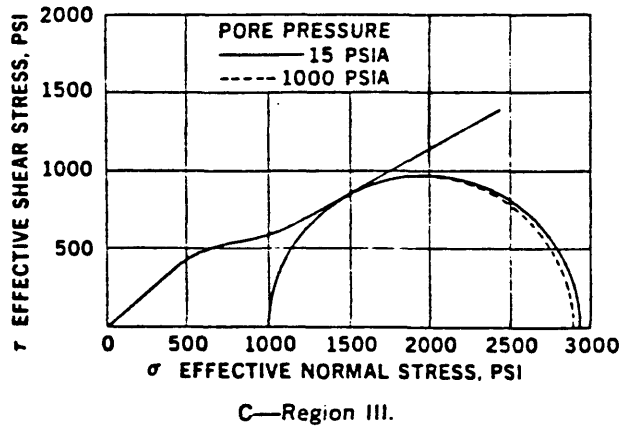
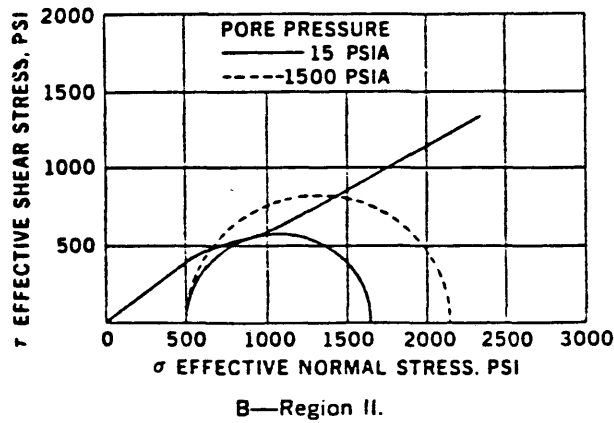
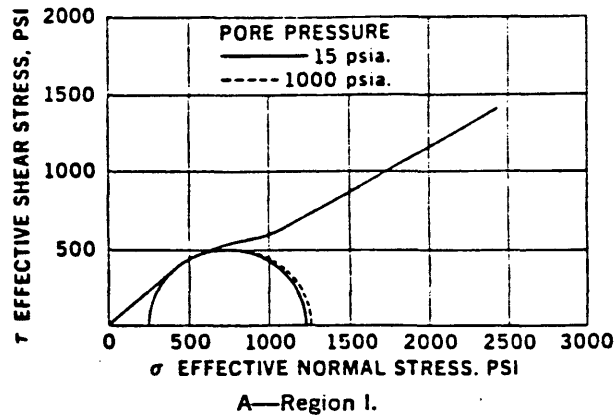


Figure 46

Effect of Pore Pressure on Sand Grain
Crushing (After Hall and Harrisberger.⁽¹¹⁾)

pressure levels. In Region II, where most sand grains crush, the sample with the higher pore pressure shows a significant increase in failure resistance.

This data showing pore pressure as a factor in reducing grain crushing helps explain the difference in fines seen in the crush test and actual lab tests. Additional work is needed with better controlled stresses and pore pressures in order to completely explain this crushing and thus build-up of fines. This increase in fines within the cell is important to quantify due to the effect they have on sand permeability and porosity. The increase in fines obviously reduces both the permeability and porosity, thus effecting the sand arch parameters. In order to do any type of permeability study with the sand cell, this fines build-up due to grain crushing would have to be accounted for.

As for trying to relate the fines increase in the sand samples to permeability in the sand pack, this could not be done due to poor inlet and outlet pressure recordings. The inlet and outlet pressures on the cell were measured using 3000 psig pressure transducers. These transducers presented two problems. First, the transducers were not sensitive enough to measure accurate pressure drop across the cell. These pressure drops are

necessary for permeability calculations. Secondly, the outlet transducer did not read consistently throughout the tests. It will have to be replaced.

In order to measure accurate pressure drops across the cell, new transducers will be needed. These transducers should have a 1000 psig limit. This will adequately handle the fluid pressure associated with the sand cell, and will give three times the accuracy for pressure measurement.

Conclusions

- 1) Arch stability is a strong function of fluid pore pressure. As the pore pressure increases, arch stability decreases.

$$Q_F = 9.822 - 0.0036 P_p$$

- 2) Arch stability increases moderately with increasing vertical and horizontal stress.
- 3) The build-up of fines within the sand pack is a result of grain crushing caused by the applied load.
- 4) No dilatant sand behavior was observed as a result of maintaining constant pore pressure. The dilatant behavior observed in past experimentation was a misinterpretation of increasing fluid pressure.
- 5) By following a set experimental procedure and maintaining constant pore pressure, more consistent data was obtained. This is due to reducing the number of variables within the experimental system.
- 6) Large flowrate steps during experimentation causes arch failure at lower flowrates. This is due to fluid surging across the arch.

- 7) The shut-in of flow during a test does not effect arch stability as long as the flowrate is brought back on at a rate roughly $2/3$ the previous rate, and then increased over several steps to the original flowrate.

Recommendations

Equipment Improvement

The greatest source of experimental error occurs when the arch grows above the simulated casing in the plexiglass port. Because the boundary conditions are changed, the rate corresponding to this growth is considered failure rate and the test is stopped. To eliminate this problem, a casing extension should be placed above the port so that arch growth is not effected by any change in boundary conditions. In order to extend the casing above the top port, the push plate on the top jack will have to be modified to let it slip by the extension. The extension will have to run up past the push plate, due to the shear stresses applied by the jack.

A second solution to the problem is to produce out of the bottom port. Since there already exists an extension connecting the two ports in the cell, the arch growth would not experience changing boundary conditions. Producing from the bottom port would require switching the two ports and adjusting the outlet lines. This second alternative seems the most practical solution unless both ports are to be used simultaneously, then the upper extension will be necessary.

In running experiments, the flowrate at arch failure is probably the single most important piece of data taken. With the present set up, this flowrate is not measured accurately. Currently the flowrate is measured with a stopwatch and graduated cylinder. This works fine throughout the test except at arch failure. Because the arches generally fail when the rate is being increased, some type of flowmeter that can measure instantaneous rates is needed. The stopwatch and cylinder method is only an approximation of this flowrate.

The currently used pressure transducers recording inlet and outlet pressure are rated to 3000 psig. For the tests being run, these transducers do not provide enough accuracy. Additionally the outlet transducer did not read consistently, so both transducers should be replaced. 1000 psig pressure transducers will be sufficient to handle the fluid pressure used in future experiments and will be three times more accurate.

To better understand the arching phenomenon within the sand cell, more knowledge is needed about the distribution of stress and strain in the cell. This will require additional strain gauges being mounted inside the cell. Additionally the triaxial gauges already in the

cell might be turned so that one gauge is directly facing the arch. This gauge would more closely monitor the stress behavior of the sand arch.

To monitor these extra gauges, additional chart recorders will need to be purchased. Due to the frequent breakdown and extreme sensitivity of the existing recorders, they should be replaced with digital recorders currently on the market. These recorders are capable of tracking thirty-two input signals simultaneously. Such a recorder would greatly expand the data gathering capacity of the system.

Future Experimentation

At the present time, there are too many unknown variables in the cell. Future experimentation needs to focus on eliminating or fully understanding these unknowns. One tool that would answer many questions about what is happening within the sand cell, is a sonic device. By placing some type of sonic device inside the cell, the porosity of the sand pack could be monitored during experimentation. Such information might show dilatant sand behavior during arch formation and also sand grain realignment during arch growth and failure. Additionally this device coupled with a density device could be used to determine the bulk and shear modulus within the sand pack.

This information is necessary in order to completely analyze the stress and strain behavior within the cell. The shear modulus might also be correlated with arch stability similar to the concept described by Stein and Hilchie(12).

Another important variable that is unknown within the sand pack is the permeability. Based on the size of the grains packed in the cell, an estimate of permeability can be obtained from various sources, or can be roughly measured in a linear flow tube. This value can not however, be measured presently within the cell. The main reason being that the flow regime and cross-sectional area are not known. In all probability the flow is probably a combination of linear and radial flow. In order to define this flow, it might be possible to inject a dye into the sand to stain the sand grains contacted by the flow. The sand would then be carefully dug out and a model developed for the flow of the fluid. With this defined, permeability could be monitored during experimentation.

It has been hypothesized(22) that permeability has a large effect on arch stability. Although this was investigated by Woods(19), a more thorough study is needed to define the effect of permeability on arch stability. Thus future experimentation should change sand grain sizes

to study the relation. In order for good correlation to be checked, the permeability will have to be strictly monitored. Additionally, a detailed fines study will have to be done. Since sand grains are crushed during experimentation, fines are generated within the sand pack. These fines will reduce the permeability of the sand and thus will effect arch behavior.

Another area to be investigated in future experimentation, is arch stability under reverse flow conditions. It is important to find out whether arches will remain stable or will reform after fluids have been injected back into the formation, such as during well stimulation. If arches remain stable with reverse flow, this knowledge might be used to improve chemical consolidation techniques as well. Chemical consolidation could be initiated after arches have formed around each perforation. This combination of sand arching and chemical consolidation might be an extremely effective sand control technique.

From the experimentation done up to this time, many optimum experimental conditions have surfaced. Benton⁽²²⁾ showed that the best location for the strain gauges is directly behind the producing port and subsequent arch. Thus future tests should continue to use this gauge placement. The gauges may however be turned to directly

face the arch. Additionally, this author has found that constant pore pressure allows for more consistent data. Based on equipment constraints, the optimum fluid pressure to conduct experimentation at is 450 psig.

As mentioned earlier, future tests should be run out of the bottom port, to eliminate the problem of arches extending above the port. Also since it has been seen that arch stability is sensitive to rate surges, future tests should use rate increments of 1/4 turn on the pump or roughly 0.25 BPD increments. It is also very important to follow a set procedure in all aspects of experimentation to eliminate all possible variables or sources of error. The outlined procedure in the appendix is the accumulation of past and present research technique found to yield the most consistent data.

NomenclatureRoman Letters

A	=	Area
B	=	Formation volume factor
c_b	=	Compressibility of the bulk rock material
c_l	=	Compressibility of the pore fluid
c_r	=	Compressibility of rock matrix
E	=	Young's modulus of elasticity
E_s	=	Dynamic shear moduli
G_b	=	Shear modulus of the rock bulk material
H	=	Proportionality constant in terms of compressibility
H	=	Sand pack height
k	=	Permeability
N	=	Number of perforations
p	=	Fluid pore pressure
P_{ob}	=	Overburden pressure
P_p	=	Pore pressure
P_R	=	Reservoir pressure
P_w	=	Wellbore pressure
Q	=	Flowrate
Q_F	=	Flowrate at arch failure
S	=	Net effective stress

Greek Letters

β = c_r/c_b

γ = Sand pack density

ϵ = Normal strain

μ = Viscosity

ν = Poisson's ratio

σ = Normal stress

σ_v = Vertical sand stress, gauge F

σ_{H1} = Horizontal sand stress (135°), gauge H

σ_{H2} = Horizontal sand stress (45°), gauge G

ϕ = Porosity

Subscripts

T = Test well

x = Rectangular coordinate system

y = Rectangular coordinate system

z = Rectangular coordinate system

Cited References

1. Suman, G.O., Jr., Ellis, R.C., and Snyder, R.E., Sand Control Handbook. Gulf Publishing Company; Houston, TX, 1983.
2. Kohlhaas, C. A., Oil and Gas Well Design: Completions. Colorado School of Mines; Golden, CO.
3. Strickland, W.T., Jr., Richardson, E.A., Hamby, T.W., and Torrest, R.S., "A Metal-Plating Process for Sand Consolidation," SPE Trans. No. 4958 (June 1975).
4. Davis, D.R. and Meijs, F.H., "'Siliclock'-A Novel Sand-Control Process for Gas Wells," SPE Trans. No. 9423 (Sept. 1980).
5. Aslesen, K.S., Short, C.J., and Terwilliger, P.L., "A New Method for Sand Control and Well Stimulation in Unconsolidated Dirty Sands," SPE Trans. No. 10172 (Oct. 1981).
6. Payzone Preparation: The New First-Step in Production. Completion Tool Company; Houston, TX.
7. Terzaghi, K.v., "Stress Distribution in Dry and in Saturated Sand Above a Yielding Trap-Door," Proceedings 1st International Congress on Soil Mechanics and Foundation Engineering, Vol. 1 (June 1936).
8. Terzaghi, K.v., Theoretical Soil Mechanics. John Wiley and Sons; New York, N.Y. 1943, pp. 66-76.
9. Terzaghi, K.v. and Peck, R., Soil Mechanics in Engineering Practice. John Wiley and Sons; New York, N.Y. 1948, p. 199.
10. McNulty, J.W., "An Experimental Study of Arching in Sand," Ph.D. Thesis, The U. of Illinois, Urbana 1965.
11. Hall, C.D., Jr. and Harrisberger, W.H., "Stability of Sand Arches: A Key to Sand Control," JPT, July 1970.

12. Stein, Nathan and Hilchie, D.W., "Estimating the Maximum Production Rate Possible from Friable Sandstones Without Using Sand Control," JPT, Sept. 1972.
13. Tippie, D.B. and Kohlhaas, C.A., "Effects of Flow Rate on Stability of Unconsolidated Producing Sands," SPE No. 4533 (Oct. 1973).
14. Tippie, D.B. and Kohlhaas, C.A., "Variations of Skin Damage with Flow Rate Associated with Sand Flow or Stability in Unconsolidated-Sand Reservoirs," SPE No. 4886 (April 1974).
15. Stein, N., Odeh, A.S., and Jones, L.G., "Estimating Maximum Sand-Free Production Rates From Friable Sands for Different Well Completion Geometries," JPT (Oct. 1974).
16. Melvan, J.J., "The Effects of Overburden Stress on the Formation and Stability of Arches in Unconsolidated Sands," MS Thesis No. 2071, Colorado School of Mines; Golden, CO (May 1978).
17. Cleary, M.P., "The Effects of Fluid Properties on Arch Stability in Unconsolidated Sands," MS Thesis No. 2072, Colorado School of Mines; Golden, CO (May 1978).
18. Cleary, M.P., Melvan, J.J., and Kohlhaas, C.A., "The Effect of Confining Stress and Fluid Properties on Arch Stability in Unconsolidated Sands," SPE No. 8426 (1979).
19. Woods, D.C., "The Effect of Sand Size on Arch Stability in Unconsolidated Sands," Ph.D. Thesis No. 2165, Colorado School of Mines; Golden, CO (May 1979).
20. Bratli, R.K. and Risnes, Rasmus, "Stability and Failure of Sand Arches," SPE No. 8427 (Sept. 1979).
21. Lasaki, G.O., "Arch Stability and Failure Behavior in Unconsolidated Natural Sands," Ph.D. Thesis No. 2299, Colorado School of Mines; Golden, CO (May 1980).

22. Benton, J.H., "Near Wellbore Stress Behavior in an Unconsolidated Sand During Sand Arch Formation and Failure," MS Thesis No. 3014, Colorado School of Mines; Golden, CO (Dec. 1984).
23. Muvdi, B.B. and McNabb, J.W., Engineering Mechanics of Materials. Macmillan Pub. Co., Inc.; New York, N.Y. 1980.
24. Biot, M.A., "General Theory of Three-Dimensional Consolidation," J. Appl. Phys., 12, 1940.
25. Geertsma, J., "Velocity-Log Interpretation: The Effect of Rock Bulk Compressibility," SPEJ Dec. 1961.
26. American Petroleum Institute, API Recommended Practices for Testing Sand Used in Hydraulic Fracturing Operations. API Production Department; Dallas, TX 1983.

AppendixExperimental Procedure Outlined

I. Initial Cell Assembly.

A. Port Installation (If necessary).

1. Turn the cell using the floor winches, to a vertical position with the two ports pointing south.
2. Loosen the 16 nuts holding the face plate on, using the proper size socket (3-1/8") and steel bar.
3. Slide the steel face plate partially off, until there is a sufficient gap between the plate and the cell to slip the electric hoist chain through. Secure the hoist chain around the face plate and then proceed removing the plate.
4. Turn the cell to a horizontal position with the ports facing up.
5. Place the small hydraulic jack inside the cell, beneath the port, and pump out the old port.
6. Clean the exposed port hole.

7. Grease the sides of the new port and slide it into the port hole. Make sure the simulated casing portion of the port is in its proper alignment.
 8. Grease and install the proper O-ring around the port face.
 9. Turn the cell back to vertical and replace the face plate and secure the 16 nuts.
 10. Insert plexiglass casing portion between the two ports.
- B. Bottom jack and end cap.
1. Turn the cell with the floor winches to a vertical position with the ports facing north (upside down).
 2. Clean the inside cell wall and grooves.
 3. Install the strain gauge assembly in the cell.
 4. Lift the bottom jack into place using the electric hoist attached to the eye-bolts screwed into the top of the jack.

5. Grease the O-rings on the jack (replace if necessary), along with the side of the jack and lower it into the cell, making sure the notch in the push plate slips over the end of the strain gauge assembly.
 6. Remove eye-bolts from the top of the jack, and grease the top surface.
 7. Install the hydraulic stem in the top of the jack.
 8. Lift the end cap into place using the electric hoist and eye-bolts attached to the cap. Lower the cap into place and screw it down using 1 inch steel bars placed in the machined holes in the side of the cap.
- C. Cell preparation for loading of sand.
1. Turn the cell 180° so that the ports are facing south.
 2. Hook up all lines.
 - a. Desaturation line to top of cell.
 - b. Drain line from bottom of cell.
 - c. Inlet line.
 - d. Outlet line including sand trap assembly.
 - e. Water injection line on outlet side.

3. Close all valves on lines hooked up to the cell.
 4. Connect the strain gauge wires to the chart recorders and check for proper operation.
 5. Connect the two pressure transducers to the inlet and outlet of the cell.
- D. Loading cell with sand.
1. Fill cell with about 4 gallons of water.
 2. Wash the sand in 3 to 4 gallon increments in a 5-gallon bucket. Wash the sand in the back parking lot using a water hose and a high velocity venture type nozzle. Continue washing the sand, until the overflow water is clear.
 3. Pour the washed sand into the cell and tamp firmly into place using a 1/2-inch galvanized pipe.
 4. Continue washing and tamping sand until the sand reaches a level 5-7/8 inches below the seat for the top jack.
 5. Dip off excess water from the top of the sand pack.
 6. Level the sand and clean the inside top jack seats and end cap grooves.

7. Save a washed sand sample (1-1/2 pint) for later analysis.
 8. Leave strain gauges on and check periodically for proper operation.
- E. Top jack and end cap.
1. Lift the top jack using the hoist, install "O"-rings, grease the jack sides, and lower the jack into the cell. The bleed valve on the side of the cell should be open in order to let air and excess water escape.
 2. Grease the top of the jack and attach the hydraulic stem to the jack.
 3. Lift the end cap, and after cleaning and greasing it, lower it into place. tighten the cap down using the 1-inch steel bars.

II. Saturating Cell with Mineral Spirits.

- A. Initial Preparation
1. Make sure all outlet valves on lines hooked up to the cell are closed, with the exception of the upper bleed valve.
 2. Set valves on flow manifold to circulate the mineral spirits through the board, bypassing the cell.

3. Turn on the pump at its lowest speed (3.0 BPD).

B. Hydrocarbon saturation.

1. Open the desaturation line into the cell and shut off all flow to the settling tank.
2. Once all air has been removed from the cell, as evidenced by fluid flow out the bleed line, close the bleed valve.
3. Open the drain valve at the bottom of the cell, thus allowing the displaced water to run into the drain barrel.
4. Continue displacing water out of the sand pack until the produced or drained water cut is less than 1% water.
5. Divert flow of mineral spirits back through the board and to the settling tank, closing off both the drain and desaturation valves. Turn off the pump.
6. Let the cell sit overnight, and then desaturate for another hour or so the following day, prior to running a test. This time allows the water and mineral spirits to separate due to gravity

segregation. This helps reduce the effects of fingering in the original hydrocarbon desaturation.

7. At some point in time skim off the mineral spirits from the drain barrel and dump it into the settling tank.

III. Preparation for Initial Run.

A. Flow equipment.

1. Check to see if all lines are hooked up tightly on the inlet and outlet of the cell.
2. Open the check valve bypass on the sand trap, and also open the air bleed valve.
3. Turn the pump on and divert flow to fill the sand trap and all outlet lines.
4. Divert flow to the inlet of the cell, with the inlet air bleed valve open. The inlet line should already be full due to the check valve, but there may be air left in between the check valve and the cell, from the packing of the sand.

- B. Zero the strain gauges and pressure transducers.
 - 1. Open the bleed valves on the transducer hook-ups, and zero the two readings on the chart recorders.
 - 2. Zero the strain gauge outputs on the chart recorders and adjust each gain to its proper value.
- C. Cycling the sand pack.
 - 1. Hook up the hydraulic lines to the top and bottom of the cell.
 - 2. Open the bleed valve on the top of the cell.
 - 3. Check hydraulic fluid level in its storage tank.
 - 4. Hook up the compressed air line to the hydraulic pump.
 - 5. Close the bleed valves on the jack manifolds (top and bottom of cell) and the bleed valve off the hydraulic pump. The two valves running to the jack manifolds near the pump should be left open.
 - 6. Turn on the hydraulic pump and pump up the jacks until the vertical gauge registers 3000 psig.

7. After 15 to 20 minutes, open the three bleed off valves and let the pressure that the jacks are inserting, bleed off.
 8. After the stress within the sand pack has completely bled off, close the valves and cycle the sand pack again.
 9. Before every test, the sand pack is stressed three times to 3000 psig and then twice more to the vertical stress being run.
 10. On the final sand stress cycle, close the valves on the hydraulic lines leading to the jacks, and disconnect the compressed air line. This will help to eliminate hydraulic pressure bleeding off during the test.
- D. Bleeding air from cell.
1. Turn on the mineral spirit pump and divert flow into the cell by way of the desaturation line.
 2. Divert flow back through the board and to the settling tank, once all air has escaped through the bleed valve at the top of the cell.

3. Close both the desaturating and the cell bleed valves.

E. Water injection.

1. Check water level in the water reservoir.
2. Turn on water pump and open water injection valve.
3. Turn off pump and shut valve after 200 cc of water has been injected.

F. Fluid pressure build up.

1. Turn on the pump, diverting the flow to both the inlet and outlet of the cell. All bleed valves should be closed.
2. Continue pumping until cell and line pressure reaches desired level.
3. Close off the valves isolating the pressure in the cell and lines, and divert the flow back through the board.
4. Close the check valve bypass on the sand trap.
5. Choke down the needle valve on the flow board in order to build up the pressure in the lines, to equal the fluid pressure in the cell.

IV. Initial Test Run.

A. Initial Data.

1. Just prior to fluid pressure build up, record the three sand stress readings on charts F, G, and H.
2. After fluid pressure build-up, again record the three stress readings, along with the inlet and outlet pressures.

B. Begin actual test.

1. Simultaneously open the valve on the outlet of the cell, and divert all flow to the inlet of the cell.
2. Adjust the needle valve to keep the entire system at desired pressure.
3. Once the pressure and flow throughout the system has stabilized, record the three stresses, inlet and outlet pressures, arch characteristics, and the flowrate.

Stability can be determined by observing the pressure response on the chart recorders.

4. The flowrate is measured by diverting the flow just prior to entering the settling tank, and then measured using a graduated cylinder and stopwatch.

5. Increase the flowrate by increasing the pump speed 1/4 turn. This corresponds to an increase of roughly 0.25 BPD.
6. Allow the rate to stabilize, and then record all pressures, stresses, and arch or cavity characteristics, along with the flowrate.
7. Continue increasing the rate until arch failure occurs. This is evidenced by the complete collapse of the arch cavity along with significant pressure drops in gauges F and G and usually a slight increase in gauge H. If the cavity extends above the port and a pressure drop is seen on the recorders, this is taken to be failure also. The test can not be run with the cavity above the port due to the different boundary conditions for the sand arch.
8. Shut-in the cell and divert the flow through the board.
9. Reduce the pump speed to its minimum and then turn it off.
10. Record the stress drop at failure for each of the gauges.

11. Open the cell bleed valve in order to bleed off all fluid pressure. Record the stress levels at zero fluid pressure.

V. Preparation of Subsequent Tests.

A. Pumping out the jacks.

1. Open all hydraulic valves and jack manifold check valves on the jack hydraulic lines. Allow the pressure to bleed off the jacks.
2. Close the cell bleed off valve and turn on the pump, diverting the flow to the inlet of the cell.
3. Monitor the inlet and outlet pressures, to tell when the jacks are pumped out. The fluid pressure as seen on the chart recorders, will rise sharply and then level off. This leveling off is evidence that the jacks are being pumped out. When the pressure starts to rise sharply again, the jacks are pumped out.
4. Turn off the pump and bleed off the cell fluid pressure by opening the bleed valve.

- B. Preparing the sand for the next run.
1. Remove the top end cap and jack. The removal of the jack can be aided by blowing air (compressed air hose) in the bleed off line.
 2. Dig out the sand down to a level below the port. Collect a 1-1/2 pint sand sample in back of the port, for future analysis.
 3. Take apart and thoroughly clean the outlet line and sand trap. The compressed air hose is useful in blowing out the lines in the trap.
 4. Check the outlet filters and replace if necessary.
 5. Blow out the simulated perforation in the port and the port outlet valve.
 6. Close the valve and hook up the outlet lines and sand trap.
 7. Dump about one gallon of mineral spirits into the cell and then proceed to repack the cell.
 8. Tamp every few scoops of sand that are added to the cell.

9. Continue adding and tamping sand until the sand level reaches 5-7/8 inches below the jack seat. Make sure the mineral spirits is always covering the added sand, in order to keep air out of the sand pack.
10. Skim off the excess mineral spirits and replace the jack and end cap.
11. Subsequent tests are run following the instructions in Sections III and IV.

VI. Dumping sand after final test.

A. Disconnecting lines.

1. After the sand has been dug out below the port, disconnect the outlet line and sand trap. Clean as before.
2. Unhook the water injection line, desaturation line, strain gauge wires, and drain line. The inlet line may be left on.
3. Turn the cell using the floor winches to a position just past horizontal, with the ports facing up.
4. Slide the sand cart under the cell to collect the sliding sand.

5. Use the water hose with the high velocity nozzle to wash out the sand cell.
6. Once the cell is clean, turn off the water and turn the cell back to its vertical position.

VII. Sieve Analysis.

A. Sand preparation.

1. The sand samples need to be dried in an oven set at 200° F for roughly 20 hours.
2. The sand is then washed with acetone to remove the dried mineral spirits that coat the sand grains.
3. The acetone is then dried off in the oven for 4 to 5 hours.

B. Sieving the sand.

1. The API recommended sieve analysis procedure(26) for frac sands was used.
2. For 20/40 frac sand, clean and weigh U.S.A. sieve sizes 16, 20, 30, 35, 40, and 50 mesh, and also a fines collection pan.
3. Weigh out approximately 100 grams of sand sample and place in sieve stack.

4. Place the sieves in a Ro-tap testing sieve shaker and sieve for ten minutes.
5. Weigh each sieve and determine the percent by weight retained on each sieve, and the cumulative retained.

VIII. Grain Crushing Test.

A. Crush test.

1. Place 40 grams of sand sample in the crush cylinder.
2. Apply increasing stress to desired level over 60 seconds.
3. Hold Desired stress for 2 minutes and then remove sample.

B. Run sample through proper sieves.